universität wien

MASTERARBEIT / MASTER'S THESIS

Titel der Masterarbeit / Title of the Master's Thesis

„An analytical and computational approach to steady-state optomechanical systems by quantum Langevin equations“

verfasst von / submitted by

Klemens Winkler, BSc.

angestrebter akademischer Grad / in partial fulfilment of the requirements for the degree of

Master of Science (MSc.)

Wien, 2018 / Vienna, 2018

Studienkennzahl lt. Studienblatt / degree programme code as it appears on the student record sheet:	A066 876
Studienrichtung lt. Studienblatt / degree programme as it appears on the student record sheet:	Masterstudium Physik
Betreut von / Supervisor:	Univ.-Prof. Dr. Markus Aspelmeyer

Danksagung

Meine ersten Worte des Dankes gelten Univ.-Prof. Dr. Markus Aspelmeyer für die Gelegenheit an einem so interessanten Thema und in so einer grandiosen Forschungsgruppe zu arbeiten. Nicht zuletzt wegen der tollen Mitglieder in dieser Gruppe war es mir möglich in den letzten Monaten so viele faszinierende sowie lehrreiche Erfahrungen zu sammeln und die Arbeitsweise im täglichen wissenschaftlichen Betrieb kennen zu lernen.

Im Speziellen gilt mein Dank dem "Membrane"-Team, welchem ich mich letzten September anschließen durfte.
Besonders möchte ich Corentin Gut für die unzählbaren Stunden an Diskussionen und Erklärungen bezüglich meiner Arbeit sowie dem dabei entstandenen Programm danken.
Vielen Dank auch an Jason Hölscher-Obermaier, Ramon Moghadas Nia und Joshua Slater für die familiäre Aufnahme in euer Team und die schöne Zeit die ich mit euch hatte. Außerdem danke ich Sebastian Hofer für jenen Teil des Codes welcher die nötige Integration im Programm durchführt .

Zuletzt möchte ich meiner ganzen Familie, meiner Freundin sowie all meinen Freunden für den Beistand in den letzten fünf Jahren meines Studiums danken. Allen voran gilt mein Dank meinen Eltern, Gabriele und Roland Winkler, denn erst durch eure Unterstützung und Ermutigung ist es mir möglich gewesen mein Studium erfolgreich abzuschließen.

Contents

Introduction

Achieving control over macroscopic objects in the quantum regime has become a topic of large interest in modern quantum science. On the one side this enables tests of quantum theory in a genuinely macroscopic setting, on the other side it can give rise to new applications in quantum information processing which use those macro-systems. Cavity optomechanics is a promising approach to obtain the required level of quantum control.
Since the first investigations of cavity optomechanics in the late 60's of the last century [BM67, BMT70] this field showed a rapid progress. Some examples for this progress are ground state cooling of mechanical resonators [TDL$^+$11], measures of mechanical motions [DK10], quantum squeezed states of motion [WLW$^+$15, PDB$^+$15, LCS$^+$15] and even quantum entanglement [PTSL13, CLRSJS$^+$11, RWM$^+$18, OKDP$^+$18].
Non-classical states between light modes and mechanical motion might play an important role as a resource for different applications in quantum computation eg. in constructing a functional network for processing quantum information or as intermediate storage for quantum states.

The motivation for this work is to gain a clear theoretical insight into the currently running optomechanical experiment at the Faculty of Physics of the University of Vienna [HO17], which aims to generate and detect entanglement between a light field and a mechanical system. In this experiment it is not possible to measure directly the mechanical component of the system, however, using the optomechanical interaction, it is possible exchange the mechanical and optical state.
By using proper filtering functions, which are applied on the measured output-light in post-processing, it is possible to define two distinct temporal pulses. The first one will contain contributions of the light from the interaction which generates the entanglement between the mechanical and optical system. The second one consist of the contribution relevant for exchange of the mechanical and optical state. With the help of these two pulses and their non-classical correlations, it is now possible to draw conclusions about the entanglement shared between the mechanics and the light field .
In addition to this, a "two-sideband"-protocol is used for extracting more non-classical cor-

relations between the first and second pulse, respectively, in order to detect more entangled states.

In the course of this thesis, the optomechanical interaction is studied by considering a system consisting of two highly reflective mirrors, one of which is attached to a spring. The moveable mirror forms the mechanical component of the system while the light field inside the cavity represents the optical part of the system. Due to the radiation pressure force acting on the moveable mirror both, the mechanical and optical system, couple to each other through optomechanical interaction. This effect makes it possible to create entanglement between the light mode and the mechanics.
During the discussion, special attention is paid to optomechanical entanglement, its generation and verification. After introducing the formalism in which covariance matrices are used and the ways of detecting entanglement using measures and witnesses, the dynamic of the system is considered by deriving the linearised quantum Langevin equation (QLE) which will finally be solved in an analytical way. This then leads to the implementation of a program which is able to generate the intra-cavity as well as the output-light covariance matrix, which hold all the important informations for the user to explore entanglement in the system for different parameter regimes.
The program is then applied to the parameters of the actual experiment taking place on the University of Vienna in order to study the occurrence of entanglement, the influence the different parameters have on the system and to find the optimal operating parameters for the detection of entanglement.

Outline

This thesis will be structured into the following chapters

- In ***Chapter 1***, I will discuss the theoretical background of this work, including continuous variable systems, covariance matrices, Gaussian states, entanglement and ways to detect it qualitatively and quantitatively.

  Followed by that, I will give a short introduction of the systems of interest, namely the mechanical oscillator, the optical cavity and the optomechanical interaction between them, and I will then characterize the dynamics of the compound system by its quantum Langevin equations.

- ***Chapter 2*** will mainly deal with the different ways of solving the quantum Langevin equations (QLE). First the solutions for the QLE of the intra-cavity modes and also the filtered output modes will be discussed in the steady state regime. Also a method for solving them analytically will be presented.

- Within ***Chapter 3*** a program is presented, which was written to generate the covariance matrices for the input- and output modes analytically.In order to see that the program generates trustworthy covariance matrices we will apply some selected tests. The entanglement between the different systems is then calculated by the methods discussed in chapter 1.
  Moreover, the two-sideband protocol is presented in order to account for intra-pulse entanglement which might detect entangled states where, without this protocol, a detection of these states would not have been possible.

Chapter 1

Theory

1.1 Continuous variable systems and entanglement

1.1.1 The covariance matrix

In cavity optomechanics the systems of interest contain mechanical and optical modes which both are continuous variables (from now on CV) systems [JCLP07]. Let us consider for example an electromagnetic field modelled as N non-interacting harmonic oscillators, described by the Hamiltonian

$$\hat{H} = \sum_{i=1}^{N} \hbar\omega_i \left(\hat{a}_i^\dagger \hat{a}_i + \frac{1}{2} \right) \tag{1.1}$$

The description of the system is based on a Hilbert-space $\mathcal{H} = \otimes_{i=1}^{N} \mathcal{H}_i$ with infinite dimensional Fock spaces $\mathcal{H}_i$, $\hat{a}_i$ and $\hat{a}_i^\dagger$ are the annihilation and creation operators of the respective modes $i = \{1, 2, ...N\}$ satisfying the bosonic commutation relation

$$\left[\hat{a}_i, \hat{a}_j^\dagger \right] = \delta_{ij} \qquad \left[\hat{a}_i, \hat{a}_j \right] = \left[\hat{a}_i^\dagger, \hat{a}_j^\dagger \right] = 0 \tag{1.2}$$

The corresponding dimensionless amplitude- and phase-quadratures are given by

$$\hat{X}_i = \frac{\hat{a}_i + \hat{a}_i^\dagger}{\sqrt{2}} \qquad \hat{Y}_i = i\frac{\hat{a}_i^\dagger - \hat{a}_i}{\sqrt{2}} \tag{1.3}$$

with its commutation relation $\left[\hat{X}_i, \hat{Y}_j \right] = i\delta_{ij}$.
In general, to completely describe a CV-system implies working in an infinite dimensional Hilbert space. To avoid this on can use a mapping of the density-matrices onto the phase space. With this it is possible to reduce the space used to characterize the system to a $2N \times 2N$-real vector space where N is the number of (boson-like) modes. Furthermore, as it will be discussed below, it is possible to gain a full description of Gaussian states via the covariance

matrix.
To achieve this, all quadrature operators are collected in a $2N$-dimensional real vector $\hat{R}$ and its commutation relation into a matrix $\Omega \in \mathbb{C}^{2N\times 2N}$, the so called symplectic form, where

$$\begin{aligned} \hat{R} &= \left(\hat{X}_1, \hat{Y}_1, ..., \hat{X}_N, \hat{Y}_N\right)^T \\ \left[\hat{R}_i, \hat{R}_j\right] = i\Omega_{ij} \qquad \Omega &= \oplus_{l=1}^{N} \Omega_l \\ \Omega_l &= \begin{pmatrix} 0 & 1 \\ -1 & 0 \end{pmatrix} \end{aligned} \tag{1.4}$$

Many physical processes, for example a beam splitter- or two mode squeezing-operation, can be described as a linear transformation which acts on the system $\hat{R}' = S\hat{R}$. Such transformations will leave the symplectic form Ω invariant. All transformation which satisfy this condition belong to the (real) symplectic group $Sp_{(2N,\mathbb{R})}$ on the $2N$-dimensional phase space ([AI07, see sec. 3.2]).

$$\hat{R}' = S\hat{R} \qquad S \in Sp_{(2N,\mathbb{R})} \Leftrightarrow S^T\Omega S = \Omega \tag{1.5}$$

In order to gain a description of a CV system with its density operator ρ, so called s-order characteristic functions χ_s and their quasi-probability distributions W_s, which are linked to the characteristic functions by Fourier-transform, are commonly used [AI07, BR97] where

$$\begin{aligned} \chi(\alpha)_s &= Tr(\rho\hat{D}_\alpha)e^{\frac{s||\alpha||^2}{2}} \\ W_s(\hat{R}) &= \frac{1}{\pi^2}\int_{\mathbb{R}^{2N}} d^{2N}\zeta e^{i\zeta^T\Omega\hat{R}}\chi_s(\zeta) \end{aligned} \tag{1.6}$$

Here, $\alpha \in \mathbb{R}^{2N}$, $||.||$ denotes the euclidean norm and $\hat{D}_\alpha$ is defined as the displacement operator acting on all modes, generating a coherent state, given as

$$\begin{aligned} |0\rangle &= \otimes_{i=1}^{N} |0\rangle_i \\ \hat{D}_\alpha = \exp(i\hat{R}^T\Omega\alpha) \qquad \hat{D}_\alpha |0\rangle &= |\alpha\rangle \end{aligned} \tag{1.7}$$

Especially worth mentioning are the quasi-probability distributions for $s = \{-1, 0, 1\}$ which corresponds to the Husimi "Q-function", the Wigner-function and the singular P-representation, respectively [AI07, see sec. 2.1].

In this work, the main focus lies on Gaussian states which can be effectively described using covariance matrices (from now on CM). A wide range of states falls into this definition, for example coherent states, two-mode squeezed states and thermal states as well as the vacuum state (see appendix A.1).

The definition of a Gaussian state is rather straight forward [WHTH07]:

$$\begin{gathered} \textit{A state } \rho \textit{ is Gaussian} \Leftrightarrow \chi(\alpha)_0 \textit{ is Gaussian} \Leftrightarrow W_0(\hat{R}) \textit{ is Gaussian} \\ \rho \text{ is Gaussian} \Leftrightarrow \chi_0(\alpha) = e^{\frac{1}{2}\alpha^T\sigma\alpha + id^T\alpha} \Leftrightarrow W_0(\hat{R}) = \frac{e^{-\frac{1}{2}(\hat{R}-d)^T\sigma^{-1}(\hat{R}-d)}}{\pi\sqrt{\det\sigma}} \end{gathered} \tag{1.8}$$

where $d = \langle\hat{R}\rangle_\rho$ is the mean displacement vector of the system and σ is the covariance matrix of the system given by:

$$\begin{aligned} d_i &= \langle\hat{R}_i\rangle_\rho = Tr(\rho\hat{R}_i) \\ \sigma_{ij} &= \frac{\langle\hat{R}_i\hat{R}_j\rangle_\rho + \langle\hat{R}_j\hat{R}_i\rangle_\rho}{2} - \langle\hat{R}_i\rangle_\rho \langle\hat{R}_j\rangle_\rho \end{aligned} \tag{1.9}$$

All information that is needed to characterize the system is therefore stored in the first and second moments of its quadratures. In addition to this, a Hamiltonian which is linear or bilinear in its modes, e.g. of the form

$$\hat{H} = \sum_i g_i\hat{a}_i + \sum_{k,l} g_{kl}\hat{a}_k\hat{a}_l + \sum_{m,n} g_{mn}\hat{a}_m^\dagger\hat{a}_n + \sum_{m,n} g_{mn}\hat{a}_m\hat{a}_n^\dagger + h.c. \tag{1.10}$$

with g_i and g_{mn} being the corresponding coefficients, preserves the Gaussian character of the state [Sch86].
It is now convenient to change into a displaced frame in order to set the mean vector of the quadratures to zero so that $d_i = \langle\hat{R}_i\rangle_\rho = 0$ which will from now on be always assumed. This can be achieved by applying a phase-space translation, which is a local operation. Since entanglement does not change under this kind of operation (see also sec. 1.1.3) the system correlations are completely described by its CM.

Not every real valued symmetric $2N \times 2N$ matrix describes a meaningful physical state, i.e. a state that lives in a Hilbert-space and needs to be normalizable. In addition to this there are some more constrains coming from the commutation relations via the Heisenberg uncertainty relation which states that the variances of the considered modes cannot be simultaneously arbitrarily small [Hol82].

$$\sigma + \frac{i\Omega}{2} \geq 0 \tag{1.11}$$

This inequality also affects the symplectic eigenvalues λ_i of the CM σ. Let us consider the symplectic transformation $S \in Sp_{(2N,\mathbb{R})}$ which diagonalizes the CM, this can be always as-

sumed through the Williams-theorem [J36]:

$$\begin{aligned} S^T \sigma S = \nu \Leftrightarrow \nu + \frac{i\Omega}{2} \geq 0 \\ \nu = \oplus_{i=1}^{N} \begin{pmatrix} \lambda_i & 0 \\ 0 & \lambda_i \end{pmatrix} \end{aligned} \tag{1.12}$$

In terms of the symplectic eigenvalues λ_i inequality 1.11 takes the form:

$$\begin{aligned} \det\left[\nu + \frac{i\Omega}{2}\right] \geq 0 \Leftrightarrow \prod_{i=1}^{N} \left(\lambda_i^2 - \frac{1}{4}\right) \geq 0 \\ \lambda_i \geq \frac{1}{2} \qquad \forall i = \{1, 2, ..., N\} \end{aligned} \tag{1.13}$$

Under any symplectic transformation of the group $Sp_{(2N,\mathbb{R})}$ the spectrum of the CM will not change which gives rise to invariants for example the determinant $\det(\sigma)$ and the seralian $\Delta(\sigma)$

$$\det(\sigma) = \prod_{i=1}^{N} \lambda_i^2 \qquad \Delta(\sigma) = \sum_{i=1}^{N} \lambda_i^2 \tag{1.14}$$

which will also play an important role in a later point of this work.
Because of the greater relevance for the following discussion of this work, vacuum and coherent states as well as two-mode squeezed and thermal states, including also the most important symplectic transformations, are presented in the Appendix A.1.

1.1.2 Definition of entanglement using covariance matrices

In order to execute some of the most famous quantum protocols, for example quantum super-dense-coding, quantum teleportation or quantum computation, the presence of non-classical correlations, entanglement, is needed. Therefore a proper definition and distinction between classical and non-classical correlation is indispensable, we consider two cases, pure and mixed states and restrict to the bipartite case:

A pure state $|\psi\rangle \in \mathcal{H} = \mathcal{H}_A \otimes \mathcal{H}_B$ of a bipartite system A and B is separable, and therefore not entangled, if and only if it can be decomposed into $|\psi\rangle = |\phi\rangle_A \otimes |\psi\rangle_B$.

By using the Schmidt decomposition of the same pure state $|\psi\rangle = \sum_{i=1}^{r} c_i |\phi_i\rangle_A \otimes |\psi_i\rangle_B$, the presence of entanglement in the system is given if the Schmidt rank $r > 1$ [Per95, see sec. 5]. Let us now consider mixed states which are commonly described by the density matrix $\rho = \sum_{i=1}^{n} p_i |\psi\rangle_i \langle\psi|_i$. This can be understood as a mixture of the state $|\psi\rangle_i$ with probability $p_i > 0$ under the condition that $\sum_i p_i = 1$.

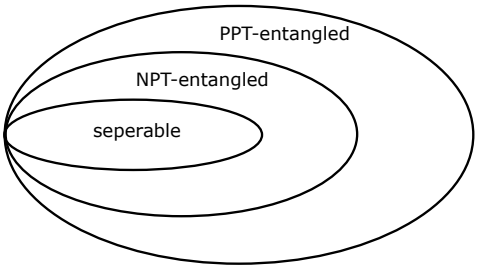

Figure 1.1: In this schematic draft different sets of quantum states are shown, the innermost set refers to all separable states, PPT-entangled states are entangled without violating the PPT-criterion while NPT-entagled states have a negative partial transpose.

A physical mixed state of a bipartite system A and B is described by a hermitian semi-definite trace-class density operator ρ with $Tr(\rho) = 1$. It is considered separable if and only if $\rho = \sum_{j=1}^{m} p_j \rho_j^A \otimes \rho_j^B$ with $p_J > 0$ and $\sum_j p_j = 1$.

In case of mixed states, the detection of entanglement is not as simple as for pure states since the decomposition for a mixed state is not unique. The question of entanglement in mixed states alone has established dedicated research areas within quantum physics. Fortunately, there are some criteria which help to detect entanglement, some even have a pendant for Gaussian states of CV systems.

The PPT-criterion is one of the most famous tools for the characterisation of separability since its computation is simple for pure and mixed states. Additionally this criterion detects many entangled states. It was stated by A. Peres and the Horodecki family [Per96, HHH96] that a state given by its density matrix ρ_s shows separability if its partial transpose over one of the subsystems A or B is also a physical density matrix and therefore is also represented by a hermitian semi-definite trace-one class operator

$$\begin{aligned} & & \rho_s \text{ is separable} \Rightarrow \rho_s^{T_i} \geq 0 \qquad i = A, B \\ \text{with} \qquad \rho_s = \sum_{ijkl} p_{kl}^{ij} \left|ik\right\rangle \left\langle jl\right| \qquad & \text{and where e.g.} \qquad \rho_s^{T_B} = \sum_{ijkl} p_{kl}^{ij} \left|il\right\rangle \left\langle jk\right| \end{aligned} \tag{1.15}$$

Only for the case of systems whose description is based on a 2×2 or 2×3 dimensional Hilbert space this is a necessary and sufficient condition. In general it is only a necessary criterion for separability, there even exist states which fulfil the PPT-criterion but are still entangled (see for example [BHN08]). Such "bound" entanglement, according to today's knowledge, cannot be distilled to pure entanglement by LOCC or used for quantum protocols as quantum teleportation. On the other side, if the partial transpose of one of the subsystems has negative eigenvalues, the system must be entangled (see also fig. 1.1).

The concept for bipartite entanglement detection of the PPT-criterion can also be brought to a handy form for Gaussian CV systems [Sim00] since it corresponds to a sign-flip of all phase-quadratures in one of the subsystems, for a separable state this sign-flip does not change the

physicality of the system. In terms of the CM σ of the system this means

$$\begin{aligned} P = \mathbb{1}_{N_A} \oplus_{i=1}^{N_B} \begin{pmatrix} 1 & 0 \\ 0 & -1 \end{pmatrix} \\ \tilde{\sigma} = P^T \sigma P \\ \sigma \text{ corresponds to a separable state} \Rightarrow \tilde{\sigma} + \frac{i\Omega}{2} \geq 0 \end{aligned} \tag{1.16}$$

Where N_A and N_B are the number of modes for the subsystem A or B respectively. This reflects the necessity for a separable state to have a positive partial transpose of the density matrix [AI07, see sec. 4.4.1]. Once again, the criterion is in general necessary but not sufficient, but for a Gaussian state where $N_A = 1$ and N_B is arbitrarily large it is also sufficient [Sim00].
The PPT-criterion can also be expressed in terms of the symplectic eigenvalues $\tilde{\lambda}_i$ of $\tilde{\sigma}$ since, for a physical CM of a Gaussian CV system, they have to satisfy 1.13 in order to be a separable state:

$$\sigma \text{ is a separable state} \Rightarrow \tilde{\lambda}_i \geq \frac{1}{2} \qquad \forall i = \{1, 2, ..., N\} \tag{1.17}$$

so whenever a symplectic eigenvalue of the "partial-transposed" CM is smaller than $\frac{1}{2}$ the corresponding state is entangled.

1.1.3 Entanglement measures and logarithmic negativity

In many cases, the need arises to not only detect entanglement in a bipartite Gaussian system, but also quantify how much entangled a state is or maybe which of two states is most entangled. Therefore, a measure for entanglement $E(\rho) : \rho \to E(\rho) \in \mathbb{R}_+$ has to show the characteristics [PV07] below:

1. ρ_s is separable $\Rightarrow E(\rho_s) = 0$
2. Local operations and classical communication (LOCC) will not increase the entanglement $\Leftrightarrow E(\hat{O}_{\text{LOCC}}\rho) \leq E(\rho)$
3. The entanglement is invariant under local unitary transformations $U = U_A \otimes U_B \Leftrightarrow E(U\rho) = E(\rho)$
4. The measure is continuous $\Leftrightarrow |\rho_1 - \rho_2| \to 0 \Rightarrow |E(\rho_1) - E(\rho_2)| \to 0$

Some other features as sub-additivity or convexity are also desired, but not required. A measure including those would be e.g. the entanglement of formation [PV07]. Unfortunately, most of the measures which fulfill 1-4 are not very user-friendly since their evaluation is difficult.

In this work, we will mainly refer to the logarithmic negativity which is, technically speaking, not a measure but an entanglement monotone since the fourth requirement is not fulfilled, but in terms of application it is the most easiest to use and is also well defined for CV systems. The negativity $\mathcal{N}(\rho)$ of a system directly quantifies how much the PPT-criterion is violated by the partial transpose of the system and is given by

$$\begin{aligned} \mathcal{N}(\rho) &= \frac{\|\rho^{T_i}\| - 1}{2} \\ \|\rho\| &= Tr\sqrt{\rho^\dagger \rho} \\ \mathcal{N}(\rho) &= \frac{\sum_i |\mu_i| - \mu_i}{2} \end{aligned} \tag{1.18}$$

Here μ_i are the eigenvalues of the corresponding partial transpose ρ^{T_i}. The logarithmic negativity $E_{\mathcal{N}}(\rho)$ is defined by

$$E_{\mathcal{N}}(\rho) = \log(\|\rho^{T_i}\|) = \log(1 + 2\mathcal{N}(\rho^{T_i})) \tag{1.19}$$

For Gaussian $1 \times N$ states the negativities are a proper quantification of entanglement and are easy to compute in terms of the symplectic eigenvalues $\tilde{\lambda}_j$ of the partial transpose of the CM [AI07, see sec. 4.5.1] which is shown in more detail in appendix A.2.

1.1.4 Entanglement witnesses and the DGCZ-sum-criterion

Another, in terms of experimental implementation, practical application for detecting inseparability are the so called entanglement witnesses. Given a state ρ is entangled, then there exist a hermitian operator $\hat{\mathcal{W}}$ such that

$$\begin{aligned} \rho \text{ is entangled } &\Leftarrow Tr(\hat{\mathcal{W}}\rho) < 0 \\ \rho \text{ is separable } &\Rightarrow Tr(\hat{\mathcal{W}}\rho) \geq 0 \end{aligned} \tag{1.20}$$

These kind of witnesses form the class of linear-witnesses since the density operator ρ appears only linearly in its definition. The set of separable states is not a convex polytope and because of that a linear witness $\hat{\mathcal{W}}_{opt}$ can be optimized to cover a tangent of the hyperplane of the set of separable states, but it will never be able to fully detect them. To gain a more precise description of the set of separable states non-linear witness e.g. of the form $Tr(\rho^2\hat{\mathcal{W}})$ can be used (see figure 1.2).
In this work we want to discuss a specific criterion in more detail which was proposed by Duan et al. in 2000 [DGCZ00], the "Duan-Giedke-Cirac-Zoller-sum-criterion" ("DGCZ-sum-citerion"). In this work I will refer to this as Duan-criterion. It is formulated in terms of sec-

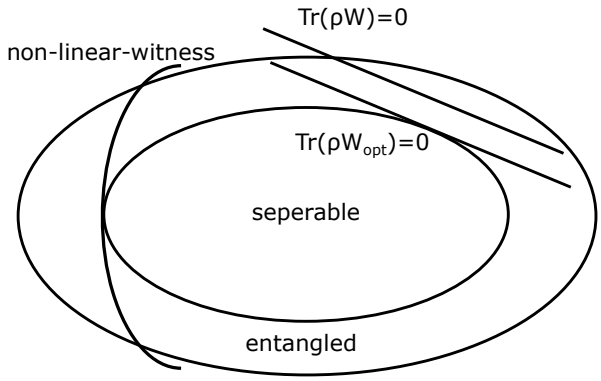

Figure 1.2: This sketch shows the geometric representation of two linear entnanglement witnesses of which one is optimized by $\hat{\mathcal{W}}_{opt}$, and a non-liear one.

ond moments and therefore very useful using CMs, for a bipartite two-mode system characterised by ρ with subsystems A and B and parameter $a \in \mathbb{R}$ it states

$$\begin{aligned} \hat{u} &= |a|\hat{X}_A + \frac{1}{a}\hat{X}_B \\ \hat{v} &= |a|\hat{Y}_A - \frac{1}{a}\hat{Y}_B \\ \rho \text{ is separable} \Rightarrow \langle(\Delta\hat{u})^2\rangle_\rho + \langle(\Delta\hat{v})^2\rangle_\rho &\geq a^2 + \frac{1}{a^2} \qquad \forall a \neq 0 \end{aligned} \tag{1.21}$$

Here we use the same definition and commutation relation for $\hat{X}_i$ and $\hat{Y}_i$ as in the former sections as well as the variances defined by $\langle(\Delta\hat{u})^2\rangle = Tr(\rho\hat{u}^2) - Tr(\rho\hat{u})^2$. Once again, if a state violates this inequality, it is entangled. From the definition of the operators $\hat{u}$ and $\hat{v}$ it follows that the Duan-criterion contains at most second moments of the two systems and can therefore be rewritten in form of CM entries by using the matrix $\hat{W}(a)$:

$$\begin{aligned} \hat{W}(a) &= \frac{1}{a^2 + \frac{1}{a^2}} \begin{pmatrix} a^2 & 0 & \frac{|a|}{a} & 0 \\ 0 & a^2 & 0 & -\frac{|a|}{a} \\ \frac{|a|}{a} & 0 & \frac{1}{a^2} & 0 \\ 0 & -\frac{|a|}{a} & 0 & \frac{1}{a^2} \end{pmatrix} \\ \rho \text{ is separable} &\Rightarrow Tr(\hat{W}(a)\sigma) \geq 1 \\ \rho \text{ is entangled} &\Leftarrow Tr(\hat{W}(a)\sigma) < 1 \end{aligned} \tag{1.22}$$

For Gaussian states it has been shown that by using the "standard form" of the CM this leads to a necessary and sufficient criterion of separability [DGCZ00, see Theorem 2] and therefore the entanglement witness can be optimized [HE06].

1.2 The mechanical system

The discussed tools in section 1.1.1 can now be directly used to characterise the coupled mechanical and optical systems which will be presented in the following. As it will be elaborated in the next sections of this work, special interest is paid to the non-classical correlations shared between both system, this can practically be achieved by the using covariance matrices.
The optomechanical system offers a wide range of possibilities for its experimental realisation [AKM14, see sec. IV], for this discussion a model of a Fabry-Pérot-cavity, where one of the mirrors is mounted on a spring as shown in figure 1.3, is used.

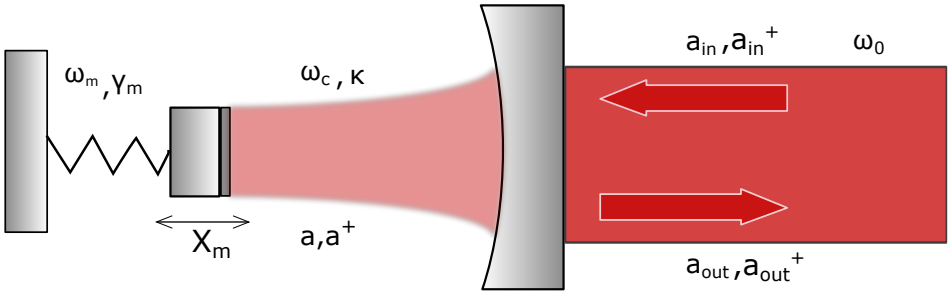

Figure 1.3: Schematic of an optomechanical cavity with its most important parameters and operators as mentioned in chapter 1. A mirror is mounted onto a spring resulting into the frequency ω_m and mechanical damping rate γ_m. The cavity of the system is formed by this movable mirror and a second one right in front of the oscillatably system yielding an intra-cavity field with the mode operators $\hat{a}/\hat{a}^\dagger$, frequency ω_c and its energy decay rate κ. The optomechanical system is driven by a laser with frequency ω_0, $\hat{a}_{out}/\hat{a}^\dagger_{out}$ and $\hat{a}_{in}/\hat{a}^\dagger_{in}$ represent the output- and input-field operators. The position of the movable mirror is given by the position-operator $\hat{X}_m$.

1.2.1 Classical mechanical oscillators

The problem of an oscillatory system in one dimension and its equation of motion is well known and studied in classical physics. A mass m attached to a spring with spring-constant k oscillates at a frequency $\omega_m = \sqrt{\frac{k}{m}}$. Neglecting all damping effects the canonical equations of motion of the systems quadratures x and p are given by:

$$\dot{p} = -m\omega_m^2 x \qquad \dot{x} = \frac{p}{m} \tag{1.23}$$

The energy of the mechanical oscillator is given by its Hamilton function $\mathcal{H}$

$$\mathcal{H} = \frac{p^2}{2m} + \frac{kx^2}{2} \tag{1.24}$$

Up to here it was always assumed that the oscillator is undamped, in order to describe

a more realistic situation, linear damping of the velocity ("viscous damping") in the system is now introduced. Therefore the equation of motion become for the position quadrature becomes

$$m\ddot{x}(t) + m\gamma_m\dot{x}(t) + m\omega_m^2 x(t) = F_{ext}(t) \tag{1.25}$$

here γ_m denotes the damping rate of the system and $F_{ext}(t)$ the sum of all external noise forces which are assumed to be stochastic. This kind of stochastic differential equation is also known as Langevin equation. It can be used e.g. to model the system dynamic when coupling to a thermal bath.
The solution of the equation of motion for this object is then found by applying the Fourier-transform and introducing the susceptibility $\chi(\omega)$

$$\begin{aligned} \tilde{x}(\omega) &= \chi(\omega)\tilde{F}_{ext}(\omega) \\ \chi(\omega) &= \frac{\omega_m}{m}\left[(\omega_m^2 - \omega^2) + i\gamma_m\omega\right]^{-1} \end{aligned} \tag{1.26}$$

By using $\chi(\omega)$ and the fluctuation-dissipation-theorem (FDT) it is now possible to calculate e.g. the noise-power-spectrum of the position in equilibrium with a thermal bath. For further purpose, the susceptibility is now used for characterising the stochastic force F (the index will from now on be dropped).
The noise-power-spectrum of the thermal force, when the oscillator is in contact with the bath at temperature T, will have the following form [Sau90]

$$S_{FF}(\omega) = \frac{4k_bT}{\hbar\omega}\mathrm{Im}(\chi(\omega)^{-1}) = \frac{4k_bT\gamma_m}{\hbar\omega_m} \tag{1.27}$$

which is connected to the auto-correlation function of the thermal force by the Wiener-Khinchin theorem

$$\langle F(t)F(t+\tau)\rangle = \frac{2k_bT\gamma_m}{\hbar\omega_m}\delta(\tau) \tag{1.28}$$

Here, $\langle . \rangle$ denotes the ensemble average and $\delta(\tau)$ is the Dirac delta function. In order to gain a quantum description for the thermal noise, this classical approach is used to introduce noise operators in the next section.

1.2.2 From classical to quantum

The transition between classical mechanics and quantum-mechanics is now made by replacing the initial quadratures x and p by their corresponding hermitian quantum operators $\hat{x}$ and $\hat{p}$ satisfying the well known commutation relation $[\hat{x}, \hat{p}] = i\hbar$. The Hamiltonian in 1.24

is also an operator valued object $\hat{H}$.

$$\hat{H} = \frac{\hat{p}^2}{2m} + \frac{k\hat{x}^2}{2} \tag{1.29}$$

For further use it is now convenient to introduce dimensionless quadrature operators $\hat{X}$ and $\hat{P}$ as well as the ladder operators already known from sec. 1.1.1 . The annihilation-operator $\hat{b}$ and the creation-operator $\hat{b}^\dagger$ are defined over $\hat{X}$ and $\hat{P}$ by:

$$\begin{aligned} \hat{b} = \frac{\hat{X} + i\hat{P}}{\sqrt{2}} \qquad \hat{b}^\dagger = \frac{\hat{X} - i\hat{P}}{\sqrt{2}} \\ \left[\hat{b}, \hat{b}^\dagger\right] = 1 \\ \hat{X} = \hat{x}/x_{zp} \qquad \hat{P} = \hat{p}/p_{zp} \\ x_{zp} = \sqrt{\frac{\hbar}{\omega_m m}} \qquad p_{zp} = \sqrt{\hbar\omega_m m} \qquad \left[\hat{X}, \hat{P}\right] = i \end{aligned} \tag{1.30}$$

The last identity is a direct consequence of the former commutation relations of $\hat{x}$ and $\hat{p}$. With those operators, the Hamiltonian of the system can be rewritten as

$$\hat{H} = \frac{\hbar\omega_m}{2}\left(\hat{X}^2 + \hat{P}^2\right) = \hbar\omega_m\left(\hat{b}^\dagger\hat{b} + \frac{1}{2}\right) = \hbar\omega_m\left(\hat{n}_b + \frac{1}{2}\right) \tag{1.31}$$

Any eigenstate $|n\rangle$ of the hermitian number operator $\hat{n}_b$ will automatically also be an eigenstate of the systems Hamiltonian. Since $\hat{n}_b$ is a positive operator (see [Sch07]) we know that its eigenvalues obey $n \geq 0$ and from different commutation relations between $\hat{n}_b$,$\hat{b}$ and $\hat{b}^\dagger$ it follows that:

$$\begin{aligned} \hat{n}_b|n\rangle = n|n\rangle \qquad n \in \mathbb{N} \\ \hat{H}|n\rangle = E_n|n\rangle \qquad E_n = \hbar\omega_m\left(n + \frac{1}{2}\right) \\ \hat{b}|n\rangle = \sqrt{n}|n-1\rangle \qquad \hat{b}^\dagger|n\rangle = \sqrt{n+1}|n+1\rangle \\ \hat{b}|0\rangle = 0 \end{aligned} \tag{1.32}$$

The states $|n\rangle$ are called Fock states and form an orthonormal basis in Fock-space. It gives the number of excitations in the mode with frequency ω_m. As we can see, even for the vacuum state $|0\rangle$ the energy of the system is non-zero with a value of $\hbar\omega_m/2$ being the zero-point fluctuation of the position and momentum operator.

Consequently, substituting the thermal force by an operator valued object $F \to \sqrt{2\gamma_m}\hat{f}$ yields

the quantum Langevin equations (QLE):

$$\dot{\hat{X}} = \omega_m \hat{P} \qquad \dot{\hat{P}} = -\omega_m \hat{X} - \gamma_m \hat{P} + \sqrt{2\gamma_m}\hat{f} \tag{1.33}$$

The correlation function of the hermitian noise operator $\hat{f}$ is now given by [Hof15]

$$\begin{aligned} &\langle \hat{f}(t)\hat{f}(t+\tau) + \hat{f}(t+\tau)\hat{f}(t)\rangle_\rho = \\ &\frac{1}{\omega_m}\int_0^\infty \frac{d\omega}{\pi}\omega \coth(\frac{\hbar\omega}{2k_B T})\cos(\omega\tau)) \overset{k_b T \gg \hbar\omega_m}{\simeq} (2\bar{n}+1)\delta(\tau) \end{aligned} \tag{1.34}$$

Here $\bar{n}$ represents the mean excitation number of the thermal bath at temperature T and at frequency ω_m. As we can see, the noise in general is not delta-correlated, but for high temperatures such that $k_b T \gg \hbar\omega_m$ and large quality factors $Q = \frac{\omega_m}{\gamma_m}$ the approximation made in 1.34 will hold.

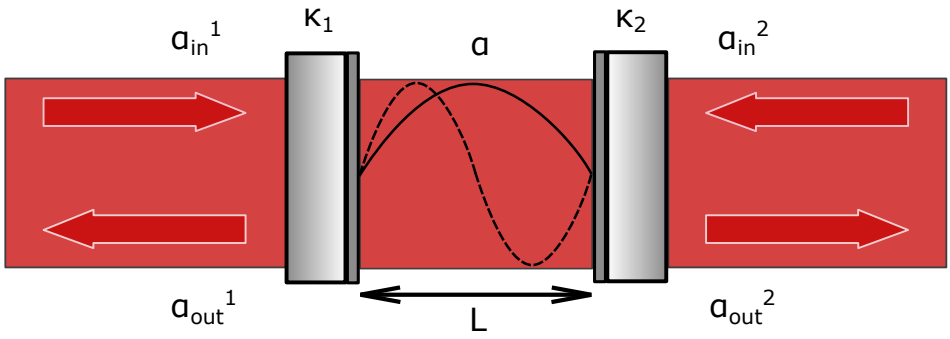

Figure 1.4: Fabry-Pérot cavity formed by two highly reflective mirrors separated by a distance L. Because of this boundary condition the standing wave between the mirrors only allows to have specific frequencies ω_n (represented by the first two modes). The field inside the cavity is described by the complex field amplitude α, each mirror has his own energy decay rate κ_i as well as an input and output-field characterized by the amplitudes $\alpha^i_{in/out}$ where $i = 1, 2$ for the input and output mirror.

1.3 The optical system

Just like in the case of the mechanical oscillators there are various realisations of the optical systems. All of them can be effectively described by one structure, the Fabry-Pérot-cavity, which will also serve as our toy-model to introduce the important concepts and tools we will use in a later part of this work.

1.3.1 Classical description of optical cavities

A Fabry-Pérot-cavity consists in its simplest version of two highly reflective mirrors which are placed parallel to each other by a distance L (see figure 1.4).
Because of this boundary condition the standing wave of the light field inside the cavity has specific frequencies ω_n (represented by the first two modes in fig. 1.4). The field inside the cavity is described by the complex field amplitude α, each mirror has its own energy decay rate κ_i as well as an input and output-field characterized by the complex amplitudes $\alpha^{(i)}_{in/out}$ where $i = 1, 2$ stands for the input and output mirror respectively. Inside the cavity, due to the properties of a standing wave, only frequencies with a specific wavelength λ_n are allowed. Those are linked to the frequency and the length of the cavity by:

$$\begin{aligned} \lambda_n &= 2nL \qquad n \in \mathbb{N} \\ \omega_n &= \frac{2c\pi}{\lambda_n} = \frac{c\pi}{nL} \\ \Delta\omega &= \frac{c\pi}{L} \end{aligned} \tag{1.35}$$

where c is the velocity of light. Two modes ω_n and ω_{n+1} with arbitrary $n \geq 1$ are therefore separated by the free-spectral range $\Delta\omega$. For the further discussion we will restrict the description to the fundamental mode $\omega_1 = \omega_c$ of the cavity. It is now convenient to define the finesse $\mathcal{F}$ of the cavity by [AKM14]:

$$\mathcal{F} = \frac{\Delta\omega}{\kappa} \tag{1.36}$$

Here κ is the decay rate of the photon intensity during a specific time interval. For high Q-factors we can express the decay rate κ as the sum of many loss channels, for example as

$$\kappa = \kappa_1 + \kappa_2 + \tilde{\kappa} \tag{1.37}$$

where κ_1 specifies the losses at the input-mirror while κ_2 stands for the very same losses at the output-mirror. $\tilde{\kappa}$ covers all other mechanism which arise in the cavity e.g. scattering and absorption losses.

The different field amplitudes in and outside the cavity, which can be seen in figure 1.4, will be now introduced. For both mirrors, denoted by the superscripts 1 (input-mirror) and 2 (output-mirror), we have an input and output field. We are mostly interested in the fields described by $\alpha_{in}^{(1)}$ and $\alpha_{out}^{(1)}$ since they can easily be accessed through the experiment. Moreover, since we want to deal with an over-coupled cavity, it will be assumed $\kappa_1 \approx \kappa \gg \kappa_2, \tilde{\kappa}$ which allows one to neglect the fields given by $\alpha_{in}^{(2)}$ and $\alpha_{out}^{(2)}$.
Now consider the case of the intra-cavity field α driven by a laser with frequency ω_0 and complex field amplitude $\mathcal{E}$ so that $\alpha_{in}^{(1)}(t) = \mathcal{E}e^{-i\omega_0 t}$. The absolute value of the amplitude $|\mathcal{E}|^2$ can be understood as observed photons per time and is connected to the power P of the laser by $\mathcal{E} = \sqrt{\frac{P}{\hbar\omega_0}}$.
The time evolution of the intra-cavity field amplitude $\alpha(t)$ is described by

$$\dot{\alpha}(t) = -\left(i\omega_c + \frac{\kappa}{2}\right)\alpha(t) + \sqrt{\kappa_1}\mathcal{E}(t)e^{-i\omega_0 t} \tag{1.38}$$

We now rotate to a frame of the laser frequency by substituting $\alpha(t) \to \alpha(t)e^{-i\omega_0 t}$. This leads to the equations of motion given by:

$$\dot{\alpha}(t) = -\left(-i\Delta_0 + \frac{\kappa}{2}\right)\alpha(t) + \sqrt{\kappa_1}\mathcal{E}(t) \tag{1.39}$$

Here we have introduced the laser detuning $\Delta_0 = \omega_0 - \omega_c$. Analogous to the case of a mechanical oscillator, we can also define the optical susceptibility by taking the Fourier transform of the upper relation and rearranging the respective terms:

$$\chi(\omega) = \frac{\tilde{\alpha}(\omega)}{\sqrt{\kappa_1}\tilde{\mathcal{E}}(\omega)} = \left(\frac{\kappa}{2} + i(\omega - \Delta_0)\right)^{-1} \tag{1.40}$$

Under the condition that the amplitude of the laser drive is constant in time $\mathcal{E}(t) = \mathcal{E}$, the intra-cavity field amplitude will arrive at a steady state so that $\dot{\alpha} = 0$ [AKM14, see sec. II.A.2], for this case the steady-state amplitude of the intra-cavity field is given by

$$\begin{aligned} \dot{\alpha} = 0 = -\left(-i\Delta_0 + \frac{\kappa}{2}\right)\alpha(t) + \sqrt{\kappa_1}\mathcal{E} \\ \alpha = \frac{\sqrt{\kappa_1}\mathcal{E}}{\frac{\kappa}{2} - i\Delta_0} \end{aligned} \tag{1.41}$$

In this situation, the average energy $\bar{E}$ inside the cavity is then given by the product of $\hbar\omega_c$ and the average photon number $\bar{n} = |\alpha|^2$:

$$\bar{E} = \hbar\omega_c\bar{n} = P\frac{\omega_c}{\omega_0}\frac{\kappa_1}{\Delta_0^2 + \frac{\kappa^2}{4}} \tag{1.42}$$

1.3.2 Quantum description of the optical system

Analogous to the mechanical system, we can describe the electromagnetic field inside the cavity by substituting the field amplitudes by operators, more precisely the intra-cavity field is substituted by $\alpha \to \hat{a}$ and the external fields by $\alpha^{(i)}_{in/out} \to \hat{a}^{(i)}_{in/out}$ where we have assumed the phases of the operators to be zero. However, as the external fields at the output mirror are not of much interest to us, especially as they would be more difficult to access experimentally, their contribution to the dynamics of the system will be neglected from now on.
These operators corresponds to that in the mechanical pendant having annihilation- and creation-operators $\hat{a}$ and $\hat{a}^\dagger$ whose action on a Fock-state is given by the very same relation as in eq. 1.32, they will create or annihilate a photon of frequency ω_c. The classical relations of the previous section are obtained by taking the expectation value $\langle\hat{O}\rangle = Tr(\rho\hat{O})$ of the corresponding operators and time derivatives.
The Hamiltonian $\hat{H}$ of the optical system has a similar form to the mechanical Hamiltonian, using the number operator $\hat{n}_a$ it is given by:

$$\begin{aligned} \hat{H} = \hbar\omega_c\left(\hat{a}^\dagger\hat{a} + \frac{1}{2}\right) = \hbar\omega_c\left(\hat{n}_a + \frac{1}{2}\right) \\ \left[\hat{a}, \hat{a}^\dagger\right] = 1 \end{aligned} \tag{1.43}$$

This is completely analogous to the relations introduced for the mechanical system in 1.31. For later use the amplitude- and phase-quadrature operators $\hat{X}$ and $\hat{Y}$, which automatically satisfy the commutation relation $\left[\hat{X}, \hat{Y}\right] = i$, are defined by :

$$\hat{X} = \frac{(\hat{a}^\dagger + \hat{a})}{\sqrt{2}} \qquad \hat{Y} = \frac{i(\hat{a}^\dagger - \hat{a})}{\sqrt{2}} \tag{1.44}$$

We can also formulate QLE in the optical system complementary to 1.38 [GC85] for the ladder-operators:

$$\begin{gathered}\dot{\hat{a}}(t) = -\left(i\omega_c + \frac{\kappa_1}{2}\right)\hat{a}(t) + \sqrt{\kappa_1}\hat{a}^1_{in}(t) \\ \left[\hat{a}_{in}(t), \hat{a}^\dagger_{in}(t+\tau)\right] = \delta(\tau) \qquad \left[\hat{a}^\dagger_{in}(t), \hat{a}_{in}(t+\tau)\right] = 0\end{gathered} \tag{1.45}$$

Here, $\hat{a}^1_{in}(t)$ is the input-field which in this work will be assumed to be in a coherent state to take into account the driving laser. This means that the mean value of $\hat{a}^1_{in}(t)$ is not equal to zero. By introducing a driving Hamiltonian (as done in eq. 1.50) it can be readjusted to $\langle \hat{a}^1_{in}(t) \rangle_\rho = 0$. In terms of the amplitude- and phase-quadrature, the corresponding QLE have the form

$$\begin{aligned}\dot{\hat{X}}(t) &= -\frac{\kappa_1}{2}\hat{X}(t) + \omega_c \hat{P}(t) + \sqrt{\kappa_1}\hat{X}^1_{in}(t) \\ \dot{\hat{P}}(t) &= -\frac{\kappa_1}{2}\hat{P}(t) - \omega_c \hat{X}(t) + \sqrt{\kappa_1}\hat{P}^1_{in}(t)\end{aligned} \tag{1.46}$$

where we have defined the input-quadratures $X^1_{in}(t)$ and $P^1_{in}(t)$ in accordance with relation 1.44. Comparing these optical QLE with the mechanical QLE in 1.33, we see that both optical quadratures show a constant decay rate of $\kappa_1/2$.
Since we are mainly interested in the experimentally accessible input- and output-mode at the first mirror, a formulation for the output-field is needed. Fortunately, there exists such a relation coming from time-reversing the QLE of the system [GC85, see sec. B]

$$\hat{a}^1_{out}(t) = \sqrt{\kappa_1}\hat{a}(t) - \hat{a}^1_{in}(t) \tag{1.47}$$

These input-output relation can also be formulated for the previously introduced channels at the second mirror $\hat{a}^2_{in/out}$.

$$\hat{a}^2_{out}(t) = \sqrt{\kappa_2}\hat{a}(t) - \hat{a}^2_{in}(t) \tag{1.48}$$

1.4 Optomechanical coupling and interaction

We now consider an optomechanical cavity where one of the mirrors of a Fabry-Pérot-cavity is mounted to a spring (see figure 1.3). As it will be shown in this section, the radiation pressure force acting on the movable mirror causes an interaction between the optical and mechanical system. This results in many interesting effects for example cooling of the mechanical motion down to its ground state, entanglement creation and state-swap between the two subsystems. This will all be described by a linearised Hamiltonian, yielding QLE which are to be solved in the next chapter 2.

1.4.1 Basics of the optomechanical interaction

In order to study the rudimentary process behind the optomechanical interaction we start with the free evolution Hamiltonian of the mechanical oscillator and the Fabry-Pérot-cavity

$$\hat{H}_0 = \hbar\omega_c \hat{a}^\dagger \hat{a} + \hbar\omega_m \hat{b}^\dagger \hat{b} \tag{1.49}$$

The vacuum contribution to the systems Hamiltonian is neglected since it will not affect the dynamics, especially the QLE. To model a constant laser drive with laser-frequency ω_0 we will add to the original Hamiltonian $\hat{H}_0$ a driving Hamiltonian $\hat{H}_{drive}$ with the, in general, time-dependent driving-strength $\mathcal{E}(t)$

$$\hat{H}_{drive} = i\hbar \left(\mathcal{E}(t)\hat{a}^\dagger e^{-i\omega_0 t} - \mathcal{E}^*(t)\hat{a} e^{i\omega_0 t} \right) \tag{1.50}$$

In the model of a Fabry-Pérot-cavity as given in fig. 1.3, the frequency of the cavity is not a constant since the length of the cavity depends on the displacement of the mirror by $L(x_m) = L - x_m$ (here x_m carries the dimension as discussed in sec. 1.2). For positive values of x_m, assuming that no displacement means $x_m = 0$, the cavity length decreases, the frequency ω_c becomes bigger, therefore the energy stored inside the cavity also increases. This energy-loss can be intuitively understood as the momentum- and energy-transfer between the mechanical oscillator and the optical field, the same holds the other way around for negative values of x_m.
The frequency, dependent on the mirrors displacement, is then given by

$$\begin{aligned} \omega_c(x_m) &= \frac{\pi c}{L(x_m)} = \frac{\pi c}{L - x_m} \\ \omega_c(x_m) &\approx \omega_c(0) + \left.\frac{\partial \omega_c(x_m)}{\partial x_m}\right|_{x_m=0} x_m + \mathcal{O}(x_m)^2 \\ \omega_c(x_m) &\approx \omega_c + \frac{\omega_c}{L} x_m + \mathcal{O}(x_m)^2 \end{aligned} \tag{1.51}$$

The approximation made here is very precise for small displacements as they are typically obtained experimentally. Neglecting terms of quadratic or higher order in the displacements and substituting the position operator $x_m \to \hat{x}_m$, original Hamiltonian takes the form:

$$\hat{H}_0 = \hbar\omega_c(\hat{x}_m)\hat{a}^\dagger\hat{a} + \hbar\omega_m\hat{b}^\dagger\hat{b} = \hbar\omega_c\hat{a}^\dagger\hat{a} + \hbar\omega_m\hat{b}^\dagger\hat{b} + \hbar\frac{\omega_c}{L}\hat{x}_m\hat{a}^\dagger\hat{a} \tag{1.52}$$

Together with the driving-Hamiltonian and the dimensionless position-operator of the mechanical system $\hat{X}_m$ the systems Hamiltonian is given by:

$$\begin{aligned}\hat{H} = \hat{H}_0 + \hat{H}_{drive} = \hbar\omega_c\hat{a}^\dagger\hat{a} + \hbar\omega_m\hat{b}^\dagger\hat{b} + \hbar g_0\hat{X}_m\hat{a}^\dagger\hat{a} \\ +i\hbar\left(\mathcal{E}(t)\hat{a}^\dagger e^{-i\omega_0 t} - \mathcal{E}^*(t)\hat{a}e^{i\omega_0 t}\right) \\ g_0 = \frac{\omega_c x_{zp}}{L}\end{aligned} \tag{1.53}$$

Here g_0 is the bare photon coupling and it describes the interaction between one cavity photon and a quantized excitation, a phonon, of the mechanical oscillator. For further use it is convenient to change into a rotating frame with the laser frequency ω_0 in order to drop the time dependence of the drive-Hamiltonian. We therefore have the Hamiltonian

$$\hat{H} = -\hbar\Delta_0\hat{a}^\dagger\hat{a} + \hbar\omega_m\hat{b}^\dagger\hat{b} + \hbar g_0\hat{X}_m\hat{a}^\dagger\hat{a} + i\hbar\left(\mathcal{E}(t)\hat{a}^\dagger - \mathcal{E}^*(t)\hat{a}\right) \tag{1.54}$$

Here we use the laser detuning $\Delta_0 = \omega_0 - \omega_c$. As it can be seen, this Hamiltonian consists of linear and non-linear terms since it also involves the interaction $\propto \hat{X}_m\hat{a}^\dagger\hat{a} = \hat{a}^\dagger\hat{a}(\hat{b}^\dagger + \hat{b})/\sqrt{2}$ with three mode operators.
With the Hamiltonian from eq. 1.54 and the relations presented in the previous section, the following QLE can be derived [GC85]

$$\begin{aligned}\dot{\hat{X}}_m &= \omega_m\hat{P}_m \\ \dot{\hat{P}}_m &= -\omega_m\hat{X}_m - \gamma_m\hat{P}_m - g_0\hat{a}^\dagger\hat{a} + \sqrt{2\gamma_m}\hat{f} \\ \dot{\hat{a}} &= (i\Delta_0 - \frac{\kappa}{2})\hat{a} - ig_0\hat{X}_m\hat{a} + \mathcal{E}(t) + \sqrt{\kappa}\hat{a}_{in}\end{aligned} \tag{1.55}$$

1.4.2 Linearising the systems QLE and Hamiltonian

The coupling between mechanics and optics characterized by the bare photon-coupling g_0 can be rather small and will not cause any observable effects. However it is possible to effectively increase the coupling between the two subsystems with the help of the driving laser. This increases the number of photons travelling inside the cavity which, as it will be shown, introduces a stronger coupling and allows to linearise the QLE. Using this method, it will be possible to neglect non-linear terms which scale with the bare photon coupling, in this ap-

proximation it is possible to extract a Hamiltonian which shows two-mode-squeezing (TMS) and also beam-splitting (BS) interaction.

Let us consider the cavity field-amplitude as the sum of an average field amplitude $\langle \hat{a} \rangle = \alpha$ and some zero-mean field-fluctuation $\delta\hat{a}$ which are small compared to α. We also apply this transformation to the mechanical latter-operators

$$\begin{aligned} \hat{a} &= \alpha + \delta\hat{a} \qquad & \langle \delta\hat{a} \rangle &= 0 \\ \hat{b} &= \beta + \delta\hat{b} \qquad & \langle \delta\hat{b} \rangle &= 0 \end{aligned} \tag{1.56}$$

The QLE for the fluctuations of $\hat{a}$ and $\hat{b}$ can be found by formally changing into a displaced frame using the unitary operator $\hat{U}(\alpha, \beta) = \hat{D}_\alpha \hat{D}_\beta$:

$$\begin{aligned} \hat{D}_\alpha \hat{D}_\beta \hat{a} \hat{D}_\alpha^\dagger \hat{D}_\beta^\dagger &= \hat{a} - \alpha = \delta\hat{a} \Leftrightarrow \delta\dot{\hat{a}} = \dot{\hat{a}} - \dot{\alpha} \\ \hat{D}_\alpha \hat{D}_\beta \hat{b} \hat{D}_\alpha^\dagger \hat{D}_\beta^\dagger &= \hat{b} - \beta = \delta\hat{b} \Leftrightarrow \delta\dot{\hat{b}} = \dot{\hat{b}} - \dot{\beta} \end{aligned} \tag{1.57}$$

In this new frame, the QLE of the fluctuations are given by

$$\begin{aligned} \delta\dot{\hat{a}} = &\left(i\Delta_0 - \frac{\kappa}{2} - i\frac{g_0}{\sqrt{2}}(\delta\hat{b}^\dagger + \delta\hat{b}) \right) \delta\hat{a} - i\frac{g_0}{\sqrt{2}}(\beta + \beta^*)\delta\hat{a} - i\frac{g_0}{\sqrt{2}}(\delta\hat{b}^\dagger + \delta\hat{b})\alpha \\ &+ \left(i\Delta_0 - \frac{\kappa}{2} - i\frac{g_0}{\sqrt{2}}(\beta + \beta^*) \right) \alpha + \mathcal{E}(t) - \dot{\alpha} + \sqrt{\kappa}\hat{a}_{in} \\ \delta\dot{\hat{b}} = &-i\omega_m \delta\hat{b} + \frac{\gamma_m}{2}(\delta\hat{b}^\dagger - \delta\hat{b}) - i\frac{g_0}{\sqrt{2}}\delta\hat{a}^\dagger\delta\hat{a} - i\frac{g_0}{\sqrt{2}}(\alpha\delta\hat{a}^\dagger + \alpha^*\delta\hat{a}) + i\sqrt{\gamma_m}\hat{f} \\ &-i\omega_m\beta - i\frac{g_0}{\sqrt{2}}|\alpha|^2 + \frac{\gamma_m}{2}(\beta^* - \beta) - \dot{\beta} \end{aligned} \tag{1.58}$$

The time-evolution of the fluctuation operators $\delta\hat{a}$ and $\delta\hat{b}$ is described by the sum of terms including the very same fluctuation operators as well as average field amplitudes α and β. Considering only these average field amplitudes and their time evolution from above, they can be demanded to fulfil the following differential equations:

$$\begin{aligned} \dot{\alpha} &= \left(i\Delta_0 - \frac{\kappa}{2} - i\frac{g_0}{\sqrt{2}}(\beta + \beta^*) \right) \alpha + \mathcal{E}(t) \\ \dot{\beta} &= -i\omega_m\beta - i\frac{g_0}{\sqrt{2}}|\alpha|^2 \end{aligned} \tag{1.59}$$

These equations correspond to the classical evolution of the amplitudes found by averaging over the non-linearised QLE in eq. 1.55. In the case of constant driving strength $\mathcal{E}(t) = \mathcal{E}$ and only looking at the steady-state, the field-amplitudes will not change any more in time

and therefore reach the following values:

$$\begin{aligned} \alpha &= \frac{\mathcal{E}}{i\Delta_0 - \frac{\kappa}{2} - i\frac{g_0}{\sqrt{2}}(\beta + \beta^*)} \\ \beta &= -\frac{g_0|\alpha|^2}{\sqrt{2}\omega_m} \end{aligned} \tag{1.60}$$

Please note that for the steady state the momentum-average will disappear since $(\beta^* - \beta) = 0$, but the position of the oscillator will be displaced to a new equilibrium-position. It depends strongly on the intra-cavity field amplitude α which can be enhanced by choosing a sufficiently big drive strength.
Assuming that the average field amplitudes satisfy 1.59, the QLE for the fluctuations (to simplify our notation I will drop the δ for all operators), keeping in mind that quantum fluctuations of the respective fields are considered here, can be rewritten in the form:

$$\begin{aligned} \dot{\hat{a}} &= \left(i\Delta - \frac{\kappa}{2}\right)\hat{a} - i\frac{g_0}{\sqrt{2}}(\hat{b}^\dagger + \hat{b})\hat{a} - i\frac{g_0\alpha}{\sqrt{2}}(\hat{b}^\dagger + \hat{b}) + \sqrt{\kappa}\hat{a}_{in} \\ \dot{\hat{b}} &= -i\omega_m\hat{b} + \frac{\gamma_m}{2}(\hat{b}^\dagger - \hat{b}) - i\frac{g_0}{\sqrt{2}}\hat{a}^\dagger\hat{a} - i\frac{g_0}{\sqrt{2}}(\alpha\hat{a}^\dagger + \alpha^*\hat{a}) + i\sqrt{\gamma_m}\hat{f} \\ \Delta &= \left(\Delta_0 - \frac{g_0}{\sqrt{2}}(\beta + \beta^*)\right) \end{aligned} \tag{1.61}$$

Here we introduced a new detuning Δ and neglect second-order fluctuation terms e.g. $\hat{b}\hat{a}$,$\hat{b}^\dagger\hat{a}$ or $\hat{a}^\dagger\hat{a}$ since they all scale with bare-photon coupling g_0. The bare photon coupling is rather small compared to $g_0\alpha$, but all linear terms now have coefficients which scale with the term $g_0\alpha$. The coupling can now be enhanced by choosing the absolute value of the drive-strength $\mathcal{E}$ sufficiently big so that $|\alpha|^2 \gg 1$. We can also choose the phase of $\mathcal{E}$ such that $\alpha \in \mathbb{R}$ (which will be assumed from now on).
Using that $\hat{X}_{in} = (\hat{a}_{in}^\dagger + \hat{a}_{in})/\sqrt{2}$ as well as $\hat{P}_{in} = i(\hat{a}_{in}^\dagger - \hat{a}_{in})/\sqrt{2}$, for the systems quadratures the final linearised QLE arise:

$$\begin{aligned} \dot{\hat{X}}_m &= \omega_m\hat{P}_m \\ \dot{\hat{P}}_m &= -\omega_m\hat{X}_m - \gamma_m\hat{P}_m - \sqrt{2}g_0\alpha\hat{X}_c + \sqrt{2\gamma_m}\hat{f} \\ \dot{\hat{X}}_c &= -\frac{\kappa}{2}\hat{X}_c - \Delta\hat{P}_c + \sqrt{\kappa}\hat{X}_{in} \\ \dot{\hat{P}}_c &= -\frac{\kappa}{2}\hat{P}_c + \Delta\hat{X}_c - \sqrt{2}g_0\alpha\hat{X}_m + \sqrt{\kappa}\hat{P}_{in} \end{aligned} \tag{1.62}$$

With the upper approximations it is possible to formulate a new linearised Hamiltonian $\hat{H}_{lin}$

which reproduces the newly found QLE of the field fluctuations.

$$\begin{aligned} \hat{H}_{lin} = -\hbar\Delta\hat{a}^\dagger\hat{a} + \hbar\omega_m\hat{b}^\dagger\hat{b} + \hbar g(\hat{b}^\dagger + \hat{b})(\hat{a}^\dagger + \hat{a}) \\ g = \frac{g_0\alpha}{\sqrt{2}} \end{aligned} \tag{1.63}$$

Here g is the optomechanical coupling-strength which emerges from the bare-photon coupling by a multiplication of the average field amplitude $\alpha/\sqrt{2}$. By choosing a sufficiently high driving-strength therefore increases the coupling between the mechanical and optical subsystems fluctuations.

Expanding the last term of this Hamiltonian, we find two interactions which can be enhanced by the right choice of the detuning Δ (see fig. 1.5). Let us first consider all terms which preserve the absolute number of photons and phonons in the system

$$\hbar g(\hat{a}^\dagger\hat{b} + \hat{a}\hat{b}^\dagger) \tag{1.64}$$

We will refer to this part of the Hamiltonian as beam-splitter-interaction (BS). For every photon annihilated there is a phonon created and vice-versa so that the absolute number of quanta is conserved trough this process. This interaction can be used as a state-swap-operation from the mechanics onto the optical mode and the other way around or, in the case of $\omega_m \gg \kappa$, for ground-state cooling of the mechanical motion [Hof15, see sec. 1.4].
On the other hand, we have an interaction-term which creates both mechanical and optical excitation at the same time and therefore might create entanglement between the mechanical and optical modes. We will refer to this as two-mode-squeezing-interaction (TMS)

$$\hbar g(\hat{a}^\dagger\hat{b}^\dagger + \hat{a}\hat{b}) \tag{1.65}$$

If we look at the Hamiltonian in the interaction picture by applying the unitary $\hat{U}(t) = \exp(-i\Delta\hat{a}^\dagger\hat{a}t + i\omega_m\hat{b}^\dagger\hat{b}t)$ we find that

$$\begin{aligned} \hat{H}^I = \hat{U}(t)\hat{H}_{lin}\hat{U}(t)^\dagger = -\hbar\Delta\hat{a}^\dagger\hat{a} + \hbar\omega_m\hat{b}^\dagger\hat{b} + \\ \hbar g(\hat{a}\hat{b}^\dagger e^{i(\Delta+\omega_m)t} + \hat{a}^\dagger\hat{b}e^{-i(\Delta+\omega_m)t}) + \hbar g(\hat{a}^\dagger\hat{b}^\dagger e^{-i(\Delta-\omega_m)t} + \hat{a}\hat{b}e^{i(\Delta-\omega_m)t}) \end{aligned} \tag{1.66}$$

If we set the detuning to $\Delta = \omega_m$, the BS interaction shows a rotation frequency which is proportional to $2\omega_m$ while the TMS part will not oscillate at all. Now taking the rotating-wave-approximation (RWA), the fast oscillating BS-terms can be neglected and the TMS-interaction becomes the leading effect in the Hamiltonian. We will call this the "blue-detuned"-regime since $\Delta > 0$.
On the other side, if we have $\Delta = -\omega_m$ and therefore work in the "red-detuned"-regime,

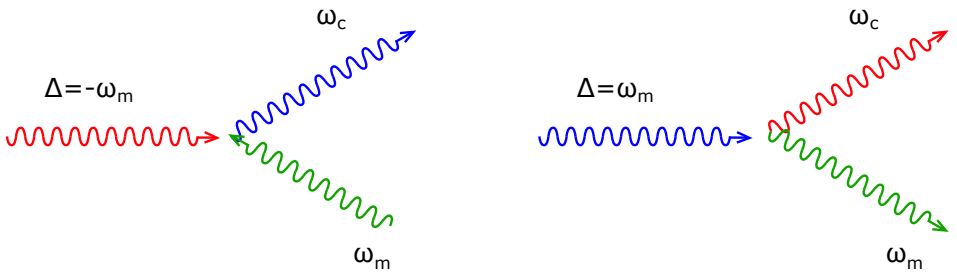

Figure 1.5: Another way of understanding the TMS- and BS-interaction is by a three-mode scattering scheme. For a red-detuned laser drive $\Delta = -\omega_m$ (left-hand side represented by the red arrow), a phonon of frequency ω_m in the mechanical system is annihilated and a photon with energy $\hbar\omega_c$ is created in the optical field. On the other hand, if the cavity is driven by a blue-detuned laser $\Delta = \omega_m$ (right-hand side represented by the blue arrow), the lasers energy is used for creating a phonon with energy $\hbar\omega_m$ and a photon in the cavity field while the laser photon is annihilated in this process.

only the BS interactions survive the RWA while the TMS terms, which are now oscillating with frequency $\propto -2\omega_m$, will "average out". In this situation it is possible to use the effect of the state-swap as well as the finite decay-width of the cavity for cooling the mechanical system down to its ground state. A more detailed discussion is given in A.4.

A collection of the most important relations, including the QLE and correlations of different operators used throughout this chapter, are summarized in appendix A.3.

Chapter 2

Solving the QLE

In this chapter I will discuss some possibilities of solving the QLE we found in section 1.4.2 in eq. 1.62 for the intra-cavity light modes and the mechanical oscillator. This will also serve as a starting point to solve the QLE for the output light field and the mechanical system. This will finally lead to the systems covariance matrix which will allow us to discuss and detect entanglement shared between two temporal separated pulses in the output-light field and the oscillator as well as between the pulses themselves.

2.1 The intra-cavity field

2.1.1 Basic definitions and relations

In the previous chapter we found the final QLE given in eq. 1.62 which we will now restructure in order to gain a clearer insight.
First, we will collect all quadratures of the mechanical and the light modes in one vector $\mathbf{X}(t) = \left(\hat{X}_m(t), \hat{P}_m(t), \hat{X}_c(t), \hat{P}_c(t)\right)^T$ which will give us the following set of stochastic differential equations for the intra-cavity system

$$\dot{\mathbf{X}}(t) = A\mathbf{X}(t) + \mathbf{N}(t) \tag{2.1}$$

Here we define $\mathbf{N}(t) = \left(0, \sqrt{2\gamma_m}\hat{f}(t), \sqrt{\kappa}\hat{X}_{in}(t), \sqrt{\kappa}\hat{P}_{in}(t)\right)^T$ is the vector of all noise operators in the system and the matrix A is given by

$$A = \begin{pmatrix} 0 & \omega_m & 0 & 0 \\ -\omega_m & -\gamma_m & -2g & 0 \\ 0 & 0 & -\frac{\kappa}{2} & -\Delta \\ -2g & 0 & \Delta & -\frac{\kappa}{2} \end{pmatrix} \tag{2.2}$$

where we use the same definitions of the parameters as in the last chapters. This set of differential equations can generally be solved by the "variation of constants"-technique which will yield

$$\mathbf{X}(t) = e^{At}\mathbf{X}(0) + \int_0^t dt' e^{A(t-t')}\mathbf{N}(t') \tag{2.3}$$

As already discussed in sec. 1.1.1, the formalism behind covariance matrices allows to deal with these type of CV systems in a very practical manner. Therefore the time-evolution of the systems CM, which is of great interest for the further discussion, is given by:

$$\begin{aligned} \dot{\sigma}(t) &= A\sigma(t) + \sigma(t)A^T + D \\ \sigma(t) &= e^{At}\sigma(0)e^{A^T t} + \int_0^t dt' e^{A(t-t')} D e^{A^T(t-t')} \\ D &= \text{diag}\left(0, \gamma_m(2\bar{n}+1), \frac{\kappa}{2}, \frac{\kappa}{2}\right) \end{aligned} \tag{2.4}$$

The matrix D collects the correlations of the different noise channels as modelled in this work. Here, it was also assumed that the correlations of the thermal bath coupling to the mechanical oscillator shows the correlations discussed in eq. 1.34, which is a good approximation for $k_b T \gg \hbar\omega_m$ and large quality factors. The matrix D, as it is discussed in more detail in sec. B.2, is found by:

$$\frac{\langle N_i(t)N_j(t') + N_j(t')N_i(t)\rangle}{2} = D_{ij}\delta(t-t') \tag{2.5}$$

Since most of the different noise channels in $\mathbf{N}$ are uncorrelated the matrix D will have the diagonal form shown above.

In this work we will restrict the discussion onto the systems steady state. The steady-state is reached after a sufficiently long time and can safely be assumed if the real part of the eigenvalues of the matrix A are all negative, this condition is well characterised by the Routh-Hurwitz-stability-criterion [GR80]. The detailed definition of Routh-Hurwitz-criterion as well as the Hurwitz matrices are given in B.1, for further discussion only the results will be used in here.

In order to ensure the steady state of the system, the following two criteria must be fulfilled:

$$\begin{aligned} \gamma_m\kappa\left(\left[\frac{\kappa^2}{4} + (\omega_m+\Delta)^2\right]\left[\frac{\kappa^2}{4} + (\omega_m-\Delta)^2\right] + \gamma_m\left[(\gamma_m+\kappa)(\frac{\kappa^2}{4}+\Delta^2)\right] + \kappa\omega_m^2\right) \\ -4\Delta\omega_m g^2(\gamma_m+\kappa)^2 > 0 \\ \omega_m\left(\frac{\kappa^2}{4} + \Delta^2\right) + 4g^2\Delta > 0 \end{aligned} \tag{2.6}$$

For the case of a blue-detuning $\Delta > 0$ the second condition is automatically fulfilled while the first one needs to be checked, and vice-versa for a red-detuning $\Delta < 0$. In the parameter regime which is of interest in this work, blue-detuning of the driving-laser will introduce instability in the system while the red-detuned case gives a wide range of stability depending on the specific choice of all the systems parameters. Using a blue detuned drive laser enhances the TMS-interaction in the optomechanical system leading to generation of phonons in the oscillator and therefore heating up the mechanical system. But from now on it will always be assumed that both conditions are satisfied.

With the above assumptions, the system will reach its steady states for $t \to \infty$ and the time evolution from eq. 2.4 simplifies to

$$\sigma_{ss} = \sigma(\infty) = \int_0^\infty dt' e^{At'} D e^{A^T t'} \tag{2.7}$$

In terms of the differential equation for $\sigma(t)$ in eq. 2.4 , the time-derivative of the systems steady-state CM σ_{ss} will be zero, it follows that the CM can also be found by solving the following system of linear equations:

$$\begin{aligned} \dot{\sigma}_{ss} = 0 &= A\sigma_{ss} + \sigma_{ss}A^T + D \\ A\sigma_{ss} + \sigma_{ss}A^T &= -D \end{aligned} \tag{2.8}$$

These type of relation is called continuous "Lyapunov"-equation, a special case of the Sylvester equation, which will yield a unique and symmetric solution for σ_{ss}. For this special problem there already exist algorithms [BS72] to find its solution supported by many computing systems for example Mathematica or MATLAB.

2.1.2 Solutions in Fourier-space

After the above discussion of the different ways of solving the QLE in an exact or approximated way, we will now have a look onto another approach which will come handy for the out-put fields we will discuss in the next sections. The now presented tools are based on the work of Genes et al. [GMTV08].
Considering the set of differential equations as we formulated them in eq. 2.1, by applying the Fourier-transform $\mathcal{F}$ and using its properties for time-derivatives we have

$$\begin{aligned} \tilde{\mathbf{X}}(\omega) = \mathcal{F}[\mathbf{X}](\omega) &= \frac{1}{\sqrt{2\pi}} \int_{-\infty}^{\infty} dt e^{i\omega t} \mathbf{X}(t) \\ \mathcal{F}[\dot{\mathbf{X}}](\omega) = -i\omega\tilde{\mathbf{X}}(\omega) &= A\tilde{\mathbf{X}}(\omega) + \tilde{\mathbf{N}}(\omega) \\ \tilde{\mathbf{X}}(\omega) &= -(i\omega\mathbb{1} + A)^{-1}\tilde{\mathbf{N}}(\omega) \end{aligned} \tag{2.9}$$

In order to get the systems dynamics, one has to find the inverse of $(i\omega\mathbb{1} + A)$ and perform an inverse Fourier-transform on both sides of the last line. However, as one can easily see, this is a demanding procedure in terms of finding an analytical solution and it would be much more interesting if there were a less complex way for this. Fortunately, if we look at the systems CM, the problem becomes much clearer and also a method for performing the exact calculation can be stated.
Referring back to the definition of the CM in 1.9, by replacing each vector-entry $X(t)_{i/j}$ by its Fourier-transform and, as already justified in sec. 1.1.1, assuming the mean vector $\langle X(t)_{i/j}\rangle$ to be zero yields

$$\sigma_{ij} = \frac{1}{4\pi}\iint_{\mathbb{R}^2} d\omega d\omega' e^{-it(\omega+\omega')}\,\langle \tilde{X}_i(\omega)\tilde{X}_j(\omega') + \tilde{X}_j(\omega')\tilde{X}_i(\omega)\rangle \tag{2.10}$$

It was also assumed that the operators collected in $\mathbf{X}$ are correlated at the same time which will result in the exponential factor under the integral as given here.
Using the previous relations for the Fourier-transform of X_i gives

$$\begin{aligned} \sigma_{ij} = \frac{1}{4\pi}\iint_{\mathbb{R}^2} d\omega d\omega' e^{-it(\omega+\omega')}\times \\ \sum_{k,l}\langle M_{ik}(\omega)M_{jl}(\omega')\tilde{N}_k(\omega)\tilde{N}_l(\omega') + M_{ik}(\omega)M_{jl}(\omega')\tilde{N}_l(\omega')\tilde{N}_k(\omega)\rangle \\ M(\omega) = (i\omega\mathbb{1} + A)^{-1} \end{aligned} \tag{2.11}$$

For further simplification, the noise correlation matrix in Fourier-space is introduced by

$$\begin{aligned} \frac{\langle \tilde{N}_k(\omega)\tilde{N}_l(\omega') + \tilde{N}_l(\omega')\tilde{N}_k(\omega)\rangle}{2} = D_{kl}\delta(\omega+\omega') \\ D = diag\left(0, \gamma_m(2\bar{n}+1), \frac{\kappa}{2}, \frac{\kappa}{2}\right) \end{aligned} \tag{2.12}$$

As already mentioned there are no expected correlations between the different noise channels and quadratures, therefore the matrix D must be of diagonal form also for its Fourier-transformation. A more detailed calculation is given in appendix B.2. In here the approximation from eq. 1.34 was used, the exact expression would be $D_{22}(\omega) = \frac{\gamma_m\omega}{\omega_m}\coth(\frac{\hbar\omega}{2k_bT})$. But as already discussed in sec. 1.2, even for temperatures around 10K the factor $\hbar\omega/2k_bT \ll 1$ for typical frequencies and in addition with a large quality factor the approximation meets the needed requirements.

Reinserting this into the expression for the CM one gets to

$$\begin{aligned}\sigma_{ij} = \frac{1}{2\pi}\iint_{\mathbb{R}^2} d\omega d\omega' e^{-it(\omega+\omega')} \sum_{k,l} M_{ik}(\omega) D_{kl}(\omega)\delta(\omega+\omega') M_{jl}(\omega') \\ \sigma = \frac{1}{2\pi}\int_{\mathbb{R}} d\omega M(\omega) D(\omega) M^T(-\omega)\end{aligned} \tag{2.13}$$

Having a closer look at $M(\omega)$ one recognizes that it can be separated into a polynomial $Q(\omega)$ in the denominator and a matrix $p_{ij}(\omega)$ in the nominator also consisting of different polynomial.

$$M_{ij}(\omega) = \frac{p_{ij}(\omega)}{Q(\omega)} \tag{2.14}$$

The matrix $p_{ij}(\omega)$ can be set to be, up to a determinant, the inverse matrix of $i\omega\mathbb{1} + A$. This is in linear algebra also known as the "adjugate matrix" of $i\omega\mathbb{1} + A$:

$$p(\omega)(i\omega\mathbb{1} + A) = (i\omega\mathbb{1} + A)p(\omega) = \det(i\omega\mathbb{1} + A) \tag{2.15}$$

With this and the definition of $M(\omega)$ the exact form of the polynomial $Q(\omega)$ is also determined

$$M(\omega)(i\omega\mathbb{1} + A) = \frac{p(\omega)}{Q(\omega)}(i\omega\mathbb{1} + A) = \mathbb{1} \Leftrightarrow Q(\omega) = \det(i\omega\mathbb{1} + A) \tag{2.16}$$

Therefore, reinserting this into eq. 2.13 the matrices can be decomposed into integrals over rational functions. This gives for the final frequency integral

$$\sigma_{ij} = \frac{1}{2\pi}\int_{-\infty}^{\infty} d\omega \sum_k \frac{p_{ik}(\omega) D_{kk}(\omega) p^T_{kj}(-\omega)}{Q(\omega)Q(-\omega)} \tag{2.17}$$

Here the diagonal form of $D(\omega)$ was already taken into account, next, a study of the degree of the polynomials seems to be useful.
The simplest polynomial, $Q(\omega)$, can only be of fourth order in ω which can easily be seen in the investigation of stability in eq. B.1. The parameter λ is thereby replaced by the frequency $-i\omega$, this will allow to make statements about the new parameter coming from the stability-criterion. For the system reaching a steady-state, the eigenvalues of the matrix A must have negative real parts or equivalently fulfil the Routh-Hurwitz-criterion. This can be directly translated into a condition for the roots of $Q(\omega)$ keeping in mind that:

$$\begin{aligned}\lambda = -i\omega \\ \mathrm{Re}(\lambda) = \mathrm{Im}(\omega) \qquad \mathrm{Im}(\lambda) = -\mathrm{Re}(\omega) \\ \mathrm{Re}(\lambda) < 0 \Leftrightarrow \mathrm{Im}(\omega) < 0\end{aligned} \tag{2.18}$$

The roots of the polynomial $Q(\omega)$ therefore have to lie on the lower half of the complex plane to guarantee the system's stability.
For the entries of the polynomials $\sum_k p_{ik}(\omega)D_{kk}(\omega)p^T_{kj}(-\omega)$, making statements about their order in ω is more difficult. Arguing with the units of the systems matrix A: it has the units of a frequency, its inverse has time units. Since the polynomial $Q(\omega)$ is fourth order in ω, the matrix entries of $p_{ij}(\omega)$ are at most of order 3. Therefore the polynomial $G_{ij}(\omega) = \sum_k p_{ik}(\omega)D_{kk}(\omega)p^T_{kj}(-\omega)$ will be maximally of sixth order in ω.

In summary, to find the CM of the intra-cavity field and the mechanics, assuming that the system has reached the steady-state, the following integral needs to be evaluated for every entry of the CM:

$$\sigma_{ij} = \frac{1}{2\pi}\int_{-\infty}^{\infty} d\omega \frac{Gij(\omega)}{Q(\omega)Q(-\omega)} \tag{2.19}$$

2.1.3 Integrals of rational functions

In the last section we have seen that, in order to find the analytical form of the CM, the integral of rational function as formulated in eq. 2.19 needs to be solved. Fortunately, there exist a solution to this special problem as it can be seen in [GR80, Hof15] and for the proof [HJ47].
For an integral consisting of polynomials of the form

$$\int_{-\infty}^{\infty} \frac{g_n(x)}{h_n(x)h_n(-x)}dx \tag{2.20}$$
$$h_n(x) = a_0x^n + a_1x^{n-1} + ... + a_n \qquad g_n(x) = b_0x^{2(n-1)} + b_1x^{2(n-2)} + ... + bn - 1$$

with all the roots of $h_n(x)$ in the upper complex half-plane. The polynomial $g_n(x)$ might also have odd powers of x, but only x^{2n-1} at most, the final solution is given by:

$$I_n = \int_{-\infty}^{\infty} \frac{g_n(x)}{h_n(x)h_n(-x)}dx = \frac{i\pi(-1)^{n+1}\Lambda_n}{a_0\Delta_n}$$
$$with\ \Delta_n = \begin{vmatrix} a_1 & a_0 & 0 & \cdots \\ a_3 & a_2 & a_1 & \cdots \\ a_5 & a_4 & a_3 & \cdots \\ \vdots & \vdots & \vdots & \vdots \end{vmatrix} \tag{2.21}$$
$$\Lambda_n = \begin{vmatrix} b_0 & a_0 & 0 & \cdots \\ b_1 & a_2 & a_1 & \cdots \\ b_2 & a_4 & a_3 & \cdots \\ \vdots & \vdots & \vdots & \vdots \end{vmatrix}$$

by looking at the definition of the Hurwitz-matrix defined for the stability criterion in eq. B.2, it is clear that Δ_n is just the determinant of the "full" Hurwitz-matrix of the polynomial $h_n(x)$ and for Λ_n one replaces the first column of the "full" Hurwitz-matrix with the coefficients of the polynomial $g_n(x)$.
To get a clear understanding of this result, the solution for the first three powers in n are given in the appendix B.3.
With the help of this relation, the solution to the CM in eq. 2.19 is found for the intra-cavity field. By using the CM's symmetry, one can reduce this to effectively ten entries which need to be taken care of. Even if the roots of the polynomial $Q(\omega)$ do not lie on the upper half of the complex plane, the roots of $Q(-\omega)$ do and therefore the newly found integration scheme can be applied.

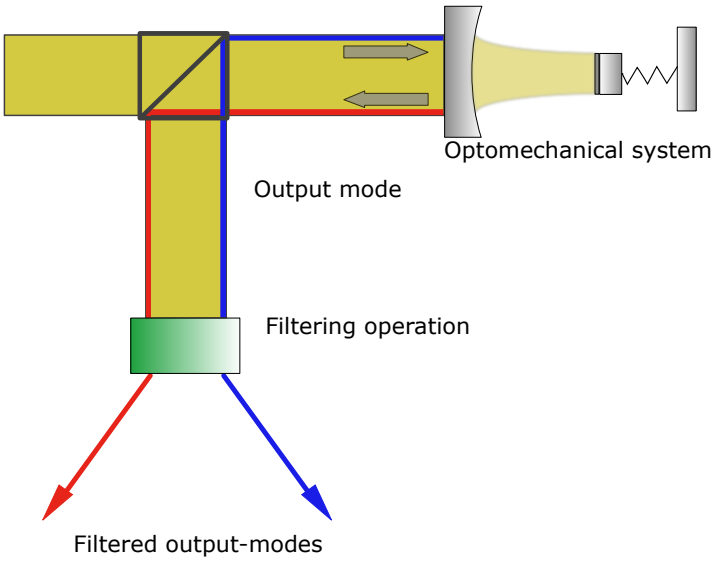

Figure 2.1: Sketch of the output field and the filtering scheme applied to the laser-driven system. As discussed below, the output field will consist of a red- and blue-detuned contribution according to the sidebands which are continously excited, in order to differentiate between those two contributions, a filtering operation is applied which enables one to only access one of the contributions.

2.2 The output field

As already discussed in sec. 1.3.2, the description of the intra-cavity field and the mechanical oscillator are more of theoretical interest since from the experimental side it is usually not possible to access them.
However, the output field can be measured in experiments and therefore it makes sense to have a look at the output mode. The main interest lies on the question whether the output light and the mechanical oscillator are entangled or not. From the experimental side, it is hard to check for the mechanical mode, but it might be possible to detect non-classical correlations in the output-field. More precise, by applying a special filtering scheme to the output-modes, it could be possible to find entanglement between two different temporal pulses. As elaborated later in this work, one of these pulses will contain the TMS-contribution of the optomechanical interaction while the other one will contain mainly the BS-part. Observing non-classical correlations between those two pulses might allow to infer on the entanglement shared between the light-mode and the mechanical system. Therefore the entanglement shared between both pulses might serve as a marker for light-mechanic entanglement in the system.

As seen in section 1.4.2, linearising the composite systems Hamiltonian leads to a BS- and TMS-interaction. Each of these interactions can be enhanced or suppressed depending on the detuning of the laser drive. Assuming a continuous resonant drive $\Delta = 0$ both interac-

tion parts are equally driven at any time and therefore will also contribute to the output light equally.
From the TMS-interaction, light with frequency $\omega_c - \omega_m$ is scattered into the output. From the BS-interaction, a state swap between the excited phonon state onto the light field takes place and will result in a mode with frequency $\omega_c + \omega_m$ (see also sec. 1.4.2). Therefore it is possible to distinguish between the TMS- and BS-interaction by their different frequencies (e.g. by applying a filtering scheme).

For the output mode, a general time-evolution as formulated for the intra-cavity field is not needed since from the (time-reversed) QLE of the system [GC85, see sec. B] the input-output relation can be formulated:

$$\hat{a}_{out}(t) = \sqrt{\kappa}\hat{a}(t) - \hat{a}_{in}(t) \qquad \left[\hat{a}_{out}(t+\tau), \hat{a}^{\dagger}_{out}(t)\right] = \delta(\tau) \tag{2.22}$$

The output field has now by its definition the same commutation relation and correlation functions as the input field. Since the input-output relation is linear in the annihilation and creation operators it will also be linear in its amplitude and phase quadratures.
Therefore, in terms of the previously introduced vector of collected quadratures and noise operators, $\mathbf{X}(t)$ and $\mathbf{N}(t)$, the input-output relation can be reformulated as:

$$\begin{aligned} \mathbf{x}_{out}(t) &= C\mathbf{X}(t) - P\mathbf{N}(t) \\ C &= \text{diag}\left(1, 1, \sqrt{\kappa}, \sqrt{\kappa}\right) \\ P &= \text{diag}\left(0, 0, \frac{1}{\sqrt{\kappa}}, \frac{1}{\sqrt{\kappa}}\right) \end{aligned} \tag{2.23}$$

As it can be seen here, for the first two entries of $\mathbf{X}(t)$, which represents the mechanical quadratures, the "output" modes equal the "input" modes from the intra-cavity quadrature vector.

2.2.1 Mode functions

As emphasized above, to extract the quantum correlations between the different light modes from the TMS- and BS-interaction, a filtering procedure for the output mode needs to be applied.
The filtering should not only sort the modes into different frequencies, but also into two distinct time intervals [HO17, see sec. 5.3.1] so that one can speak of two pulses. The red-detuned contribution from the TMS at earlier times can then be extracted and correlated with the later blue-detuned BS light mode.

The mode functions are chosen to have the form:

$$\begin{aligned} \alpha(t) &= N_\alpha e^{\Gamma t} e^{-i\omega_m t} \qquad \textit{for } t \leq 0 \\ \beta(t) &= N_\beta e^{-\Gamma t} e^{i\omega_m t} \qquad \textit{for } t \geq 0 \end{aligned} \tag{2.24}$$

The first one will filter the TMS-contribution with an exponential envelope $e^{-\Gamma t}$ while the other one has a filtering effect on the BS-contribution. To see this, the impact of the filter functions onto a general signal field-operator $\hat{a}_{sig}(t)$ can be investigated (the next steps follow directly from sec 5.3.1 in [HO17]). This signal field is thought to have three contributions, one part at zero carrier-frequency, the two other parts at frequencies $\pm\omega_m$ given by:

$$\hat{a}_{sig}(t) = \hat{a}_0(t) + \hat{a}_+(t)e^{-i\omega_m t} + \hat{a}_-(t)e^{i\omega_m t} \tag{2.25}$$

Here, $\hat{a}_0(t)$,$\hat{a}_+(t)$ and $\hat{a}_-(t)$ represent amplitudes which show small variation when looking at mechanical time-scales $\tau = 1/\omega_m$. Therefore, the following relation holds:

$$\left| \int_t^{t+\tau} dt' \hat{a}_{0,+,-}(t') e^{\mp i\omega_m t'} \right| \ll \left| \int_t^{t+\tau} dt' \hat{a}_{0,+,-}(t') \right| \tag{2.26}$$

Now consider the multiplication of $\hat{a}_{sig}(t)$ with the mode-function $\alpha(t)$ to study the effect of filtering on a signal:

$$\begin{aligned} \int_{-\infty}^{0} dt \alpha(t) \hat{a}_{sig}(t) &\approx \int_{-\infty}^{0} dt e^{\Gamma t} \left(\hat{a}_0(t) e^{-i\omega_m t} + \hat{a}_+(t) e^{-2i\omega_m t} + \hat{a}_-(t) \right) \\ &\approx \int_{-\infty}^{0} dt e^{\Gamma t} \hat{a}_-(t) \end{aligned} \tag{2.27}$$

In the last approximation-step, the relation from eq. 2.26 was used as it was shown here, the mode function "averages", with weight-function $e^{\Gamma t}$, the contribution $\hat{a}_-(t)$ with carrier-frequency $-\omega_m$ of the output signal while all other contributions are suppressed.
The very same calculation can be done for the mode function $\beta(t)$ but with an averaging over the upper-frequency contribution $\hat{a}_+(t)$. Depending on the "pulse"-width Γ the function will gather more or less information about the chosen mode from future/past times. This will also have a great impact on the entanglement shared between the different modes as it will be shown later on.

The mode functions are applied to the output operators in the following way:

$$\begin{aligned}\hat{a}^{\alpha}_{out}(t) &= \int_{-\infty}^{t} dt' \alpha(t'-t)\hat{a}_{out}(t') \\ \hat{a}^{\beta}_{out}(t) &= \int_{t}^{\infty} dt' \beta(t'-t)\hat{a}_{out}(t')\end{aligned} \tag{2.28}$$

In terms of a convolution, which comes in handy for further use, new mode-functions will be introduced by choosing $\alpha^{new}(t) = \alpha(-t)$ and $\beta^{new}(t) = \beta(-t)$. The filtered output-modes will then have the form:

$$\begin{aligned}\hat{a}^{\alpha}_{out}(t) &= \int_{-\infty}^{\infty} dt' \alpha^{new}(t-t')\hat{a}_{out}(t') = \left(\alpha^{new} * \hat{a}_{out}\right)(t) \\ \hat{a}^{\beta}_{out}(t) &= \int_{-\infty}^{\infty} dt' \beta^{new}(t-t')\hat{a}_{out}(t') = \left(\beta^{new} * \hat{a}_{out}\right)(t)\end{aligned} \tag{2.29}$$

This result will be used later on to simplify the Fourier-transform of the filtered signal.
But for the gained output modes there are still some requirements which need to be fulfilled. First of all, the commutator for different filtered modes should vanish. This allows to finally calculate correlations between the different filtered modes and detect entanglement. It also helps to interpret and understand the two temporal pulses as quantum systems and therefore apply the introduced tools of covariance matrices and entanglement detection in this formalism. Second, for the same output the operators should obey the bosonic commutation relations so that:

$$\begin{aligned}\left[\hat{a}^{\alpha}_{out}(t)^{(\dagger)}, \hat{a}^{\beta}_{out}(t)^{(\dagger)}\right] &= 0 \\ \left[\hat{a}^{\alpha}_{out}(t), \hat{a}^{\alpha}_{out}(t)^{\dagger}\right] = \left[\hat{a}^{\beta}_{out}(t), \hat{a}^{\beta}_{out}(t)^{\dagger}\right] &= 1\end{aligned} \tag{2.30}$$

The first requirement is automatically fulfilled since the mode functions do not have any overlap in time, for the second one, the normalisation factors of the two functions have to be adapted. This can be achieved by having a deeper look onto the bosonic commutations relations:

$$\begin{aligned}\left[\hat{a}^{\alpha}_{out}(t), \hat{a}^{\alpha}_{out}(t)^{\dagger}\right] = \iint_{-\infty}^{t} dt_1 dt_2 \alpha(t_1-t)\alpha^*(t_2-t) \underbrace{\left[\hat{a}_{out}(t_1), \hat{a}^{\dagger}_{out}(t_2)\right]}_{\delta(t_1-t_2)} = \\ \int_{-\infty}^{t} dt_1 |\alpha(t_1-t)|^2 \overset{!}{=} 1 \\ \int_{-\infty}^{0} d\tau |\alpha(\tau)|^2 = |N_\alpha|^2 \int_{-\infty}^{0} d\tau e^{2\Gamma\tau} = \frac{|N_\alpha|^2}{2\Gamma} \overset{!}{=} 1\end{aligned} \tag{2.31}$$

The very same relation will also hold for N_β (which will not be shown here explicitly), consequently the normalisation factor have to be $N_{\alpha/\beta} = \sqrt{2\Gamma}$.

The next question one has to deal with is how this filtering scheme can be applied to the systems quadratures. By defining the filtered output quadratures as $\hat{X}_{out}^{\alpha/\beta}(t) = (\hat{a}_{out}^{\alpha/\beta}(t) + \hat{a}_{out}^{\alpha/\beta}(t)^\dagger)/\sqrt{2}$ and $\hat{P}_{out}^{\alpha/\beta}(t) = i(\hat{a}_{out}^{\alpha/\beta}(t)^\dagger - \hat{a}_{out}^{\alpha/\beta}(t))/\sqrt{2}$ the following transformation arises for the X-quadrature with the mode function $\alpha(t)$

$$\begin{aligned}\hat{X}_{out}^{\alpha}(t) = \frac{\hat{a}_{out}^{\alpha}(t) + \hat{a}_{out}^{\alpha}(t)^\dagger}{\sqrt{2}} = \int_{-\infty}^{t} dt' \frac{\alpha(t'-t)\hat{a}_{out}(t') + \alpha^*(t'-t)\hat{a}_{out}(t')^\dagger}{\sqrt{2}} = \\ \int_{-\infty}^{t} dt' \mathrm{Re}(\alpha)(t'-t)\hat{X}_{out}(t') - \int_{-\infty}^{t} dt' \mathrm{Im}(\alpha)(t'-t)\hat{P}_{out}(t')\end{aligned} \tag{2.32}$$

This very same consideration can be made for all other quadratures so that at the end, the filtering transformation can be reduced to:

$$\begin{aligned}\mathbf{X}_{out}(t) &= \int_{-\infty}^{\infty} dt' T(t'-t)\mathbf{x}_{out}(t') \\ \mathbf{X}_{out}(t) &= \left(\hat{X}_m(t), \hat{P}_m(t), \hat{X}_{out}^{\alpha}(t), \hat{P}_{out}^{\alpha}(t), \hat{X}_{out}^{\beta}(t), \hat{P}_{out}^{\beta}(t)\right)^T \\ T(t) &= \begin{pmatrix} \delta(t) & 0 & 0 & 0 & 0 & 0 \\ 0 & \delta(t) & 0 & 0 & 0 & 0 \\ 0 & 0 & \mathrm{Re}(\alpha)(t) & -\mathrm{Im}(\alpha)(t) & 0 & 0 \\ 0 & 0 & \mathrm{Im}(\alpha)(t) & \mathrm{Re}(\alpha)(t) & 0 & 0 \\ 0 & 0 & 0 & 0 & \mathrm{Re}(\beta)(t) & -\mathrm{Im}(\beta)(t) \\ 0 & 0 & 0 & 0 & \mathrm{Im}(\beta)(t) & \mathrm{Re}(\beta)(t) \end{pmatrix}\end{aligned} \tag{2.33}$$

The vector $\mathbf{x}_{out}(t)$ had been extended by adding two more entries at the end which are equal to the third and fourth ones. It would also be possible to define the filtering matrix $T(t)$ as a 6×4-matrix instead of a 6×6-matrix. However, this will not make any difference for the computation of the output-CM.

In order to later make use of the convolution theorem, we introduce the filtering matrix $T(t) = T^{new}(-t)$, the whole integral is then given by the convolution of the matrix $T^{new}(t)$ and the vector $\mathbf{x}_{out}(t)$

$$\mathbf{X}_{out} = \int_{-\infty}^{\infty} dt' T(t'-t)\mathbf{x}_{out}(t') = \left(T^{new} * \mathbf{x}_{out}\right)(t) \tag{2.34}$$

2.2.2 Covariance matrix for the filtered output modes

Collecting all the insights of the last sections, for the filtered output-field the following vector of quadrature-operators arises:

$$\begin{aligned} \mathbf{X}_{out} = \int_{-\infty}^{\infty} dt' T(t'-t)\mathbf{x}_{out}(t') = \\ \int_{-\infty}^{\infty} dt' T(t'-t)\left(C\mathbf{X}(t') - P\mathbf{N}(t')\right) = \left(T^{new} * (C\mathbf{X} - P\mathbf{N})\right)(t) \end{aligned} \tag{2.35}$$

Here also the relation from eq. 2.23 was used, keeping in mind that the intra-cavity and noise-quadratures as well as the matrices C and P need to be adapted, e.g. P and C are now 6×4-matrices in order to be able to apply a different filtering scheme onto the same light mode.

$$\begin{aligned} \mathbf{X}(t) &= \left(\hat{X}_m(t), \hat{P}_m(t), \hat{X}_c(t), \hat{P}_c(t),\right)^T \\ \mathbf{N}(t) &= \left(0, \sqrt{2\gamma_m}\hat{f}(t), \sqrt{\kappa}\hat{X}_{in}(t), \sqrt{\kappa}\hat{P}_{in}(t)\right)^T \\ C = \begin{pmatrix} 1 & 0 & 0 & 0 \\ 0 & 1 & 0 & 0 \\ 0 & 0 & \sqrt{\kappa} & 0 \\ 0 & 0 & 0 & \sqrt{\kappa} \\ 0 & 0 & \sqrt{\kappa} & 0 \\ 0 & 0 & 0 & \sqrt{\kappa} \end{pmatrix} &\qquad P = \frac{1}{\sqrt{\kappa}} \begin{pmatrix} 0 & 0 & 0 & 0 \\ 0 & 0 & 0 & 0 \\ 0 & 0 & 1 & 0 \\ 0 & 0 & 0 & 1 \\ 0 & 0 & 1 & 0 \\ 0 & 0 & 0 & 1 \end{pmatrix} \end{aligned} \tag{2.36}$$

Finding the solutions for the output-field will therefore require solving the intra-cavity problem stated in eq. 2.9 which includes finding a very complex integral. This solution needs then to be put into the previous relations, multiplied with different matrices and then once again integrated.

On the other side, the CM stores all information of the system, this means knowing the systems CM amounts to knowing the whole system. The definition of the CM in eq.1.9 and already using the Fourier-transform therefore yields:

$$\begin{aligned} \sigma_{ij}^{out} = \frac{1}{4\pi}\iint_{\mathbb{R}^2} d\omega d\omega' e^{-it(\omega+\omega')} \left\langle \tilde{X}_i^{out}(\omega)\tilde{X}_j^{out}(\omega') + \tilde{X}_j^{out}(\omega')\tilde{X}_i^{out}(\omega)\right\rangle = \\ \frac{1}{2}\iint_{\mathbb{R}^2} d\omega d\omega' e^{-it(\omega+\omega')} \tilde{T}_{ik}^{new}(\omega)\tilde{T}_{jm}^{new}(\omega')\left(C_{kl}\tilde{X}_l(\omega) - P_{kl}\tilde{N}_l(\omega)\right)\left(C_{mn}\tilde{X}_n(\omega') - P_{mn}\tilde{N}_n(\omega')\right) \\ + \tilde{T}_{ik}^{new}(\omega)\tilde{T}_{jm}^{new}(\omega')\left(C_{mn}\tilde{X}_n(\omega') - P_{mn}\tilde{N}_n(\omega')\right)\left(C_{kl}\tilde{X}_l(\omega) - P_{kl}\tilde{N}_l(\omega)\right) \end{aligned} \tag{2.37}$$

Here, Einstein summation convention as well as the convolution theorem onto the identity of eq. 2.35 were used, reinserting the relations found for the Fourier-transform $\tilde{\mathbf{X}}(\omega)$ (see

also eq. 2.9), the final output-covariance-matrix is given by

$$\sigma^{out} = \iint_{\mathbb{R}^2} d\omega d\omega' e^{-it(\omega+\omega')} \tilde{T}^{new}(\omega) \left(CM(\omega) + P\right) D\delta(\omega+\omega') \left(CM(\omega') + P\right)^T \tilde{T}^{new}(\omega')^T \tag{2.38}$$

D is given by the noise correlations as already defined in eq. 2.12, since the noise channels are only self-correlated, the matrix D is given by a 4×4 diagonal matrix :

$$D = \text{diag}\left(0, \gamma_m(2\bar{n}+1), \frac{\kappa}{2}, \frac{\kappa}{2}\right) \tag{2.39}$$

The matrix $M(\omega) = (i\omega\mathbb{1} + A)^{-1}$ has the same form as in the previous sections, $\tilde{T}^{new}(\omega)$ is simply the Fourier-transform of $T^{new}(t)$. For further simplification, the matrices $CM(\omega) + P$ will be brought together into one matrix $V(\omega)$.
Altogether, the systems output-CM takes the simple form

$$\sigma^{out} = \int_{\mathbb{R}} d\omega \tilde{T}^{new}(\omega) V(\omega) D V(-\omega)^T \tilde{T}^{new}(-\omega)^T \tag{2.40}$$

Now the question arises: Does there exist a possibility to solve this integral similar to the way it was done for the intra-cavity field by using an integral over rational functions?
Consider first the matrix $V(\omega)$: as shown in the previous section the matrix $M(\omega)$ can be decomposed into a rational function. By applying this knowledge onto $V(\omega)$ it can be decomposed into

$$V(\omega) = CM(\omega) + P = \frac{Cp(\omega) + PQ(\omega)}{Q(\omega)} \tag{2.41}$$

with $p(\omega)$ and $Q(\omega)$ being the same as in eq.2.15 and 2.16. So indeed it is possible to decompose this part of the integral.
The matrix $\tilde{T}^{new}(\omega)$, which is simply the Fourier-transform of $T^{new}(t) = T(-t)$, is given by:

$$\tilde{T}^{new}(\omega) = \begin{pmatrix} \frac{1}{\sqrt{2\pi}} & 0 & 0 & 0 & 0 & 0 \\ 0 & \frac{1}{\sqrt{2\pi}} & 0 & 0 & 0 & 0 \\ 0 & 0 & \sqrt{\frac{\Gamma}{\pi}}\frac{-\Gamma+i\omega}{pol(-\omega)} & \sqrt{\frac{\Gamma}{\pi}}\frac{\omega_m}{pol(-\omega)} & 0 & 0 \\ 0 & 0 & \sqrt{\frac{\Gamma}{\pi}}\frac{-\omega_m}{pol(-\omega)} & \sqrt{\frac{\Gamma}{\pi}}\frac{-\Gamma+i\omega}{pol(-\omega)} & 0 & 0 \\ 0 & 0 & 0 & 0 & \sqrt{\frac{\Gamma}{\pi}}\frac{-\Gamma-i\omega}{pol(\omega)} & \sqrt{\frac{\Gamma}{\pi}}\frac{\omega_m}{pol(\omega)} \\ 0 & 0 & 0 & 0 & \sqrt{\frac{\Gamma}{\pi}}\frac{-\omega_m}{pol(\omega)} & \sqrt{\frac{\Gamma}{\pi}}\frac{-\Gamma-i\omega}{pol(\omega)} \end{pmatrix} \tag{2.42}$$

$$pol(\omega) = \left[\omega - (-\omega_m + i\Gamma)\right]\left[\omega - (\omega_m + i\Gamma)\right]$$

As it can be checked, the roots of the polynomial $pol(\omega)$ lie in the upper half of the complex plane. This now allows to pull out all the polynomials in the denominator from the matrix

$\tilde{T}^{new}(\omega)$, which leaves a new (reduced) matrix $\tilde{T}^{red}(\omega)$ of polynomials (e.g. $T^{red}(\omega)_{11} = pol(\omega)pol(-\omega)/\sqrt{2\pi}$), which gives:

$$\tilde{T}^{new}(\omega) = \frac{1}{pol(\omega)pol(-\omega)}\tilde{T}^{red}(\omega) \tag{2.43}$$

Recombining all the steps discussed in this section, the output-CM is given by

$$\sigma^{out} = \int_{\mathbb{R}} d\omega \frac{\tilde{T}^{red}(\omega)\left(Cp(\omega) + PQ(\omega)\right)}{pol(\omega)pol(-\omega)Q(\omega)} D \frac{\left(Cp(-\omega) + PQ(-\omega)\right)^T \tilde{T}^{red}(-\omega)^T}{pol(\omega)pol(-\omega)Q(-\omega)} \tag{2.44}$$

In the nominator of this integral, a 6×6-matrix with polynomials in each entry appears. What needs to be checked is if the order of all polynomials satisfies the condition assumed for the integral in eq. 2.20.
The maximal power of ω in $\tilde{T}^{red}(\omega)$ is given by its first and second diagonal elements. It is of fourth order at most, this clearly holds for its counterpart $\tilde{T}^{red}(-\omega)^T$.
The sum $Cp(\omega) + PQ(\omega)$ is dominated in its power of ω by the polynomial $Q(\omega)$ since the matrix $p(\omega)$ needs to be (with the same arguments as in the intra-cavity case) of order $n \leq 3$. Therefore this sum must be of order 4 in ω at most because of the appearing polynomial $Q(\omega)$.
Altogether, the polynomials which appear in the now defined nominator-matrix $G_n(\omega)$ will be bounded by the order of 14 from above while the integration scheme presented in Appendix B.3 also allows for fifteenth order in ω.

$$G_n(\omega)_{ij} := \tilde{T}^{red}_{ik}(\omega)\left(Cp(\omega) + PQ(\omega)\right)_{kl} D_{lm}(\omega)\left(Cp(-\omega) + PQ(-\omega)\right)_{nm} \tilde{T}^{red}_{nj}(-\omega) \tag{2.45}$$

On the other side, in the denominator the overall polynomial, which has all its roots in the upper plane, is given by

$$H_n(\omega) := pol(\omega)pol(\omega)Q(-\omega) \tag{2.46}$$

Looking at $pol(\omega)$ and knowing that $Q(\omega)$ is a fourth order polynomial, one could check that $H_n(\omega)$ shows terms of order 8 in ω at most. Therefore, the matrix $G_n(\omega)$ and the polynomial $H_n(\omega)$ indeed fulfil the conditions for solving the integral below using Hurwitz-matrices and the same procedure as in the previous section can be applied.

$$\sigma^{out}_{ij} = \int_{-\infty}^{\infty} d\omega \frac{G_n(\omega)_{ij}}{H_n(\omega)H_n(-\omega)} \tag{2.47}$$

To generate the output-CM, $6 \times 6 = 36$ integrals need to be evaluated, using once again the special symmetry of σ^{out} this reduces to a maximal number of 21 integrals. Using this aspect, it might be possible to save up to 40 % of computational time.

Chapter 3

The program

In this chapter, the main discussion will be about the explanation of the program which is used to generate the intra-cavity and, most importantly, the output-CM. The structure of the program is roughly presented followed by some tests of already known physical effect, such as ground-state cooling of the mechanical system, in order to convince the reader of the correctness of the implemented code.

3.1 The intra-cavity program

As already mentioned in sec. 1.3.2, the knowledge of the intra-cavity fields dynamics has no further experimental interest since this field might not be accessible for the experiment. Still, a short presentation of the program structure as well as some tests will be presented.

3.1.1 Basic structure

The whole program was written in Mathematica which allows to handle symbolic calculations and to treat problems in an analytical way. If there is an interest in numerical values it is possible to hand parameters to the program which then generates the CMs of the intra-cavity mechanics-light-system.
First, the matrix A and the noise-correlation D, given by its definition in eq. 2.2 and 2.4 , are initialized into the program. Those two are the only inputs which the program effectively needs since all other matrices and polynomials are derived from A and D. Using the very same relations found in the previous chapter, the program generates $p(\omega)$ and $Q(\omega)$, together with D the "polynomial" matrix $G(\omega)$ (see also eq. 2.19) is calculated.
The source code, which was implemented to solve the integral in eq.2.19, was kindly provided by Dr. Sebastian Hofer. It uses the Hurwitz-matrices of each entry of $G(\omega)$ and from there constructs the determinants Δ_n and Λ_n by using the polynomial $Q(\omega)$.

At the end of each calculation routine, the program returns a CM which only depends on the systems parameters ω_m,γ_m, Δ, κ, g and $\bar{n}$. By the variation of these parameters the system can be examined for entanglement between the mechanical oscillator and the intra-cavity light-field. Therefore another routine was written which calculates the logarithmic negativity in this two-mode system by using eq. A.7.

3.1.2 Testing the intra-cavity field program

It is now of interest to see if the program indeed reproduces correct and meaningful CMs. Therefore, a few test are applied to the system to study its dynamics in order to gain trust in the program.

One of the easiest tests which can be applied to the program is the zero-coupling case. Assuming that the coupling g between the optical and mechanical system is zero, both modes will evolve independently and therefore the light mode will show a shot-noise covariance matrix (see e.g. A.1) while the mechanical oscillator will end up in a thermal state (see eq. A.2). This can be understood by the fact that in this situation both systems couple only to their noise-channel, more precisely the mechanics to the thermal bath given by $\hat{f}$ and the intra-cavity field only to the optical noise which arises from $\hat{X}_{in}$ and $\hat{P}_{in}$ in the linearised QLE. Moreover, the bath was modelled to initially be in a thermal state and the optical noise channel is assumed to be in a vacuum state since we changed into a displaced frame where only fluctuations are considered.
This should also be independent of all parameters except the number of excitation in the mechanical thermal bath $\bar{n}$ assuming initial thermalisation of the system with the environment. For testing the program, the thermal bath is assumed to be at temperature $T \approx 10K$ which corresponds to $\bar{n} \approx 1.76 \times 10^5$ when $\omega_m = 2\pi \times 1.18$MHz.

As it can be seen in fig. 3.1, the matrix plot of the CM shows the expected behaviour. The only non-zero entries are the diagonals which are formed by the variances of the position- and momentum-quadratures of the mechanical system (σ_{11} and σ_{22}) and the intra-cavity light field amplitude- and phase-quadratures (σ_{33} and σ_{44}).
The off-diagonal elements are all equal to zero which matches the interpretation of two non-interacting systems. This is in direct contrast to a system in a TMS-state discussed in eq. A.5. Therefore calculating the logarithmic negativity $E_{\mathcal{N}}(\sigma)$ from eq. A.7 will yield zero as well as the Duan-criterion given in eq. 1.22 will not show any violation independent from the choice of the parameter a as defined in section 1.1.4 since there is no entanglement stored in this system.

$$\begin{pmatrix} \frac{352\,001}{2} & 0 & 0 & 0 \\ 0 & \frac{352\,001}{2} & 0 & 0 \\ 0 & 0 & \frac{1}{2} & 0 \\ 0 & 0 & 0 & \frac{1}{2} \end{pmatrix}$$

Figure 3.1: Matrix plot of the CM with zero coupling ($g = 0$) with a thermal bath temperature $T = 10K$. For a mechanical frequency $\omega_m = 2\pi \times 1.18MHz$ this yields $\bar{n} \approx 1.76 \times 10^5$. The first two diagonal entries correspond to the position- and momentum-quadratures of the mechanical oscillator being in a thermal state as discussed in sec. 1.1.1 , the third and fourth entries represent the intra-cavity light field amplitude- and phase-quadratures being in shot-noise state. No correlations between the mechanical and the optical system, which would be represented by non-zero off-diagonal element (e.g. $\sigma_{13} \neq 0$), are observed in this case.

Another test for the program which was taken into account for this work is the ground-state cooling of the mechanical system [AKM14, see sec. VII.A] as presented in more detail in A.4.

The information about the photon number in the mechanical system can be extracted from the CM since it is stored in the first diagonal entries:

$$n = \langle \hat{n} \rangle = \frac{\langle \hat{X}_m^2 \rangle + \langle \hat{P}_m^2 \rangle - 1}{2} = \frac{\sigma_{11} + \sigma_{22} - 1}{2} \tag{3.1}$$

Here n represents the mean phonon number in the mechanical oscillator. From a theoretical point of view, ground-state cooling is well known and studied so that it is also possible to calculate the expected n for a given system. Introducing the rates $A_\pm$, which characterise the absorption or emission of one phonon by scattering one laser photon, n is given by [GVT+08]:

$$\begin{aligned} A_\pm &= \frac{g^2 \kappa}{\frac{\kappa^2}{4} + (\Delta \mp \omega_m)} \\ n &\approx \frac{\gamma_m \bar{n} + A_+}{\gamma_m + A_- - A_+} \end{aligned} \tag{3.2}$$

With greater red-detuning of the drive-laser the rate A_- becomes greater than A_+, effectively decreasing n. For the limits of $\omega_m \gg \bar{n}\gamma_m, g, \kappa$ and $\kappa \gg \gamma_m, g$, eq.3.1 and eq.3.2 yield approximately the same result (for more details see [GVT+08]).

Ideally the program reproduces this behaviour of the mechanical system with different laser-detuning, but it is more likely that the results between the program and the theoretical prediction only differ slightly from each other since the expression given in 3.2 is only an approximation.

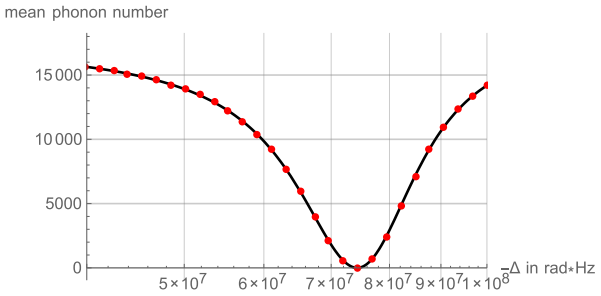

Figure 3.2: Plotted in this graph are the effective mean phonon number coming from the theoretical approach in eq. 3.2 (solid black line) as well as the prediction made by the intra-cavity program from eq.3.1 (red dots in the plot) for different red-detuning of the drive-laser. For this plot, the parameters from table 3.1 where used in accordance with the conditions $\omega_m \gg \bar{n}\gamma_m, g, \kappa$ and $\kappa \gg \gamma_m, g$.

$\omega_m/2\pi$ [Hz]	$\gamma_m/2\pi$ [Hz]	$g/2\pi$ [Hz]	$\kappa/2\pi$ [Hz]	$\bar{n}$
1.18×10^7	1.62×10^{-1}	4.06×10^3	4.06×10^5	1.76×10^4

Table 3.1: Table with parameters used for the plots in fig. 3.2.

In fig. 3.2 both predictions are plotted using the parameters from table 3.1. As it can be seen in the figure, the program makes the same predictions on the phonon number as the theory, the maximal cooling is reached for a red-detuning of the drive-laser of $\Delta = -\omega_m$.
Also considered, but not shown in this work, was the maximal relative error between the prediction in eq. 3.1 and 3.2 which is in this regime smaller than 10^{-3}. Therefore it can be safely assumed that the program reproduces the ground-state-cooling of the mechanical oscillator in a trustworthy way.

3.1.3 Entanglement in the intra-cavity field

Although the intra-cavity light field is harder to access in the experiment, it can be of great interest to study its dynamics, especially the occurrence of entanglement in dependence of multiple parameters. These insights can be used for the output-field program in order to get an estimation in which parameter regime entanglement might be expected.

First of all the stability of the system needs to be studied by considering the results found in sec. 2.1.1. From the Ruth-Hurwitz stability criterion it follows that for a red-detuned drive-laser, the first condition from eq. 2.6 is automatically satisfied while the second one needs to be checked in order to find a stable parameter-regime.
For the plot of the stability region in fig. 3.3, the systems parameters of table 3.2 where used. These parameters are also observed in the experiment, which is currently being carried out at the University of Vienna. This is also why they are also of great interest for the further

$\omega_m/2\pi$ [Hz]	$\gamma_m/2\pi$ [Hz]	$\kappa/2\pi$ [Hz]	$\bar{n}$
1.18×10^6	1.62×10^{-1}	4.06×10^6	1.76×10^5

Table 3.2: Table with parameters used for the plots in fig. 3.3 and 3.4.

discussion in this work.
For the exploration of entanglement in the system it is crucial that stability is always guaranteed, the whole discussion done in chapter 2 is based on the assumption that the system is found in its steady state. If this is not given, the program reproduces CMs which will not fulfil the requirement discussed in sec. 1.1.1, e.g. the CMs will not have real valued entries. Therefore also the generated plots of the entanglement between the mechanical and optical system cannot be considered to be credible.

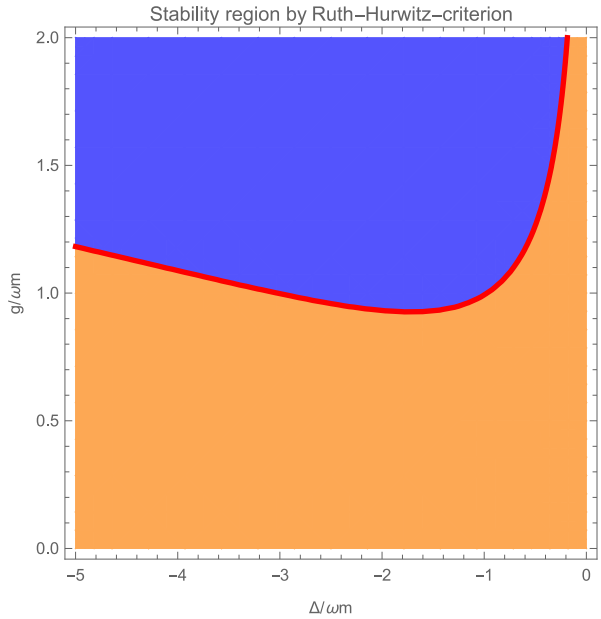

Figure 3.3: Plotted in this graph is the stability region of the system which parameters are given by table 3.2 in dependence from the detuning Δ and the coupling g. The blue area represents regions where the second condition coming from the Ruth-Hurwitz criterion in eq. 2.6 is not satisfied while the orange region will yield stability. The red line in this plot represents the transition from stability to instability. The criterion is fulfilled for a wide region for a detuning Δ from zero up to five times the mechanical frequency ω_m and a coupling from zero up to less than one ω_m. It should also be emphasized that for detuning around $\Delta > -0.5\omega_m$ the condition is even given for coupling higher than $g = \omega_m$.

The entanglement shared between the mechanical and optical subsystems is measured by the logarithmic negativity discussed in sec. 1.1.3. Values under zero are therefore also allowed in order to get an insight about how far away the two subsystems are away from

being entangled. In fig. 3.4, the values of the logarithmic negativity in dependence of both, the detuning and the coupling are shown. Once again, the parameters of table 3.2 were used as well as the stability region were chosen for Δ and g.
The plot shows that entanglement between the intra-cavity field and the mechanical oscillator is expected for sufficiently high detuning and coupling. Especially the detuning plays an important role since for Δ close to zero, independent of the coupling g, no entanglement is detected at all. But already for a slight detuning $\Delta \approx 0.1\omega_m$ the border of entanglement is shifted towards smaller coupling. The green contour in fig. 3.4 underlines this effect by showing the effective mean phonon number of the mechanical system being $n = 1$. The cooling of the mechanics, mediated trough the BS-interaction and the finite energy decay κ of the optical subsystem, even though the BS-part benefits in favour of the TMS-interaction. Therefore it supports the generation of entanglement and suppresses the effects of the coupling between the thermal bath and the mechanics.

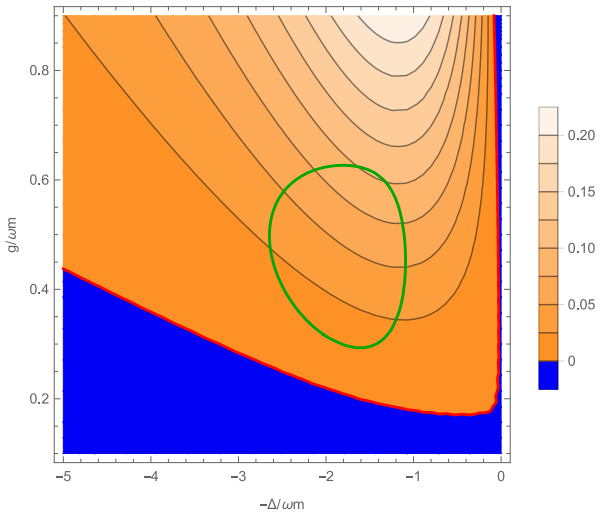

Figure 3.4: Logarithmic negativity as a function of detuning Δ and coupling g. The red line represents the border of entanglement, all CMs which are generated with parameters under this line do not show non-classical correlation at all. Between zero detuning and $\Delta \approx -0.1\omega_m$ the border of entanglement decreases for decreasing detuning, the maximum logarithmic negativity is found for $\Delta \approx -\omega_m$ and a maximal coupling $g = 0.9$. The green contour shows region of $n = 1$ and represents ground-state cooling of the mechanical system. Please note that the range of g was adapted in comparison to 3.3 in order to assure a stable system.

3.2 The output-field program

The output field of the system is, in comparison to the intra-cavity field, the one which is the easiest to access in terms of the experiment. The output-field part of the program allows now to directly generate the CM of the experimental measurable filtered output modes and the mechanical system. With the results from the previous section 3.1 it might also be possible to find a parameter regime where entanglement between the two filtered output modes could be achieved.
In extension to this, an optimized protocol called "two-sideband"-evaluation is discussed in terms of the final program. This enables the program to extract even higher entanglement in the output-field and detect entangled states which would have been considered as separable in the first case.

3.2.1 Basics structure

The same matrix A and D as in the intra-cavity system is handed to the program as well as the filter matrix $\tilde{T}^{new}(\omega)$ from eq. 2.42. The filtering matrix includes the information about the mode-functions as discussed in sec. 2.2.1. In addition to this, the matrices C and P as in eq. 2.36 are constructed by the program. With those matrices, the main objects of interest, namely the matrix of polynomials $G_n(\omega)$ and the denominator polynomial $H_n(\omega)$ (according to eq. 2.45 and 2.46) are generated.
The integration scheme which solves the final integrals is once again the same one as for the intra-cavity case, everything is done by the polynomials Hurwitz-matrices and determinants. At the end of the routine, the program returns CM which solely depend on the systems parameters ω_m,γ_m, Δ, κ, g and $\bar{n}$. Additionally, the pulse-width Γ needs to be handed to the program to evaluate the CMs numerically.

3.2.2 Testing the output-field program

In order to test the output part of the program, once again, the zero-coupling situation for the output field and the mechanical oscillator can be considered. As in the case of the intra-cavity field the parameters used for this are $\omega_m = 2\pi \times 1.18\text{MHz}$ and $T \approx 10K$ which corresponds to $\bar{n} \approx 1.76 \times 10^5$.
In fig. 3.5 the 6×6-covariance matrix of the system is shown. The mechanical subsystem is indeed generated to be in a thermal state while the filtered output modes are in shot-noise state. Once again, no-correlations between the different subsystems are observed since all non-diagonal matrix elements $\sigma_{ij} = 0$ with $i \neq j$.
On the other side, testing the program via the effect of ground-state cooling also seems to be a good approach for testing the mechanical side of the CM.

$$\begin{pmatrix} \frac{352\,001}{2} & 0 & 0 & 0 & 0 & 0 \\ 0 & \frac{352\,001}{2} & 0 & 0 & 0 & 0 \\ 0 & 0 & \frac{1}{2} & 0 & 0 & 0 \\ 0 & 0 & 0 & \frac{1}{2} & 0 & 0 \\ 0 & 0 & 0 & 0 & \frac{1}{2} & 0 \\ 0 & 0 & 0 & 0 & 0 & \frac{1}{2} \end{pmatrix}$$

Figure 3.5: Matrix plot of the output-CM with zero coupling ($g = 0$) with a thermal bath temperature $T = 10K$. For a mechanical frequency $\omega_m = 2\pi \times 1.18\text{MHz}$ this yields $\bar{n} \approx 1.76 \times 10^5$. The first two diagonal elements correspond to the quadratures of the position and momentum in the mechanical system which are in a thermal state, the third and fourth as well as the fifth and sixth entries represent the amplitude- and phase-quadratures of the first and second output mode filtered by the mode functions $\alpha(t)$ and $\beta(t)$ in eq. 2.24 respectively. Both of the output-light modes are found to be in a shot-noise state and no correlations are observed between the mechanical and optical subsystems.

This time we test the effects of ground state cooling using a slightly other parameter regime where the previous assumptions as formulated in sec. 3.1.2, namely $\omega_m \gg \bar{n}\gamma_m, g, \kappa$ and $\kappa \gg \gamma_m, g$, do not hold. As discussed in [GVT+08], the theory gives the following prediction on the mean phonon number n in the mechanical system:

$$\begin{aligned} n = \frac{\langle \hat{X}_m^2 \rangle + \langle \hat{P}_m^2 \rangle - 1}{2} \approx \\ \frac{1}{\gamma_m + A_- - A_+} \left[(1+a)\frac{A_- + A_+}{2} + \gamma_m \bar{n} \left(1 + \frac{1}{\eta}\right) + \frac{\gamma_m \bar{n}(A_- - A_+)}{2\kappa} \left(1 + \frac{b}{\eta}\right) \right] \\ a = \frac{\kappa^2 + 4\Delta^2 + 4\eta\omega_m^2}{\eta(\kappa^2 + 4\Delta^2 + 4\omega_m^2)} \\ b = \frac{(4\Delta^2 - \kappa^2) - 2\omega_m^2}{\frac{1}{2}(\kappa^2 + \Delta^2)} \\ \eta = 1 + \frac{4g^2\Delta}{\omega_m(\kappa^2 + 4\Delta^2)} \end{aligned} \tag{3.3}$$

The two scattering rates $A_\pm$ are defined in the very same way as in eq. 3.2. With this more complicated expression for n it is now possible to access other parameter-regimes for the ground state cooling of the mechanical system.

This time, the parameters are chosen to have the same typical values as for the experiment done at the University of Vienna on generation and verification of optomechanical entanglement, the systems parameters are given in table 3.3.

In fig. 3.6 the mean phonon number for the theoretical approach as well as for the prediction by the programs CM can be seen. Once again, both expressions yield very close results,

therefore the maximal relative error is of the order 10^{-3}.
Also for the output-field part of the program the effect of ground-state cooling in the mechanical oscillator is trustworthy reproduced.

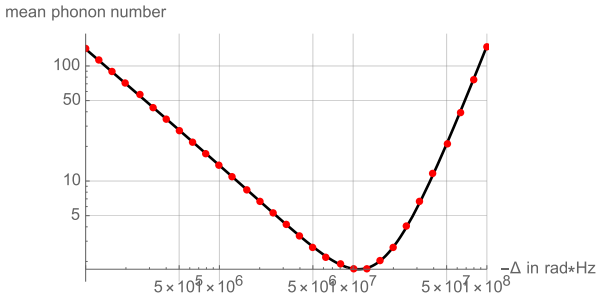

Figure 3.6: This graph shows the effective mean phonon number of the mechanical system as a function of the detuning Δ, the red dots represent the results from the output-field program while the solid black line gives the theory's prediction from eq. 3.3. The laser is always assumed to be red-detuned to ensure the systems steady-state-stability condition, all other parameters used for this plot are given in table 3.3.

3.2.3 Entanglement in the output-field

In contrast to the intra-cavity system, the output-field program allows to distinguish between three different parties which might share some entanglement. On the one hand there is the mechanical system, on the other hand the two differently filtered output-modes which characterize the two temporal separated pulses.
One could for example consider the reduced system of the mechanical subsystem and the first-light mode whose information is stored in the third and fourth entries of the CM. This first light-mode is filtered by the mode function $\alpha(t)$ given in 2.24. Therefore the mode-function filters the light-field in such a way that this light-mode mainly contains contributions from the TMS-interaction as discussed in sec. 2.2.1.
But also the second reduced system of the mechanics and the other filtered output-light-mode can be considered. This light-mode, generated by the use of $\beta(t)$, is dominated by the contribution from the BS-interaction of the linearised Hamiltonian.
Finally, it is also possible to extract and detect the entanglement between the two different output-light-modes, the whole situation is shown graphically in fig. 3.7.

$\omega_m/2\pi$ [Hz]	$\gamma_m/2\pi$ [Hz]	$g/2\pi$ [Hz]	$\kappa/2\pi$ [Hz]	$\bar{n}$
1.18×10^6	1.62×10^{-1}	2.05×10^5	4.06×10^6	1.76×10^5

Table 3.3: Table with parameters used for ground-state cooling and entanglement detection in the output-field program.

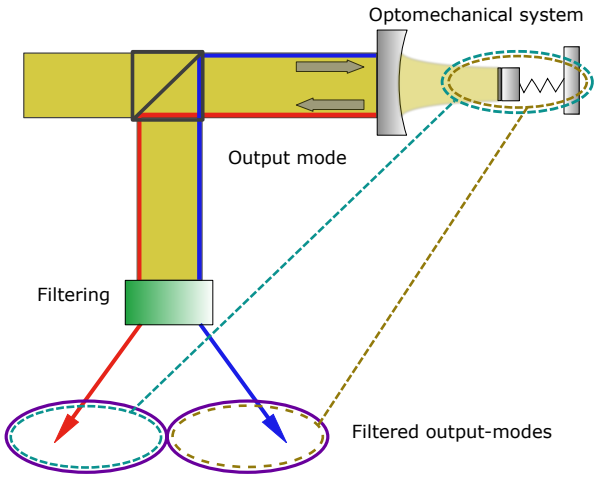

Figure 3.7: In this graphic the different types of entanglement parties are represented in the optomechanical system.Turquoise dotted-line: the reduced system is formed by the mechanical subsystem and the first filtered-light-mode which mainly includes contribution from the TMS-interaction. Brown dotted-line: on the other side, the contribution from the upper-sideband (the BS-interaction) is contained in the second filtered-output-mode. This interaction, as discussed in sec. 1.4.2, will perform a state-swap between the intra-cavity field and the mechanics, and will not generate any entanglement. Violet solid-line: the third reduced system is formed by the two output-light modes.

Intuitively now the question arises where entanglement is expected and which of the reduced systems share the highest non-classical correlations?

Consider first the reduced system formed by the mechanics and the different filtered output-modes. The first output-mode is generated by the mode function $\alpha(t)$ from eq. 2.24, as already discussed in sec. 2.2.1 this mode contains mainly the contributions from the TMS-interaction. This interaction, which arises from the linearised Hamiltonian (see A.8), generates non-classical correlations between the intra-cavity field and the mechanical system. These correlations are mediated onto the out-put field trough the input-output-relation so that entanglement between the upper-sideband and the mechanical oscillator can be expected.
The other reduced system is formed by the mechanics and the second output-mode filtered by $\beta(t)$. This filter function suppresses contributions from the TMS-interaction, the BS-interaction is the dominant part in this mode. The interaction acts as a state-swap-operation on the mechanics and the intra-cavity light mode, therefore the entangled state of the mechanics, which was previously introduced, is exchanged onto the intra-cavity mode. Once again, through the input-output relation this mediates onto the output-field where this contribution is filtered.

This intuitive image can already be tested with the program by examining the various en-

tries of the covariance matrix of the full system. The entanglement is once again measured by the logarithmic negativity from sec. 1.1.3, the results are shown in fig. 3.8 as a function of the pulse-width Γ, while the parameters from table 3.3 are used.
From the plot it can indeed be seen that the entangling-mode, containing the TMS-contribution, and the mechanics (blue dots) shows definitely entanglement in contrast to the system formed by swap-mode with the BS-contributions and the mechanics (red dots). For smaller pulse-widths Γ the non-classical correlations decrease for the entangling-mode. The effect can be understood via the decoherence of the mechanical system since smaller pulse-widths correspond to longer interaction times in the optomechanical system. But this favours the coupling to the thermal bath of the oscillator which destroys the shared correlations. On the other side, if Γ becomes too large, and therefore the interaction time too short, the systems will not build up any entanglement which manifests in a decrease of the logarithmic negativity and a state similar to the shot-noise state is achieved by the program which also reflect in the values of the logarithmic negativity as it can be seen in fig. 3.8.

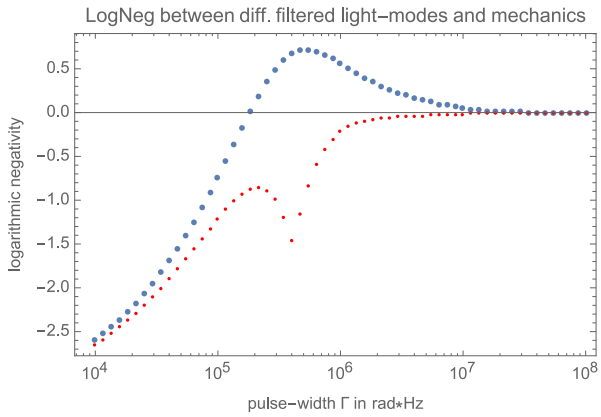

Figure 3.8: Plot of the entanglement shared between the entangling-mode (blue dots) and the swap-mode (red dot) with the mechanical system respectively generated with the parameters from table 3.3 and a detuning of $\Delta = -200$kHz. The first output-light-mode is, in contrast to the other one, definitely entangled with the mechanics , due to the mechanical decoherence, the logarithmic negativity decreases for smaller pulse-widths Γ as well as for broader pulses which can be argued by the limited time for the optomechanical interaction. This will leave the optical system in a state similar to shot-noise state and no correlations are gathered by the mode-function.

In the further course of this work, the entanglement between the entangling-mode and the mechanics is discussed in more detail. The task is to find a parameter regime where the entanglement between the two subsystems are sufficiently large so that also non-classical correlations between the different filtered output-modes is expected. For further discussion,

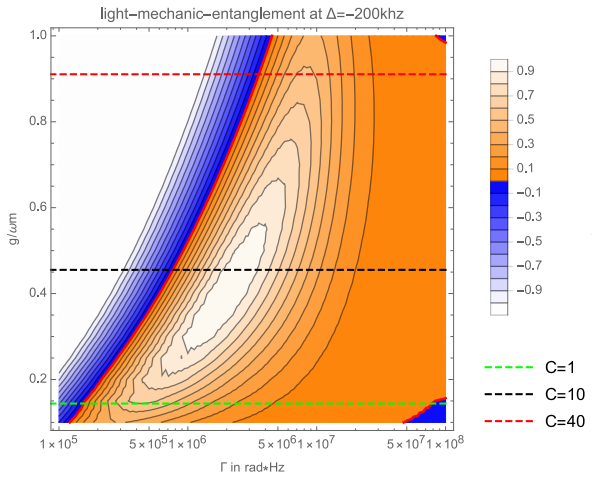

Figure 3.9: $\Delta = -200kHz$

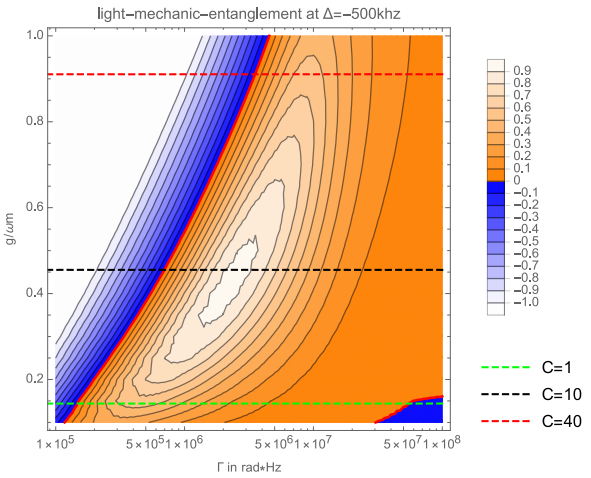

Figure 3.10: $\Delta = -500kHz$

Shown here are the different contour plots of the logarithmic negativity as a function of the pulse-width Γ and the coupling strength g. The detuning of the driving-laser is given by $\Delta = -200kHz$ in fig. 3.9 and $\Delta = -500kHz$ in fig. 3.10 , all other parameters are the same as for the previous plot 3.8 and can be found in table 3.3. The solid red line indicates the border to separable states where the logarithmic negativity is found to be below or equal zero, the dotted lines represent regions of equal cooperativities $C = 1$ (green), $C = 10$ (black) and $C = 40$ (red). The most entanglement is found in a parameter regime of $g = 0.2 - 0.7\omega_m$ and $\Gamma = 5 \cdot 10^5 - 10^7 \text{rad} \cdot \text{Hz}$.

we will now introduce the systems cooperativity C:

$$C = \frac{4g^2}{\kappa\gamma_m(\bar{n}+1)} \tag{3.4}$$

It compares the optomechanical interaction with the coupling of the mechanics to the thermal bath and the optical system to its noise channel. Bigger cooperativity is connected to a stronger optomechanical interaction and therefore favours the generation of entanglement in the system. For the typical systems parameters of table 3.3, the cooperativity is given by $C = 1.45$.

In fig. 3.9 and 3.10 the entanglement, measured by the logarithmic negativity, for the reduced system of the oscillator and the entangling-pulse are plotted as a function of the pulse-width Γ and the coupling strength g , all other parameters of the system, as found in table 3.3, where kept constant.
The logarithmic negativity is maximal in a region around $\Gamma = 5 \cdot 10^5 - 10^7 \text{rad} \cdot \text{Hz}$ as well as for high couplings. Typical experimental values for the cooperativity are found between $C = 1$–10 so that all other values above are more of theoretical interest. But already for reasonable cooperativity around $C = 10$ the program definitely generates and detects non-classical correlations.

Furthermore, an investigation of the entanglement between the filtered output-modes, which is also accessible in the experiment, is more interesting because it can be regarded as a marker of entanglement between mechanics and light field.

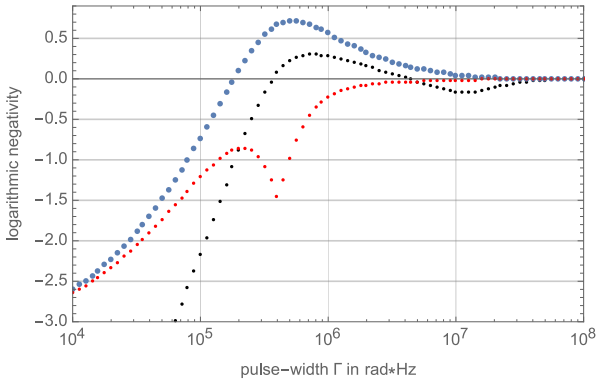

Figure 3.11: Shown in this plot is the logarithmic negativity as a measure for entanglement, shared between first and second pulse, in dependence of the pulse width Γ, the detuning is set to $\Delta = -200$kHz all other parameters are the same as for fig. 3.6. The pulses show entanglement for pulse-widths around $\Gamma = 4 \cdot 10^5 - 4 \cdot 10^6 \text{rad} \cdot \text{Hz}$ and decreases for higher pulse widths before returning to a state with only classical correlations and therefore no entanglement.

In fig. 3.11, the entanglement, given by the logarithmic negativity, for the two temporal pulses (black dots) is shown in dependence of the pulse-width. In addition to this, the logarithmic negativity for the reduced system of the mechanics and the earlier/later pulse from fig 3.8 is also shown for comparison. Interestingly, the light-light curve shows a drop below logarithmic negativity values of zero, which leads to the interpretation that there are no detectable non-classical correlations, for pulse widths of about $\Gamma = 4 \cdot 10^6 \text{rad} \cdot \text{Hz}$ in contrast to the entanglement curve of the first pulse and the mechanical system given by the blue dots. Even for pulses with $\Gamma > 5 \cdot 10^6 \text{rad} \cdot \text{Hz}$ there are still non-classical correlations between the oscillator and the first pulse and therefore also a two-mode-squeezed like state in this reduced system, thus, the entanglement process is still present in this regime. The effect can perhaps be understood by the small interaction times of the optomechanical system which suppresses the optimal state-swap between the mechanics and the light modes and results in a separable state. The critical pulse-width from the left-hand side is once again given due to the decoherence time of the mechanical system since smaller pulses correspond to longer interaction times in which the mechanical system also has a higher opportunity for exchanging photons and phonons with the thermal bath.
For broad pulses, due to the limited interaction time, the mode-functions only collect noise which decreases the entanglement in the system and results in a state similar to the two-mode-shot-noise state.

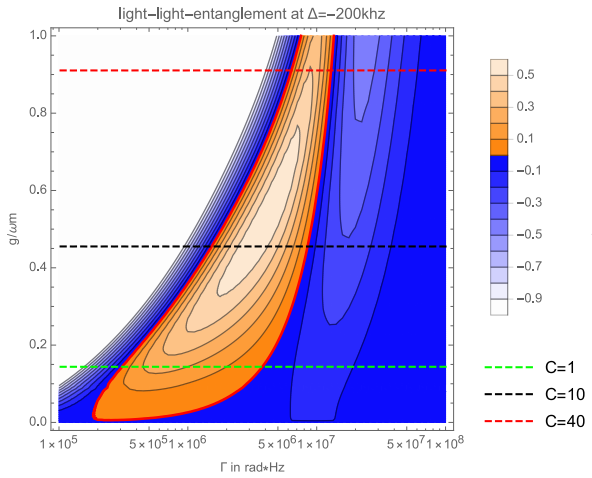

Figure 3.12: $\Delta = -200kHz$

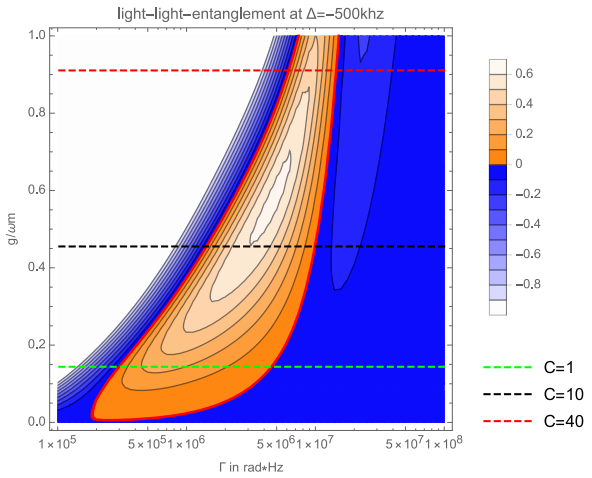

Figure 3.13: $\Delta = -500kHz$

Different contour plots of the logarithmic negativity as a function of the pulse-width Γ and the coupling g , with detuning given by $\Delta = -200kHz$ in fig. 3.12 and $\Delta = -500kHz$ in fig. 3.13. The other parameters are the same as for the previous plots and are collected in 3.3. The solid red line again indicates the border to logarithmic negativities below or equal zero. In contrast to fig. 3.9and 3.10 the logarithmic negativity drops below zero for larger pulse widths independently of the coupling. Nevertheless, bigger detuning results in higher logarithmic negativities and wider entanglement regions.

The program now allows the user to explore a wide range of parameters which can be changed in the system. Which are the parameters which improve the entanglement stored in the system? From an experimental point of view, which parameters can be varied and how much?

From the experimental side, changing the detuning of the drive-laser might be an uncomplicated adaptation to the experiment. This is why a more detailed exploration of the detunings influence on the system and the entanglement shared between the two pulses might be helpful to find the optimal working regime for the experiment. Is it possible to increase the entanglement with higher detuning?

In fig. 3.12 and 3.13 the logarithmic negativity as a function of the cooperativity, varied by the coupling strength g and the pulse widths Γ is shown. As it can be seen in those plots, the entanglement in the system decreases once again for bigger pulse widths Γ while higher detuning improves the entanglement shared between the different pulses, in addition, the possible pulse width for which it occurs also slightly increases.

On the one hand, a stronger red-detuning results in lower generation of quantum correlated photon-phonon pairs of the mechanical state with the intra-cavity field. On the other hand, the BS-interaction is enhanced which, due to the ground-state cooling effect as discussed in sec. 3.2.2, mainly reduces the mean phonon number of the oscillator. In addition to this, enhancing the BS-interaction together with the cooling effect optimizes the state-swap between

the intra-cavity light and the mechanics.
To confirm this thought, the maximal entanglement for different red-detuning of the drive-laser as a function of the cooperativity is shown in fig. 3.14. In this case, the pulse-width generated between $\Gamma = 10^5 - 10^8 \text{rad} \cdot \text{Hz}$ was considered and the maximal logarithmic negativity extracted while keeping the coupling constant. For coupling-strengths $g \leq 0.3\omega_m$ different red-detuning will not lead to a significant rise in the maximal logarithmic negativity, but for bigger values, there is indeed a difference for higher detuning of the laser resulting in more detected entanglement in the system.

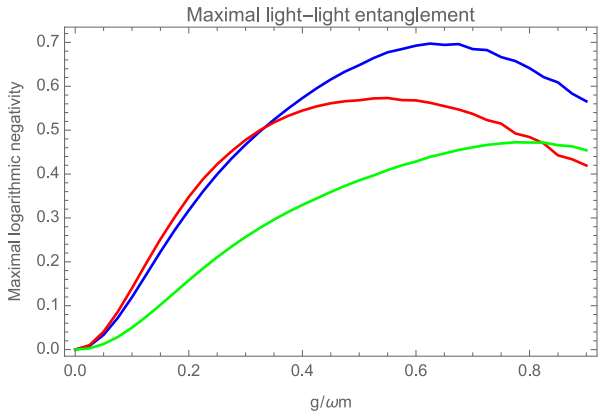

Figure 3.14: Plot of the maximal entanglement as a function of the coupling for different detuning $\Delta = -200\text{khz}$ (red curve),$-\omega_m$ (blue curve),$-3\omega_m$ (green curve). The maximum of the logarithmic negativity was found by generating pulse widths between $\Gamma = 10^5 - 10^8 \text{rad} \cdot \text{Hz}$ while keeping the coupling constant. For higher optomechanical coupling $g > 0.3\omega_m$ bigger red-detuning improves the maximal logarithmic negativity found in the system. The other systems' parameters are the same as in the plots before.

In fig. 3.15 the maximal logarithmic negativity, found by scanning over a pulse width $\Gamma = 10^5 - 10^8 \text{rad} \cdot \text{Hz}$, is shown in dependence of the detuning Δ and the coupling g, both in terms of the mechanical frequency ω_m. From this plot one can see, in accordance with the results from fig. 3.14, that higher detuning does not affect the maximal logarithmic negativity significantly for lower couplings $g < 0.3\omega_m$. On the other side, for higher coupling strengths the right choice of the laser-detuning can enhance the logarithmic negativity, and therefore the entanglement. For example, consider a coupling of $g = 0.5\omega_m$ which corresponds to a cooperativity of $C \approx 12$ with the parameters used for the plot (as given in table 3.3). For this high coupling of the system, adjusting the detuning towards $\Delta = -\omega_m$ also helps in improving the systems logarithmic negativity. With the detuning of $\Delta = -200\text{kHz}$ considered in the previous plots of this section, the logarithmic negativity yields a value of around $\text{logneg}(\sigma) = 0.56$ while for a detuning at resonance with the mechanical frequency the maximal value is generated to be $\text{logneg}(\sigma) = 0.65$.

It seems that the influence of the detuning in the system becomes evident with higher coupling and cooperativities, therefore choosing a red-detuning of the drive-laser around $\Delta \approx -\omega_m$ does not decrease the entanglement found between the two temporal pulses in the "worst" case of small coupling. On the other hand, in the best case scenario of sufficiently high coupling and cooperativites, a more red-detuned drive-laser improves the generation of entanglement in the system and could as well be a serious option for the optimization of the experiment.
From now on, if not stated otherwise, a detuning of $\Delta = -200\text{kHz}$ is considered, keeping in mind that even higher red-detuning might increase the detected entanglement in the system.

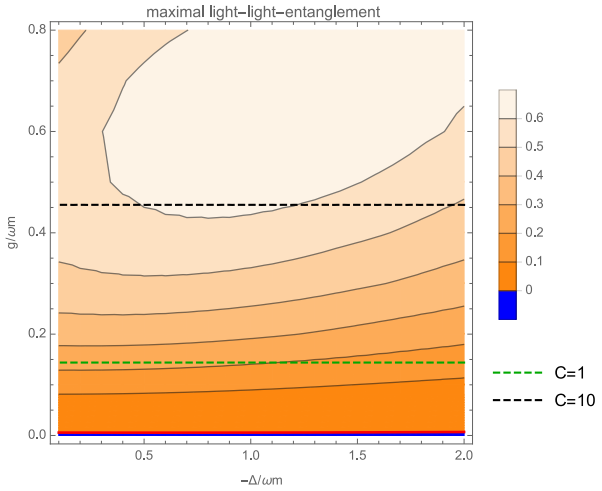

Figure 3.15: Plot of the maximal entanglement as a function of the coupling and detuning maximized by scanning trough a pulse-width of $\Gamma = 10^5 - 10^8 \text{rad} \cdot \text{Hz}$, all other parameters can be found in table 3.3. For coupling $g < 0.3\omega_m$ the detuning has almost no effect on the maximal logarithmic negativity while for higher couplings the improvement is significant especially for detuning around the mechanical frequency $\Delta = -\omega_m$. The dashed lines indicate parameters of equal cooperativity $C = 1$ (green) and $C = 10$ (black). The solid red line represents the border between entangled and separable states.

Let us now consider the mechanics quality factor Q and the coupling strength g in the system. The latter can be changed by the input power of the laser-drive as discussed in sec. 1.3 as long as the stability in the system is given (see sec. 2.1.1 and fig. 3.3). The mechanical quality factor scales with γ_m^{-1}, therefore lower damping rates will improve Q.
In fig. 3.16 the maximal logarithmic negativity, found by scanning over pulse widths from $\Gamma = 10^5 - 10^8 \text{rad} \cdot \text{Hz}$, as a function of the coupling strength and the quality factor are shown. Improving the systems Q-factor results in an increasing logarithmic negativity and more entanglement in the output-modes. However, also increasing the systems coupling g will not automatically yield higher entanglement. In fact from fig. 3.16 one can learn that there indeed is a optimal region around $g = 0.2 - 0.8\omega_m$ for which a stronger optomechanical

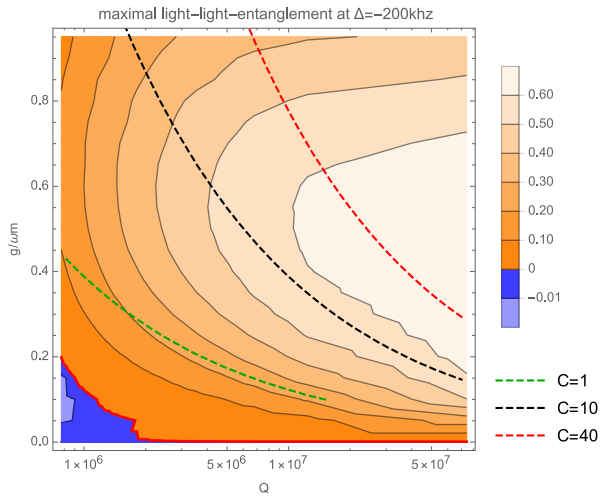

Figure 3.16: The logarithmic negativity as a function of the quality factor and coupling, the detuning of the driving-laser is given by $\Delta = -200kHz$, other system parameters are given in table 3.3. The solid red line indicates the border to logarithmic negativity below or equal zero. The dashed lines represent contours of equal cooperativites with $C = 1$ (green), $C = 10$ (black) and $C = 40$ (red).

coupling will not improve the logarithmic negativity significantly.
In addition, it is questionable to what extent the Q-factor can be increased in the experiment. In most cases the quality factor is given for a certain geometry of the mechanical system and the bath temperature, so that it can realistically only be improved by cooling the entire system.

This leads to the next parameter of interest namely the influence of the temperature T of the system characterized by the thermal occupation number $\bar{n}(T)$ as discussed in sec. A.1. The temperature of the system can be assumed to be at $T = 10$K ($\bar{n} \approx 1.76 \cdot 10^5$) which can be achieved helium cooling, using a dilution refrigerator might enable the experimentalists to even access regions below one Kelvin.
For further discussion the considered minimal thermal occupation will be at around $\bar{n}_{min} = 10^4$ which, for this oscillator, corresponds to approximately $T = 570$mK and a maximal value of $\bar{n}_{max} = 2 \cdot 10^5$ with $T = 11.3$K.
The plot generated by the program for this situation is presented in fig. 3.17. A lowering of the temperature allows to detect higher entanglement for smaller optomechanical coupling which can intuitively be understood by the decoherence time of the mechanical system. It is given by $(\bar{n}\gamma_m)^{-1}$ and improves with lower thermal occupation numbers. Therefore the system tends to lose its quantum correlations time-scales above this critical value.

As discussed and shown in detail in this chapter, the program allows the user to explore various relationships between entanglement and the parameters of the system. Starting with

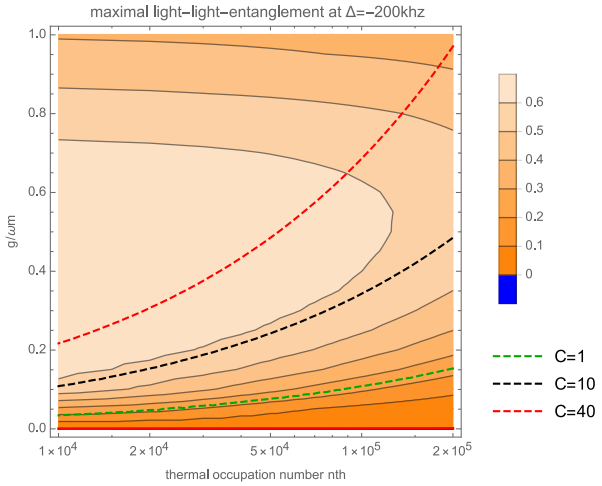

Figure 3.17: Plots of the logarithmic negativity as a function of the coupling and thermal occupation $\bar{n}$. The detuning is chosen to be $\Delta = -200kHz$, all other parameters are given in table 3.3. The solid red line indicates the border where the logarithmic negativity is found to be below zero, the dotted lines represent the systems cooperativity of $C = 1$ (green), $C = 10$ (black) and $C = 40$ (red).

the linearised QLE, it is now possible to study the steady-state dynamics of the optomechanical system in a very idealised situation. This makes the program particularly interesting for considerations before the actual experiment, or advantageous precise knowledge about entanglement regions without resorting to (usually time-consuming) simulations.

3.3 The two-sideband protocol

Up to now, only the lower-sideband in the pulse at early times and the upper-sideband at later times were correlated by the mode-functions $\alpha(t)$ and $\beta(t)$. This was argued by the fact that first the TMS-interaction generates the entanglement while the BS-interaction swaps the states between the mechanics and the intra-cavity light which is then mediated onto the output-field.
In reality, both processes take place at the very same time so that there also exists an upper-sideband in the earlier pulse and a lower one for later pulse times. Therefore only taking into account the correlations between those two pulses separated in time neglects effects of correlations between upper- and lower-sideband in the same pulse, this will be referred to as intra-pulse-correlations/entanglement from now on (see also sec. 5.8 in [HO17]). This leads to a decrease in entanglement detected in the system, in the extreme case it might be possible to even detect a non-entangled state while, with the two-sideband protocol, the state would be inseparable.
To improve the entanglement detection in the program, it is useful to define two more mode-functions which extract the contribution for the upper-sideband, due to the BS-interaction, in the earlier pulse and the lower-sideband, due to the TMS-interaction, in the later second pulse. All together, in this detection scheme the four mode functions are given by:

$$\begin{aligned} \alpha(t)_{\pm} &= \sqrt{2\Gamma} e^{\Gamma t} e^{\pm i\omega_m t} \qquad \textit{for } t \leq 0 \\ \beta(t)_{\pm} &= \sqrt{2\Gamma} e^{-\Gamma t} e^{\pm i\omega_m t} \qquad \textit{for } t \geq 0 \end{aligned} \tag{3.5}$$

The mode functions $\alpha(t)_-$ and $\beta(t)_+$ are the ones considered for the filtering of the lower-sideband and upper-sideband in the earlier and later pulses respectively as they were already introduced in sec. 2.2.1.
On the other side, $\alpha(t)_+$ and $\beta(t)_-$ extract the discussed contribution of the BS/TMS-interaction in the earlier/later pulses as discussed above, now enabling the program to detect intra-pulse correlations. Still, the newly introduced mode-functions need to satisfy the output-field bosonic commutation relation which effectively means they need to be orthogonormalised with respect to each other, the more precise argument is given in the appendix C.1.
For the mode functions in two different pulses, this is automatically given since they do not have a time-overlap, this means only the inter-pulse functions $\alpha(t)_+$ and $\alpha(t)_-$ as well as $\beta(t)_+$ and $\beta(t)_-$ need to be considered. This orthonormalization can be e.g. carried out by

the Gram-Schmidt process and yields for the new mode-functions $\alpha(t)_+$ and $\beta(t)_-$:

$$\begin{aligned} \alpha(t)_+ &= \frac{\sqrt{2\Gamma(\Gamma^2+\omega_m^2)}}{\omega_m} e^{\Gamma t}\left(e^{i\omega_m t} - \frac{\Gamma}{\Gamma - i\omega_m} e^{-i\omega_m t}\right) \qquad \textit{for } t \leq 0 \\ \beta(t)_- &= \frac{\sqrt{2\Gamma(\Gamma^2+\omega_m^2)}}{\omega_m} e^{-\Gamma t}\left(e^{-i\omega_m t} - \frac{\Gamma}{\Gamma - i\omega_m} e^{i\omega_m t}\right) \qquad \textit{for } t \geq 0 \end{aligned} \tag{3.6}$$

Now the mode functions $\{\ \alpha(t)_\pm, \beta(t)_\pm\}$ form an orthonormal set of functions with the scalar product $\langle f, g\rangle = \int_{-\infty}^{\infty} f(t)^* g(t) dt$, therefore also the bosonic commutation relation for the ouput-modes are satisfied. Unfortunately the newly introduced mode-functions lose their optimal shape of eq. 3.5, which, however, has to be accepted for the application of the already discussed analytical approach.

To pass the mode functions to the program and include them in the systems CM it is now also needed to evaluate the Fourier-transformations of the real and imaginary parts of the functions $\alpha(t)_+$ and $\beta(t)_-$ as discussed in 2.2.1. This will also yield informations about how the functions enter the matrix $\tilde{T}^{new}(\omega)$ from eq. 2.42 and how the polynomial $H_n(\omega)$ from eq. 2.46 needs to be adapted.
The filtering matrix $\tilde{T}_{ts}^{new}(\omega)$, which appears for the two-sideband protocol, is then a 10×10 matrix formed by the direct sum of:

$$\tilde{T}_{ts}^{new}(\omega) = \tilde{T}^{new}(\omega) \bigoplus \tilde{T}_{ts}(\omega) \tag{3.7}$$

With the matrix $\tilde{T}_{ts}(\omega)$:

$$\begin{pmatrix} \mathcal{F}\left[\mathrm{Re}(\alpha_+(-t))\right](\omega) & -\mathcal{F}\left[\mathrm{Im}(\alpha_+(-t))\right](\omega) & 0 & 0 \\ \mathcal{F}\left[\mathrm{Im}(\alpha_+(-t))\right](\omega) & \mathcal{F}\left[\mathrm{Re}(\alpha_+(-t))\right](\omega) & 0 & 0 \\ 0 & 0 & \mathcal{F}\left[\mathrm{Re}(\beta_-(-t))\right](\omega) & -\mathcal{F}\left[\mathrm{Im}(\beta_-(-t))\right](\omega) \\ 0 & 0 & \mathcal{F}\left[\mathrm{Im}(\beta_-(-t))\right](\omega) & \mathcal{F}\left[\mathrm{Re}(\beta_-(-t))\right](\omega) \end{pmatrix} \tag{3.8}$$

Also the matrices P and C in eq. 2.36, which account for the input-output relation of the intra-cavity light field, need to be extended to 10×4 matrices so that for the two-sideband

protocol the new matrices C_{ts} and P_{ts} arise in the following way:

$$C_{ts} = \begin{pmatrix} C \\ C' \end{pmatrix} \qquad P_{ts} = \begin{pmatrix} P \\ P' \end{pmatrix}$$
$$C' = \begin{pmatrix} 0 & 0 & \sqrt{\kappa} & 0 \\ 0 & 0 & 0 & \sqrt{\kappa} \\ 0 & 0 & \sqrt{\kappa} & 0 \\ 0 & 0 & 0 & \sqrt{\kappa} \end{pmatrix} \qquad P' = \frac{1}{\sqrt{\kappa}} \begin{pmatrix} 0 & 0 & 1 & 0 \\ 0 & 0 & 0 & 1 \\ 0 & 0 & 1 & 0 \\ 0 & 0 & 0 & 1 \end{pmatrix} \tag{3.9}$$

The final stems covariance matrix will then also be of dimension 10×10 with the new intra-pulse output-mode functions in the last four entries of the CM.

The two-sideband protocol in the program is once again tested via a zero coupling system and the ground-state cooling as in the case of the intra-cavity and output-field code. Also for this protocol the program correctly reproduces these effects, the result of the ground state cooling will not be discussed in more detail in here. The zero-coupling CM of the two-sideband protocol generated by the program with $\bar{n} = 1.76 \cdot 10^5$ and $g = 0$ is given in fig. 3.18, again the mechanics is found in a thermal state while all four light-modes end up in the shot-noise state since both systems only couple to their respective noise-channels.

$$\begin{pmatrix} \frac{352\,001}{2} & 0 & 0 & 0 & 0 & 0 & 0 & 0 & 0 & 0 \\ 0 & \frac{352\,001}{2} & 0 & 0 & 0 & 0 & 0 & 0 & 0 & 0 \\ 0 & 0 & \frac{1}{2} & 0 & 0 & 0 & 0 & 0 & 0 & 0 \\ 0 & 0 & 0 & \frac{1}{2} & 0 & 0 & 0 & 0 & 0 & 0 \\ 0 & 0 & 0 & 0 & \frac{1}{2} & 0 & 0 & 0 & 0 & 0 \\ 0 & 0 & 0 & 0 & 0 & \frac{1}{2} & 0 & 0 & 0 & 0 \\ 0 & 0 & 0 & 0 & 0 & 0 & \frac{1}{2} & 0 & 0 & 0 \\ 0 & 0 & 0 & 0 & 0 & 0 & 0 & \frac{1}{2} & 0 & 0 \\ 0 & 0 & 0 & 0 & 0 & 0 & 0 & 0 & \frac{1}{2} & 0 \\ 0 & 0 & 0 & 0 & 0 & 0 & 0 & 0 & 0 & \frac{1}{2} \end{pmatrix}$$

Figure 3.18: Zero coupling matrix ($g = 0$) in the two-sideband protocol with a thermal bath temperature $T = 10K$ and mechanical frequency $\omega_m = 2\pi \times 1.18$MHz so that $\bar{n} \approx 1.76 \times 10^5$. The mechanical system, represented by the first two diagonal entries, is found to be in a thermal state due to the coupling to the thermal bath. The four light modes only couple to the optical noise channel, this is also the reason why all modes are found around shot-noise state.

In the next plot, we compare the entanglement detected between the mechanical system and the first pulse as well as for both temporal pulses using the two-mode-protocol and the regular protocol introduced in the previous section 3.2. Defining and implementing two additionally mode functions, which extract the upper- and lower-sideband contribution in the

first and second pulse, helps to increase the entanglement found in both reduced systems as it can be seen in fig. 3.19. Shown is the logarithmic negativity as a function of the pulse width for the two-sideband- as well as for the "single-sideband"-protocol as formulated in sec. 3.2. All points which are plotted in circles represent the entanglement between the earlier pulse and the mechanical system. The dots on the other side give the entanglement between the two temporal pulses. Once again the logarithmic negativity was used as measure of entanglement, red colour refers to the single-sideband evaluation as performed in the former section, the black colour represents the two-sideband protocol.
The entanglement found in the two-sideband protocol is always larger or equal to the one found without using the additional mode functions. Expanding the program onto the two-sideband protocol now allows one to find a wider pulse-regime for light-mechanics and light-light entanglement as for the single-sideband case. The logarithmic negativity for the mechanical system and the earlier temporal pulse is positive (and therefore the systems are entangled) for $\Gamma > 7 \cdot 10^4 \text{rad} \cdot \text{Hz}$ while in the single-sideband protocol the same holds for pulse widths $\Gamma > 10^5 \text{rad} \cdot \text{Hz}$. Also for the entanglement shared between the earlier and the later temporal pulse the detection range increases from $\Gamma > 3 \cdot 10^5 \text{rad} \cdot \text{Hz}$ in the single-sideband scenario to $\Gamma > 10^5 \text{rad} \cdot \text{Hz}$ in the two-sideband protocol. Additionally, there is no dip of the logarithmic negativity observed as in light-light entanglement as in the single-sideband protocol.

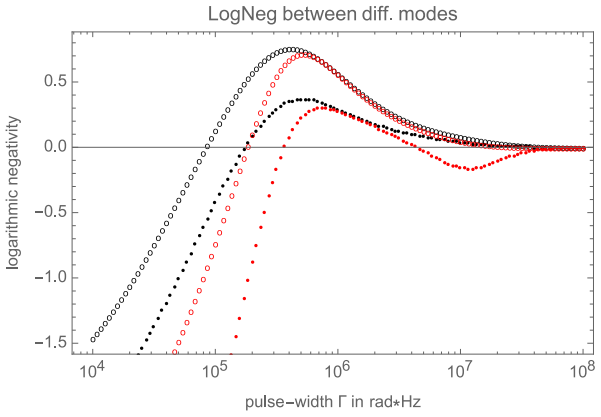

Figure 3.19: Logarithmic negativity in dependence of the pulse width Γ plotted for the system formed by the mechanics and earlier pulse in the two-sideband (black circles) and single-sideband protocol (red circles). Also included in this plot is the reduced system of the earlier and later pulse (black dots for two-sideband evaluation and red dots for single sideband evaluation). As for the plots before, the parameters from table 3.3 where used.

As we have seen in this section it is indeed possible to increase the detectable entanglement for the reduced system of the mechanical oscillator and the earlier temporal pulse as well as for the system of the two distinct temporal pulses by introducing proper additional mode

functions and therefore also account for intra-pulse non-classical correlations.
Moreover, we are also able to detect entangled states in this two-sideband protocol where using the single-sideband evaluation from the former section 3.2 would have detected a separable state.

Chapter 4

Conclusion and outlook

In this work it was shown that, starting from the linearised quantum Langevin equations, it is possible to find the steady-state covariance matrix of an optomechanical system, consider the intra-cavity field as well as a special filtered output-light field and to extract the entanglement shared between the various parties. This is done without any further approximation and in a completely analytical way such that the results of the proposed program can be considered exact.
In addition, a "two-sideband"-protocol was proposed which can be incorporated into the code without major complications and leads to an increase in the detected entanglement in the system.

Using this code it was possible to study the experiment currently running at the University of Vienna. As it was shown in the last chapter, with the help of the program the dependence of the occurring entanglement on the different systems parameters can be studied.
As shown in section 3.2, a higher red-detuning and power (which also increases the coupling strength of the optomechanical interaction) of the drive-laser might be a simple adaptation in terms of experimental realisation to increase the detectable entanglement for the two temporally separated pulses. Especially for higher cooperativity, and therefore also for a sufficiently high coupling strength, choosing the right detuning of the drive-laser also increases the values of the logarithmic negativity in the system and therefore also the entanglement stored.
While it is probably more tedious from the experimental side, reducing the temperature of the systems environment as well as improving the mechanical quality factor clearly has positive effects on the maximal entanglement in the system. In this cases it is also possible to find an optimal coupling strength.

The proposed scheme for finding the systems steady state dynamics has some interesting

advantages, for example it could be used before realising the actual experiment for scanning a wide variety of parameter regimes to get an initial impression of the entanglement in the system as well as the numerical values of the necessary parameters. Moreover, the computational time needed for this program is short compared to the simulations currently used in the running experiment.
One of the disadvantages is clearly that the whole scheme works only for an idealised experiment e.g. no losses in the detection are modelled, furthermore classical noise is completely neglected.

In addition to this, we also considered an oscillator where only one mechanical mode takes part in the optomechanical interaction, but it might be interesting for future applications of the program to implement multiple modes which show no interaction among themselves. Having a multi-mode mechanical system and neglecting some of the modes in the final entanglement detection might leave the user unable to detect non-classical correlations even if they are present in the first place [HO17, see sec. 5.7].
Let us consider two non-interacting modes in order to give a rough idea of the expansion to multi-mode structures.In this case, the form of eq. 2.1 changes slightly since one has to also account for another mechanical mode so that:

$$\begin{aligned}
\dot{\mathbf{X}}(t) &= A\mathbf{X}(t) + \mathbf{N}(t) \\
\mathbf{X}(t) &= \left(\hat{X}_{m1}(t), \hat{P}_{m1}(t), \hat{X}_{m2}(t), \hat{P}_{m2}(t), \hat{X}_c(t), \hat{P}_c(t)\right)^T \\
\mathbf{N}(t) &= \left(0, \sqrt{2\gamma_{m1}}\hat{f}(t), 0, \sqrt{2\gamma_{m2}}\hat{f}(t), \sqrt{\kappa}\hat{X}_{in}(t), \sqrt{\kappa}\hat{P}_{in}(t)\right)^T \\
A &= \begin{pmatrix}
0 & \omega_{m1} & 0 & 0 & 0 & 0 \\
-\omega_{m1} & -\gamma_{m1} & 0 & 0 & -2g_1 & 0 \\
0 & 0 & 0 & \omega_{m2} & 0 & 0 \\
0 & 0 & -\omega_{m2} & -\gamma_{m2} & -2g_2 & 0 \\
0 & 0 & 0 & 0 & -\frac{\kappa}{2} & -\Delta \\
-2g_1 & 0 & -2g_2 & 0 & \Delta & -\frac{\kappa}{2}
\end{pmatrix}
\end{aligned} \tag{4.1}$$

The indices $\{m1, m2\}$ correspond to the first and second modes of the mechanical system. Both modes couple to the intra-cavity light-field by the, in general different, couplings g_1 and g_2. This change in matrix A has consequences for all other variables and matrices discussed in sec. 2.1 and 2.2, only the most important are discussed here.
One of those consequences can be observed on the noise-correlation matrix D given in eq.

2.12, since the additional mechanical mode completely loses its diagonal shape:

$$D = \begin{pmatrix} 0 & 0 & 0 & 0 & 0 & 0 \\ 0 & \gamma_{m1}(2\bar{n}+1) & 0 & \sqrt{\gamma_{m1}\gamma_{m2}}(2\bar{n}+1) & 0 & 0 \\ 0 & 0 & 0 & 0 & 0 & 0 \\ 0 & \sqrt{\gamma_{m1}\gamma_{m2}}(2\bar{n}+1) & 0 & \gamma_{m2}(2\bar{n}+1) & 0 & 0 \\ 0 & 0 & 0 & 0 & \frac{\kappa}{2} & 0 \\ 0 & 0 & 0 & 0 & 0 & \frac{\kappa}{2} \end{pmatrix} \tag{4.2}$$

The matrix $M(\omega)$ from eq. 2.11 and the polynomial $Q(\omega)$ from eq. 2.16 will be defined the very same way as for the initial intra-cavity system as discussed in sec. 2.1 so that with those small adaptations the intra-cavity field can be generated in the multi-mode case.

For the output field, however, the situation is not as trivial and simple as for the intra-cavity field. First, new mode-functions must be introduced which filter the lower- and upper-sideband for each mechanical mode in the first and second pulse. In the situation of two mechanical modes, this means two additional mode-functions, one for the lower-sideband in the earlier, and one for the upper-sideband in the later one. For the output-field-modes to obey the bosonic commutation-relation, the mode functions must form an orthonormal set, this will lead to a non-idealized form of at least two, temporal separated, mode functions as already discussed in sec. C.1.
Should it then be of further interest to implement a two-sideband protocol, then two intra-pulse filter functions must be defined for each mechanical mode, increasing the size of the systems CM onto a 20×20-matrix, the integration scheme behind this program would not change at all, but the computing time would be higher than for the simple case of a single-mode system.
In general, for m non-interacting mechanical modes, the final CM will be of the dimension $6m \times 6m$ without using the two-sideband protocol, including the intra-pulse correlations this increases to $10m \times 10m$ dimensions.
From a theoretical point of view, based on enough computing power and time, there is nothing against the implementation, testing and application of a multi-mode program.

Finally, it should be noted that it still requires further testing e.g. by computing power spectral densities of the output light quadratures and comparing the results with theoretical predictions. This should prove that the program reproduces the correct CMs and right physical effects, even though the zero-coupling and ground-state cooling test we applied to it in the last chapter were already promising.
Once fully tested it might be interesting for a larger optomechanics community to make the

presented program publicly available.

Appendix

A Appendix to "Theory"

A.1 Important Gaussian states and symplectic transformations

The simplest Gaussian state probably is the N-mode vacuum state $|0\rangle = \otimes_{i=1}^{N} |0_k\rangle$ (note that all other number states in general are not Gaussian) whose CM can be calculated straight forwardly from its definition in 1.9.This is also one of the states which yields an equality in 1.11 and 1.13:

$$\sigma_{|0\rangle} = \oplus_{i=1}^{N} \frac{1}{2} \begin{pmatrix} 1 & 0 \\ 0 & 1 \end{pmatrix} \tag{A.1}$$

Another state of great interest is the state at thermal equilibrium with temperature T of a single mode described by the density matrix $\rho(\bar{n})$ where $\bar{n} = Tr(\rho \hat{a}^\dagger \hat{a})$ is the mean thermal excitation number in the specific mode with frequency ω. Also in this case, the CM follows directly from 1.9

$$\begin{aligned} \bar{n} &= \left(e^{\hbar\omega / k_b T} - 1 \right)^{-1} \\ \rho(\bar{n}) &= \sum_{n=0}^{\infty} \frac{\bar{n}^n}{(1+\bar{n})^{1+n}} |n\rangle \langle n| \\ \sigma_{Th} &= \frac{2\bar{n}+1}{2} \begin{pmatrix} 1 & 0 \\ 0 & 1 \end{pmatrix} \end{aligned} \tag{A.2}$$

This can also easily be expanded to the multi-mode thermal state.
The action of an ideal (phase free) beam-splitter on two modes is described by the symplectic transformation

$$S(\theta)_{BS} = \begin{pmatrix} \cos\theta & 0 & \sin\theta & 0 \\ 0 & \cos\theta & 0 & \sin\theta \\ \sin\theta & 0 & -\cos\theta & 0 \\ 0 & \sin\theta & 0 & -\cos\theta \end{pmatrix} \tag{A.3}$$

where θ determines the transitivity of the beam-splitter, for example $\theta = \pi/4$ corresponds to a *50:50*-beam-splitter.

The action of the two-mode-squeezing operator with squeezing parameter $\zeta = re^{i\theta}$ is represented by the symplectic transformation

$$S(\zeta)_{TMS} = \begin{pmatrix} \cosh r & 0 & -\cos\theta \sinh r & \sin\theta \sinh r \\ 0 & \cosh r & \sin\theta \sinh r & -\cos\theta \sinh r \\ -\cos\theta \sinh r & \sin\theta \sinh r & \cosh r & 0 \\ \sin\theta \sinh r & \cos\theta \sinh r & 0 & \cosh r \end{pmatrix} \tag{A.4}$$

By applying the two-mode-squeezing symplectic transformation onto the CM of the two-mode vacuum state $\sigma_{|00\rangle}$ it is possible to generate the CM of the two-mode squeezed state σ_{TMS}

$$\sigma(\zeta)_{TMS} = S(\zeta)^T_{TMS}\sigma_{|00\rangle}S(\zeta)_{TMS} = \frac{1}{2}\begin{pmatrix} \cosh 2r & 0 & -\cos\theta \sinh 2r & \sin\theta \sinh 2r \\ 0 & \cosh 2r & \sin\theta \sinh 2r & \cos\theta \sinh 2r \\ -\cos\theta \sinh 2r & \sin\theta \sinh 2r & \cosh 2r & 0 \\ \sin\theta \sinh 2r & \cos\theta \sinh 2r & 0 & \cosh 2r \end{pmatrix} \tag{A.5}$$

A.2 Logarithmic negativity in covariance matrix formalism

The negativity $\mathcal{N}(\sigma)$ of a CM σ as well as the logarithmic negativity $E_{\mathcal{N}}(\sigma)$ can be formulated in a practical and easy to calculate way using the symplectic eigenvalues $\tilde{\lambda}_j$ of the partial transpose of the CM defined in 1.16:

$$\begin{aligned} \mathcal{N}(\sigma) &= \begin{cases} \frac{1}{2}\prod_j \left(\tilde{\lambda}_j^{-1} - 2\right) & \text{for } j : \tilde{\lambda}_j < \frac{1}{2} \\ 0 & \text{if } \forall j : \tilde{\lambda}_j \geq \frac{1}{2} \end{cases} \\ E_{\mathcal{N}}(\sigma) &= \begin{cases} -\sum_j \log(2\tilde{\lambda}_j) & \text{for } j : \tilde{\lambda}_j < \frac{1}{2} \\ 0 & \text{if } \forall j : \tilde{\lambda}_j \geq \frac{1}{2} \end{cases} \end{aligned} \tag{A.6}$$

For this work we will relax the last condition for the logarithmic negativity which will allow us to get a feeling of how far away the state is from being entangled.
Especially for a two-mode Gaussian state, since the numbers of eigenvalues N_{NPT} which violate 1.17 is bounded from above by $N_{NPT} = \min(N_A, N_B)$, the only possible existing eigenvalue with $\tilde{\lambda}_- < \frac{1}{2}$ can be computed by the invariants of the CM $\det(\sigma)$ and $\Delta(\sigma)$ [AIDS03]:

$$\tilde{\lambda}_- = \frac{1}{\sqrt{2}}\sqrt{\Delta(\sigma) - \sqrt{\Delta(\sigma)^2 - 4\det(\sigma)}} \tag{A.7}$$

A.3 Linearised QLE and important relations

$$
\begin{aligned}
\langle \hat{f}(t)\hat{f}(t+\tau) + \hat{f}(t+\tau)\hat{f}(t)\rangle \simeq (2\bar{n}+1)\delta(\tau) \qquad \langle \hat{f}(t)\rangle = 0 \\
\left[\hat{a}_{in}(t), \hat{a}_{in}^{\dagger}(t+\tau)\right] = \delta(\tau) \qquad \left[\hat{a}_{in}^{\dagger}(t), \hat{a}_{in}(t+\tau)\right] = 0 = \langle \hat{a}_{in}^{\dagger}(t)\hat{a}_{in}(t+\tau)\rangle \\
\hat{a}_{out}(t) = \sqrt{\kappa}\hat{a}(t) - \hat{a}_{in}(t) \\
g_0 = \frac{\omega_c x_{zp}}{L} \qquad g = \frac{g_0\alpha}{\sqrt{2}} \\
\Delta_0 = \omega_0 - \omega_c \qquad \Delta = \left(\Delta_0 - \frac{g_0}{\sqrt{2}}(\beta+\beta^*)\right) \\
\hat{H}_{lin} = -\hbar\Delta\hat{a}^{\dagger}\hat{a} + \hbar\omega_m\hat{b}^{\dagger}\hat{b} + \hbar g(\hat{b}^{\dagger}+\hat{b})(\hat{a}^{\dagger}+\hat{a}) \\
\dot{\hat{X}}_m = \omega_m\hat{P}_m \\
\dot{\hat{P}}_m = -\omega_m\hat{X}_m - \gamma_m\hat{P}_m - 2g\hat{X}_c + \sqrt{2\gamma_m}\hat{f} \\
\dot{\hat{X}}_c = -\frac{\kappa}{2}\hat{X}_c - \Delta\hat{P}_c + \sqrt{\kappa}\hat{X}_{in} \\
\dot{\hat{P}}_c = -\frac{\kappa}{2}\hat{P}_c + \Delta\hat{X}_c - 2g\hat{X}_m + \sqrt{\kappa}\hat{P}_{in}
\end{aligned}
\tag{A.8}
$$

A.4 Ground state-cooling of the mechanical system

As already discussed in section 1.4.2 the optomechanical coupling of the mechanical and optical system gives rise to the Hamiltonian $\hat{H}_{lin}$ (see also A.8). This new Hamiltonian shows a TMS- and BS-interaction which can be enhanced or suppressed by a proper choice of the laser detuning.

Choosing a red-detuning on the one side will suppress the direct transition from a state $|0,m\rangle \rightarrow |1,m\rangle$ and the one which adds a phonon to the mechanical system $|0,m\rangle \rightarrow |0,m+1\rangle$ as illustrated in fig. A.1. On the other side, the BS-interaction is enhanced and therefore the initial state is brought from $|0,m\rangle \rightarrow |1,m-1\rangle$.Because of the finite decay rate $\kappa \ll \omega_m$ of the cavity this state decays to $|0,m-1\rangle$ and a photon shifted to higher frequencies by ω_m will leave the cavity effectively cooling the system. This effect can even be used to cool the mechanics down to its ground state.

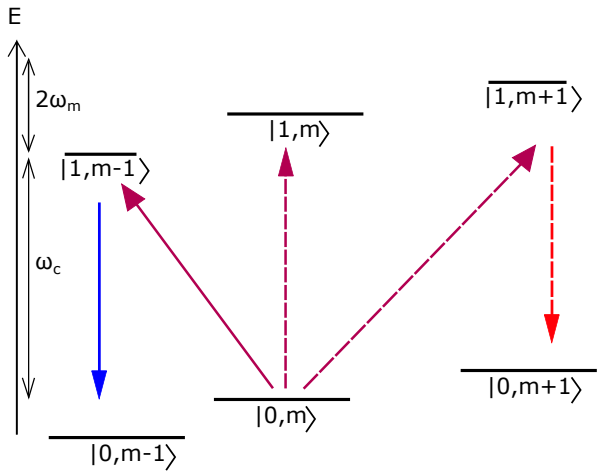

Figure A.1: Level diagram of groundstate cooling where $|0,m\rangle = |0\rangle_c |m\rangle_m$ represents a state with zero photons in the optics and m excitations in the mechanical system . The transitions, in here the direct transition $|0,m\rangle \rightarrow |1,m\rangle$ and the one mediated by the TMS-interaction $|0,m\rangle \rightarrow |0,m+1\rangle$, represented by dotted lines are suppressed due to the red-detuning of the laser while the one coming from the BS-interaction $|0,m\rangle \rightarrow |1,m-1\rangle$ is enhanced. Due to the finite decay rate κ of the cavity, this state will decay and emit one photon of energy $\hbar\omega_c$, effectively lowering the phonon number in the mechanical system to a state $|0,m-1\rangle$.

B Appendix to "Solving the QLE"

B.1 Ruth-Hurwitz-criterion and matrices

The Ruth-Hurwitz criterion states that for a $n \times n$- matrix to have eigenvalues with negative real parts, the corresponding $1,...,n$ Hurwitz matrices will have positive determinants. The criterion is discussed in here by using the matrix A defined in eq. 2.2, lets consider its characteristic polynomial

$$\chi_A(\lambda) = \det(A - \lambda \mathbb{1}_4) = a_0\lambda^4 + a_1\lambda^3 + a_2\lambda^2 + a_3\lambda + a_4 \tag{B.1}$$

Here we assume that $a_0 \neq 0$ and that all coefficients are real numbers which can be easily checked. The Hurwitz-matrices are given by [Hof15, see appendix B.4]

$$\begin{aligned} H(n)_{ij} &= a_{2i-j} \qquad 1 \leq i,j \leq n \\ H(n)_{ij} &= 0 \qquad j > 2i \\ \textit{eigenvalues of } A \textit{ have negative real parts} &\Leftrightarrow \det(H(n)) > 0 \qquad \forall n \leq 4 \end{aligned} \tag{B.2}$$

The four Hurwitz-matrices which need to be consider in the case of matrix A are given by:

$$\begin{aligned} H(1) &= a_1 \\ H(2) &= \begin{pmatrix} a_1 & a_0 \\ a_3 & a_2 \end{pmatrix} \\ H(3) &= \begin{pmatrix} a_1 & a_0 & 0 \\ a_3 & a_2 & a_1 \\ 0 & a_4 & a_3 \end{pmatrix} \\ H(4) &= \begin{pmatrix} a_1 & a_0 & 0 & 0 \\ a_3 & a_2 & a_1 & a_0 \\ 0 & a_4 & a_3 & a_2 \\ 0 & 0 & 0 & a_4 \end{pmatrix} \end{aligned} \tag{B.3}$$

The stability of the system is then given if the determinants of all Hurwitz-matrices are positive, in this case the real parts of the corresponding eigenvalues of A will have negative values which is needed for reaching the systems steady state:

$$\textit{eigenvalues of A have negative real parts} \Leftrightarrow \det(H(n)) > 0 \qquad \forall n \leq 4 \tag{B.4}$$

For the first two Hurwitz-matrices, the criterion is automatically fulfilled so that only the determinants of $H(3)$ and $H(4)$ need to be considered. The determinants are given by:

$$\begin{aligned} &\det(H(3)) = \\ &\gamma_m\kappa\left(\left[\frac{\kappa^2}{4}+(\omega_m+\Delta)^2\right]\left[\frac{\kappa^2}{4}+(\omega_m-\Delta)^2\right]+\gamma_m\left[(\gamma_m+\kappa)(\frac{\kappa^2}{4}+\Delta^2)\right]+\kappa\omega_m^2\right) \\ &-4\Delta\omega_m g^2(\gamma_m+\kappa)^2 > 0 \\ &\det(H(4)) = \det(H(3))\left[\omega_m^2\left(\frac{\kappa^2}{4}+\Delta^2\right)-4g^2\Delta\omega_m\right] > 0 \end{aligned} \tag{B.5}$$

This can be reduced to two conditions for the stability of the system since the determinant of the third Hurwith-matrix appears in the determinant of the fourth one:

$$\begin{aligned} &\gamma_m\kappa\left(\left[\frac{\kappa^2}{4}+(\omega_m+\Delta)^2\right]\left[\frac{\kappa^2}{4}+(\omega_m-\Delta)^2\right]+\gamma_m\left[(\gamma_m+\kappa)(\frac{\kappa^2}{4}+\Delta^2)\right]+\kappa\omega_m^2\right) \\ &-4\Delta\omega_m g^2(\gamma_m+\kappa)^2 > 0 \\ &\omega_m\left(\frac{\kappa^2}{4}+\Delta^2\right)+4g^2\Delta > 0 \end{aligned} \tag{B.6}$$

B.2 Derivation of the noise-correlation matrix and its Fourier-transformation

It is of interest to study the noise-correlations which arise in section 2.1.1 in eq. 2.5 in more detail. The vector $\mathbf{N}(t) = \left(0, \sqrt{2\gamma_m}\hat{f}(t), \sqrt{\kappa}\hat{X}_{in}(t), \sqrt{\kappa}\hat{P}_{in}(t)\right)^T$ contains the noise-operators which appear in the final linearised QLE equations as summarized in sec. A.3. The different noise-channels coming from the thermal bath of the mechanical oscillator $\hat{f}(t)$ as well as the optical noise characterised by $\hat{X}_{in}$ and $\hat{P}_{in}$ do not show any correlations.
In addition to this, there is no correlation observed for the different optical noise-quadratures, for simplicity only terms which have non-zero correlators will be kept in this derivation:

$$\begin{aligned} \langle \hat{X}_{in}(t)\hat{P}_{in}(t') + \hat{P}_{in}(t')\hat{X}_{in}(t)\rangle = \\ \frac{i}{2}\langle \hat{a}_{in}(t)\hat{a}^\dagger_{in}(t') - \hat{a}_{in}(t')\hat{a}^\dagger_{in}(t)\rangle = 0 \end{aligned} \tag{B.7}$$

But the optical noise-quadratures as well as the mechanical noise-operator $\hat{f}(t)$ are indeed self correlated, using the relations summarized in A.3 this yields

$$\begin{aligned} \langle \hat{X}_{in}(t)\hat{X}_{in}(t') + \hat{X}_{in}(t')\hat{X}_{in}(t)\rangle = ... = \\ \frac{1}{2}\langle \hat{a}_{in}(t)\hat{a}^\dagger_{in}(t') + \hat{a}_{in}(t')\hat{a}^\dagger_{in}(t)\rangle = \delta(t-t') \\ \langle \hat{P}_{in}(t)\hat{P}_{in}(t') + \hat{P}_{in}(t')\hat{P}_{in}(t)\rangle = ... = \\ \frac{i^2}{2}\langle -\hat{a}_{in}(t)\hat{a}^\dagger_{in}(t') - \hat{a}_{in}(t')\hat{a}^\dagger_{in}(t)\rangle = \delta(t-t') \\ \langle \hat{f}(t)\hat{f}(t') + \hat{f}(t')\hat{f}(t)\rangle \simeq (2\bar{n}+1)\delta(t-t') \end{aligned} \tag{B.8}$$

For the last relation we used the approximation discussed in 1.34 assuming hight temperatures such that $k_b T \gg \hbar\omega_m$ as well as high quality factors.
In this derivation we modelled the noise to be Markovian which means that the thermal bath as well as the optical noise-channel behave as if they have no memory of previous times. These results can now be used to construct the noise-correlation matrix as it will be used throughout this work (see eq. 2.5):

$$\begin{aligned} \frac{\langle N_i(t)N_j(t') + N_j(t')N_i(t)\rangle}{2} = D_{ij}\delta(t-t') \\ D = \mathrm{diag}\left(0, \gamma_m(2\bar{n}+1), \frac{\kappa}{2}, \frac{\kappa}{2}\right) \end{aligned} \tag{B.9}$$

Within our approximations, the different noise-channels are strictly uncorrelated and even cross-correlation between the optical noise-quadratures vanish. Alone this allows us to apply the discussed method of finding the solution to the QLE in sec. 2 and is therefore the centre of the whole approach in this thesis.

The found relations can be used as a starting point for the derivation of the Fourier-transformed noise-correlation operator as it is used for the discussion in sec. 2.1.2

$$\begin{aligned} \frac{\langle \tilde{N}_i(\omega)\tilde{N}_j(\omega') + \tilde{N}_j(\omega')\tilde{N}_i(\omega)\rangle}{2} = \\ \frac{1}{2\pi}\iint_{\mathbb{R}^2} dt'dt e^{-i\omega t}e^{-i\omega' t'}\frac{\langle N_i(t)N_j(t') + N_j(t')N_i(t)\rangle}{2} = \\ \frac{1}{2\pi}\iint_{\mathbb{R}^2} dt'dt e^{-i\omega t}e^{-i\omega' t'}D_{ij}\delta(t-t') = \frac{1}{2\pi}\int_{\mathbb{R}} dt e^{-i(\omega+\omega')t}D_{ij} = \\ \delta(\omega+\omega')D_{ij} \end{aligned} \tag{B.10}$$

B.3 Integrals over rational functions

An integral over rational functions of the form:

$$\int_{-\infty}^{\infty} \frac{g_n(x)}{h_n(x)h_n(-x)}dx \tag{B.11}$$

with the two polynomials:

$$h_n(x) = a_0x^n + a_1x^{n-1} + ... + a_n \qquad g_n(x) = b_0x^{2(n-1)} + b_1x^{2(n-2)} + ... + bn - 1 \tag{B.12}$$

can be solved by using Hurwitz-matrices of the polynomial $h_n(x)$. One condition for these schemes to be successfully applied is that the roots of the polynomial need to lie in the upper-half of the complex-plane so that the path of integration C closes all poles in this plane [GR80], this is illustrated in fig. B.1.

The other condition on the polynomials states that the polynomial $g_n(x)$ is of order $2n-1$ at most, it can even contain lower odd powers since they will not contribute in the final integral.

If the two conditions are satisfied, the integral can be solved by using the nth Hurwitz matrix

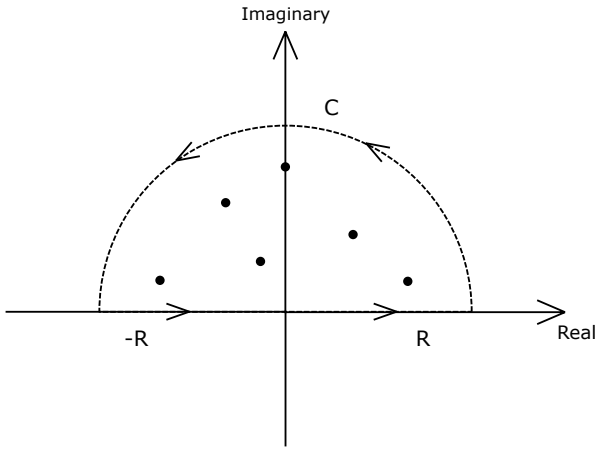

Figure B.1: In order to apply the discussed Integration scheme, all roots of the polynomial $h_n(x)$, illustrated by black dots, need to lie in the upper-half complex-plane. The integration path is given by the semicircle C with radius R, in the limit of $R \to \infty$ the integral approaches zero [HJ47, sec. 7.9] and therefore has no contribution to the final results.

$H_h(n)$ of $h(x)$ as defined in B.2 (see also [HJ47, Hof15]):

$$\begin{aligned} \Delta_n = \det(H_h(n)) &= \begin{vmatrix} a_1 & a_0 & 0 & \cdots \\ a_3 & a_2 & a_1 & \cdots \\ a_5 & a_4 & a_3 & \cdots \\ \vdots & \vdots & \vdots & \vdots \end{vmatrix} \\ \Lambda_n &= \begin{vmatrix} b_0 & a_0 & 0 & \cdots \\ b_1 & a_2 & a_1 & \cdots \\ b_2 & a_4 & a_3 & \cdots \\ \vdots & \vdots & \vdots & \vdots \end{vmatrix} \\ I_n = \int_{-\infty}^{\infty} \frac{g_n(x)}{h_n(x)h_n(-x)} dx &= \frac{i\pi(-1)^{n+1}\Lambda_n}{a_0\Delta_n} \end{aligned} \tag{B.13}$$

The second variable Λ_n is found by substituting the first column of $H_h(n)$ by the coefficients of the polynomial $g_n(x)$.
For a clearer understanding, the results for the integrals for polynomials $h_n(x)$ with $n \leq 3$ and any general polynomial $g_n(x)$ is presented:

$$\begin{aligned} I_1 = \int_{-\infty}^{\infty} \frac{g_1(x)}{h_1(x)h_1(-x)} dx &= \frac{i\pi b_0}{a_0 a_1} \\ I_2 = \int_{-\infty}^{\infty} \frac{g_2(x)}{h_2(x)h_2(-x)} dx &= \frac{i\pi(a_0 b_1 - b_0 a_2)}{a_2 a_1 a_0} \\ I_3 = \int_{-\infty}^{\infty} \frac{g_3(x)}{h_3(x)h_3(-x)} dx &= i\pi \frac{(a_0 b_1 - b_0 a_2)a_3 - a_0 a_1 b_2}{(a_0 a_3 - a_2 a_1)a_0 a_3} \end{aligned} \tag{B.14}$$

C Appendix to "The program"

C.1 Orthonormalization in the two-sideband protocol

In the two-sideband protocol, in order to encounter for correlations between lower and upper sidebands in each of the temporal pulses, the following mode functions were introduced

$$\begin{aligned} \alpha(t)_{\pm} &= \sqrt{2\Gamma} e^{\Gamma t} e^{\pm i\omega_m t} \qquad \textit{for } t \leq 0 \\ \beta(t)_{\pm} &= \sqrt{2\Gamma} e^{-\Gamma t} e^{\pm i\omega_m t} \qquad \textit{for } t \geq 0 \end{aligned} \tag{C.1}$$

These mode functions are then applied to the output-mode operator $\hat{a}_{out}$ so that the following filtered output-modes arise

$$\begin{aligned} \hat{a}_{out}^{\alpha_{\pm}}(t) &= \int_{-\infty}^{t} dt' \alpha_{\pm}(t'-t) \hat{a}_{out}(t') \\ \hat{a}_{out}^{\beta_{\pm}}(t) &= \int_{t}^{\infty} dt' \beta_{\pm}(t'-t) \hat{a}_{out}(t') \end{aligned} \tag{C.2}$$

However, to use the introduced tools of covariance matrices to detect the shared entanglement, the bosonic commutation relations for those new output modes need to be fulfilled meaning that

$$\begin{aligned} \left[\hat{a}_{out}^{\alpha_{\pm}}(t), \hat{a}_{out}^{\alpha_{\mp}}(t)^{\dagger}\right] &= 0 \\ \left[\hat{a}_{out}^{\beta_{\pm}}(t), \hat{a}_{out}^{\beta_{\mp}}(t)^{\dagger}\right] &= 0 \\ \left[\hat{a}_{out}^{\alpha_{\pm}}(t), \hat{a}_{out}^{\alpha_{\pm}}(t)^{\dagger}\right] = \left[\hat{a}_{out}^{\beta_{\pm}}(t), \hat{a}_{out}^{\beta_{\pm}}(t)^{\dagger}\right] &= 1 \end{aligned} \tag{C.3}$$

Please note that all other commutation relation which are automatically satisfied are not shown in here, e.g. the ones between output-modes of the different temporal pulses due to the non-temporal overlap of the mode functions.
The consequences on the mode functions can be illustrated on the example of $\left[\hat{a}_{out}^{\alpha_{+}}(t), \hat{a}_{out}^{\alpha_{-}}(t)^{\dagger}\right]$ as well as $\left[\hat{a}_{out}^{\alpha_{+}}(t), \hat{a}_{out}^{\alpha_{+}}(t)^{\dagger}\right]$ and can be extended to all other mode functions with same argu-

ment

$$\begin{aligned}
\left[\hat{a}_{out}^{\alpha_+}(t), \hat{a}_{out}^{\alpha_-}(t)^\dagger\right] &= \iint_{\mathbb{R}^2} dt_1 dt_2 \alpha_+(t_1 - t)\alpha_-^*(t_2 - t) \underbrace{\left[\hat{a}_{out}(t_1), \hat{a}_{out}^\dagger(t_2)\right]}_{\delta(t_1 - t_2)} = \\
&\int_{-\infty}^{t} dt_1 \alpha_+(t_1 - t)\alpha_-^*(t_1 - t) \stackrel{!}{=} 0 \\
\left[\hat{a}_{out}^{\alpha_+}(t), \hat{a}_{out}^{\alpha_+}(t)^\dagger\right] &= \iint_{\mathbb{R}^2} dt_1 dt_2 \alpha_+(t_1 - t)\alpha_+^*(t_2 - t) \underbrace{\left[\hat{a}_{out}(t_1), \hat{a}_{out}^\dagger(t_2)\right]}_{\delta(t_1 - t_2)} = \\
&\int_{-\infty}^{t} dt_1 |\alpha_+(t_1 - t)|^2 \stackrel{!}{=} 1
\end{aligned} \tag{C.4}$$

Therefore the mode functions $\{\, \alpha(t)_\pm, \beta(t)_\pm \}$ must form a set of orthonormal functions using the scalar product $\langle f, g \rangle = \int_{-\infty}^{\infty} f(t)^* g(t) dt$. This orthonormalisation can now be carried out by the Gram-Schmidt process, however one will lose the optimal shape of eq. C.1 of the two mode functions $\alpha_-(t)$ and $\beta_+(t)$.

Abstract

The motivation behind my master thesis is to gain a clear theoretical insight into the currently running experiment at the University of Vienna within the research group of Univ.-Prof. Dr. Markus Aspelmeyer for the generation and detection of CV entanglement in optomechanical systems [HO17].
In this experiment, non-classical correlations between the light field and the mechanical component of an optomechanical structure are to be demonstrated. Since the mechanical component of the experiment is difficult to access for detection, this type of correlations is detected via two temporally separated pulses in the light field emerging from the cavity, whereby the state of the mechanical subsystem is be transferred to the light field by the optomechanical interaction.

In the first part of my work, we consider an optomechanical system consisting of a Fabry-Pérot cavity wiht a moving end mirror. We are especially interested in the interaction between the optical and the mechanical subsystem, which are described by the linearised quantum Langevin equations (QLE).
In the second part of my thesis, I present a way to analytically solve the obtained linearised QLE for the steady state of the system. In addition to this, I discuss the application of two filter functions to the emerging light field, which makes it possible to define two temporally separated modes corresponding to the pulses in the actual experiment and to explore their entanglement.

All discussed aspects will ultimately culminate in the implementation of a program which allows the user to generate the covariance matrices for different constellations of subsystems. With the help of this program, influences of different parameters on the entanglement in the system of the above mentioned experiment will be studied that enable predictions for optimal experimental parameters.

Zusammenfassung

Die Motivation hinter meiner Masterarbeit ist es einen klaren theoretischen Einblick in das gerade laufende Experiment an der Universität Wien innerhalb der Arbeitsgruppe von Univ.-Prof. Dr. Markus Aspelmeyer zur Erzeugung und Detektion von CV Verschränkung in optomechanischen Systemen [HO17] zu erhalten.
In diesem Experiment sollen nicht-klassische Korrelationen zwischen Lichtfeld und mechanischen Komponente eines optomechanischen Aufbaus nachgewiesen werden. Da die mechanische Komponente des Experiments jedoch nur schwer für die Detektion zugänglich ist wird diese Art der Korrelationen über zwei zeitlich getrennten Pulsen im aus der Cavity austretenden Lichtfeld nachgewiesen wobei durch die optomechanische Interaktion der Zustand des mechanischen Subsystems auf das Lichtfeld übertragen wird.

Im ersten Teil meiner Arbeit betrachten wir ein optomechanisches System bestehend aus einem Fabry-Pérot-cavity mit einem beweglichen Endspiegel. Im speziellen sind wir an der Interaktion zwischen dem optischen und dem mechanischen Subsystem interessiert, welche durch die linearisierten Quanten Langevin Gleichungen (QLG) beschrieben wird.
Im zweiten Teil meiner Arbeit präsentiere ich einen Weg um die erhaltenen linearisierten QLG für den Gleichgewichtszustands des Systemes auf analytische Weise zu lösen. Zusätzlich diskutiere ich die Anwendung zweier Filterfunktionen auf das austretende Lichtfeld wodurch es möglich ist zwei zeitlich getrennte Moden entsprechend den Pulsen im eigentlichen Experiment zu definieren und ihre Verschränkung zu untersuchen.

Alle diskutierten Aspekte gipfeln letztendlich in der Implementation eines Programmes welches es dem Anwender erlaubt die Kovarianzen Matrizen für unterschiedliche Konstellationen von Subsysteme zu generieren. Mit Hilfe dieses Programmes werden Einflüsse verschiedener Parameter auf die Verschränkung im System des oben genannten Experimentes untersucht und so sodass Vorhersagen für optimale experimentelle Parameter gemacht werden können.

Bibliography

[AI07] G. Adesso and A. Illuminati. Entanglement in continuous-variable systems: recent advances and current perspectives. *Journal of Physics A: Mathematical and Theoretical*, 2007.

[AIDS03] S. Alessio, F. Illuminati, and S. De Siena. Symplectic invariants, entropic measures and correlations of gaussian states. *Journal of Physics B: Atomic, Molecular and Optical Physics*, 2003.

[AKM14] Markus Aspelmeyer, Tobias J. Kippenberg, and Florian Marquardt. Cavity optomechanics. *Rev. Mod. Phys.*, 86:1391–1452, Dec 2014.

[BHN08] B. Baumgartner, B.C. Hiesmayr, and H. Narnhofer. The geometry of bipartite qutrits including bound entanglement. *Physics Letters A*, 372(13):2190 – 2195, 2008.

[BM67] V.B. Braginskii and A.B. Manukin. Ponderomotive effects of electromagnetic radiation. *Journal of Experimental and Theoretical Physics*, 25(4):653, 1967.

[BMT70] V.B. Braginskii, A.B. Manukin, and M. Yu. Tikhonov. Investigation of dissipative ponderomotive effects of electromagnetic radiation. *Journal of Experimental and Theoretical Physics*, 31(5):829, 1970.

[BR97] S. Barnett and P. Radmore. *Methods in Theoretical Quantum Optics*. Oxford: Clarendon Press, Oxford, 1997.

[BS72] R. H. Bartels and G. W. Stewart. Solution of the matrix equation ax + xb = c [f4]. *Commun. ACM*, 15(9):820–826, September 1972.

[CLRSJS+11] K C Lee, M R Sprague, B J Sussman, J Nunn, Nathan Langford, Xian-Min Jin, Tessa Champion, Patrick Michelberger, K F Reim, Duncan England, Dieter Jaksch, and Ian Walmsley. Entangling macroscopic diamonds at room temperature. 334:1253–6, 12 2011.

[DGCZ00] Lu-Ming Duan, G. Giedke, J. I. Cirac, and P. Zoller. Inseparability criterion for continuous variable systems. *Phys. Rev. Lett.*, 84:2722–2725, Mar 2000.

[DK10] J. M. Dobrindt and T. J. Kippenberg. Theoretical analysis of mechanical displacement measurement using a multiple cavity mode transducer. *Phys. Rev. Lett.*, 104:033901, Jan 2010.

[GC85] C. W. Gardiner and M. J. Collett. Input and output in damped quantum systems: Quantum stochastic differential equations and the master equation. *Phys. Rev. A*, 31:3761–3774, Jun 1985.

[GMTV08] C. Genes, A. Mari, P. Tombesi, and D. Vitali. Robust entanglement of a micromechanical resonator with output optical fields. *Phys. Rev. A*, 78:032316, Sep 2008.

[GR80] I. S. Gradshteyn and I. M. Ryzh. *Table of Integrals, Series and Products*. Academic Press, Orlando, FL, 1980.

[GVT+08] C. Genes, D. Vitali, P. Tombesi, S. Gigan, and M. Aspelmeyer. Ground-state cooling of a micromechanical oscillator: Comparing cold damping and cavity-assisted cooling schemes. *Phys. Rev. A*, 77:033804, Mar 2008.

[HE06] P. Hyllus and J. Eisert. Optimal entanglement witnesses for continuous-variable systems. *New Journal of Physics*, Volume 8, 2006.

[HHH96] Michal Horodecki, Pawel Horodecki, and Ryszard Horodecki. Separability of mixed states: necessary and sufficient conditions. *Physics Letters A*, 223(1):1 – 8, 1996.

[HJ47] R. Philips H. James, N. Nichols. *Theory Of Servomechanisms*. McGraw-Hill Book Co., 1947.

[HO17] Jason Hoelscher-Obermaier. *Generation and Detection of Quantum Entanglement in Optomechanical Systems*. PhD thesis, Universität Wien, 2017.

[Hof15] Sebastian Hofer. *Quantum Control of Optomechanical Systems*. PhD thesis, Universität Wien, 2015.

[Hol82] Alexander Holevo. *Probabilistic and Statistical Aspects of Quantum Theory*. North-Holland Pub. Co, 1982.

[J36] Williamson J. On the algebraic problem concerning the normal forms of linear dynamical systems. *American Journal of Mathematics*, 58:141–163, 1936.

[JCLP07] Nicolas J Cerf, Gerd Leuchs, and E Polzik. *Quantum Information With Continuous Variables of Atoms and Light*. Cambridge University Press, 01 2007.

[LCS+15] F. Lecocq, J. B. Clark, R. W. Simmonds, J. Aumentado, and J. D. Teufel. Quantum nondemolition measurement of a nonclassical state of a massive object. *Phys. Rev. X*, 5:041037, Dec 2015.

[OKDP+18] C. F. Ockeloen-Korppi, E. Damskägg, J.-M. Pirkkalainen, M. Asjad, A. A. Clerk, F. Massel, M. J. Woolley, and M. A. M. A. Sillanpää. Stabilized entanglement of massive mechanical oscillators. *Nature*, 556:478, 2018.

[PDB+15] J.-M. Pirkkalainen, E. Damskägg, M. Brandt, F. Massel, and M. A. Sillanpää. Squeezing of quantum noise of motion in a micromechanical resonator. *Phys. Rev. Lett.*, 115:243601, Dec 2015.

[Per95] A. Peres. *Quantum Theory: Concepts and Methods*. Springer Netherlands, 1995.

[Per96] Asher Peres. Separability criterion for density matrices. *Phys. Rev. Lett.*, 77:1413–1415, Aug 1996.

[PTSL13] T. A. Palomaki, J. D. Teufel, R. W. Simmonds, and K. W. Lehnert. Entangling mechanical motion with microwave fields. *Science*, 342(6159):710–713, 2013.

[PV07] Martin B. Plbnio and Shashank Virmani. An introduction to entanglement measures. *Quantum Info. Comput.*, 7(1):1–51, January 2007.

[RWM+18] Ralf Riedinger, Andreas Wallucks, Igor Marinkovic, Clemens Löschnauer, Markus Aspelmeyer, Sungkun Hong, and Simon Gröblacher. Remote quantum entanglement between two micromechanical oscillators. *Nature*, 556(473), 2018.

[Sau90] Peter R. Saulson. Thermal noise in mechanical experiments. *Phys. Rev. D*, 42:2437–2445, Oct 1990.

[Sch86] B. L. Schumaker. Quantum mechanical pure states with gaussian wave functions. *Physics Reports*, 135:317–408, April 1986.

[Sch07] Franz Schwabl. *Quantenmechanik (QM I) : eine Einführung*. Springer Verlag, 7. edition, 2007.

[Sim00] R. Simon. Peres-horodecki separability criterion for continuous variable systems. *Phys. Rev. Lett.*, 84:2726–2729, Mar 2000.

[TDL+11] J. D. Teufel, T. Donner, Dale Li, J. W. Harlow, M. S. Allman, K. Cicak, A. J. Sirois, J. D. Whittaker, K. W. Lehnert, and R. W. Simmonds. Sideband cooling of micromechanical motion to the quantum ground state. *Nature*, 475(359), July 2011.

[WHTH07] Xiang-Bin Wang, Tohya Hiroshima, Akihisa Tomita, and Masahito Hayashi. Quantum information with gaussian states. *Physics Reports*, 448(1):1 – 111, 2007.

[WLW+15] E. E. Wollman, C. U. Lei, A. J. Weinstein, J. Suh, A. Kronwald, F. Marquardt, A. A. Clerk, and K. C. Schwab. Quantum squeezing of motion in a mechanical resonator. *Science*, 349(6251):952, August 2015.

List of Figures

List of Tables